Energy Efficiency Oriented Full Duplex Wireless Communication Systems

Thesis submitted in accordance with the requirements of
the University of Liverpool for the degree of Doctor in Philosophy
by
Zhongxiang Wei

November 2017

Declaration

The work in this thesis is based on research carried out at the University of Liverpool. No part of this thesis has been submitted elsewhere for any other degree or qualification and it is all my own work unless referenced to the contrary in the text.

Abstract

Full-duplex (FD) transmission is a promising technique for fifth generation (5G) wireless communications, enabling significant spectral efficiency (SE) improvement over existing half-duplex (HD) systems. However, FD transmission consumes higher power than HD transmission, especially for millimetre wave band. Therefore, energy efficiency (EE) for FD systems is a critical yet inadequately addressed issue. This thesis addresses the critical EE challenges and demonstrates promising solutions for implementing FD systems, as detailed in the following contributions.

In the first contribution, a comprehensive EE analysis of the FD and HD amplify-and-forward (AF) relay-assisted 60 GHz dual-hop indoor wireless systems is presented. An opportunistic relay mode selection scheme is developed, where FD relay with different self-interference (SIC) techniques or HD relay is opportunistically selected. Together with transmission power adaptation, EE is maximised with given channel gains. A counter-intuitive finding is shown that, with a relatively loose maximum transmission power constraint, FD relay with two-stage SIC is preferable to both FD relay with one-stage SIC and HD relay, resulting in a higher optimised EE. A full range of power consumption sources are considered to rationalise the analysis. The effects of imperfect SIC at relay, drain efficiency and static circuit power on EE are investigated. Simulation results verify the theoretical analysis.

In the second contribution, EE oriented resource allocation for FD decode-of-forward (DF) relay-assisted 60 GHz multiuser systems is investigated. In contrast to the existing SE oriented designs, the proposed scheme maximises EE for FD relay systems under cross-layer constraints, addressing the typical problems at 60 GHz. A low-complexity EE-orientated resource allocation algorithm is proposed, by which the transmission power allocation, subcarrier allocation and throughput assignment are performed jointly across multiple users. Simulation results verify the analytical results and confirm that the FD relay systems with the proposed algorithm achieve a higher EE than the FD relay systems with SE oriented approaches, while offering a comparable SE. In addition, a much lower throughput outage probability is guaranteed by the proposed resource allocation algorithm, showing its robustness against channel estimation errors.

In the third contribution, it is noticed that in wireless power transfer (WPT)-aided relay systems, the SE of the source-relay link plays a dominant role in the system SE due

to limited transmission power at the WPT-aided relay. A novel asymmetric protocol for WPT-aided FD DF relay systems is proposed in multiuser scenario, where the time slot durations of the two hops are designed to be uneven, to enhance the degree of freedom and hence the system SE. A corresponding dynamic resource allocation algorithm is developed by jointly optimising the time slot durations, subcarriers and transmission power at the source and the relay. Simulation results confirm that, compared to the symmetric WPT-aided FD relay (Sym-WPT-FR) and the time-switching based WPT-aided FD relay (TS-WPT-FR) systems in the literature, the proposed asymmetric WPT-aided FD relay system achieves up to twice the SE and higher robustness against the relay's location and the number of users.

In the final contribution, to strike the balance between high SE and low power consumption, a hybrid duplexing strategy is developed for distributed antennas (DAs) systems, where antennas are capable of working in hybrid FD, HD, and sleeping modes. To maximise the system EE with low complexity, activation/deactivation of transmit/receive chain is first performed, by a proposed channel-gain-based DA clustering algorithm, which highlights the characteristics of distributed deployment of antennas. Based on the DAs' configuration, a novel distributed hybrid duplexing (D-HD)-based and EE oriented algorithm is proposed to further optimise the downlink beamformer and the uplink transmission power. To rationalise the system model, self-interference at DAs, co-channel interference from uplink users to downlink users, and multiuser interference in both uplink and downlink are taken into account. Simulation results confirm that the proposed system provides significant EE and SE enhancements over the co-located FD MIMO system, showing the advantages in alleviating high path loss as well as in cutting the carbon footprint. Compared to the sole-FD DA system, the proposed system shows much higher EE with marginal loss in SE. Also, the SIC operation in the proposed system is much more simplified compared to the two benchmarks.

Contents

List of Figures

List of Tables

Acknowledgement

This thesis would not have been finished without loads of support and help from the following people.

I would like to give my deepest gratitude to my supervisor Dr. Xu Zhu, who has been teaching me with great patient and guiding me from a graduate student to a mature researcher. This work can not be finished without her invaluable comments and constant encouragement. I also appreciate concerns from Prof. Yi Huang for my research. I am grateful to Dr. Sumei Sun at Institute for Infocomm Research, Singapore, where I spent one year as a research assistant and obtained lots of advices and guidance in my research work.

I would like to thank the University of Liverpool, as well as the Department of Electrical Engineering and Electronics, for financing me throughout my Ph.D. period, and providing outstanding training to research students.

I would also like to thank my colleagues: Dr. Yufei Jiang, Dr. Yang Li, Dr. Jun Yin, Dr. Chao Zhang, Ahmed Al-Tahmeesschi, Yanghao Wang, Kainan Zhu, Teng Ma, Yiwei Liu and Boda Liu for creating a family-like atmosphere in the lab. I am pleasure to share my good and tough times with you. Many thanks to Dr. Linhao Dong for your active work on mm-wave communications, which is a corner stone for my research.

Finally, my gratitude is dedicated to my parents, my wife CC and my little angle Yingge. I would had no chance to pursue my dreams in my life without their great support, patience and love. This thesis is dedicated to them.

Haec Otia Studia Fovent

These days of peace foster learning

Nomenclature

3D	three-dimensional
5G	fifth generation
AC	analogue cancellation
ADC	analogue-to-digital converter
AF	amplify-and-forward
AWGN	additive white Gaussian noise
BnB	branch-and-bound
BS	base station
cm	centimetre
CNR	channel-to-noise ratio
CoMP	coordinated multiple points
CP	cyclic prefix
CR	cognitive radio
CSI	channel state information
DA	distributed antenna
DAC	digital-to-analogue converter
DAS	distributed antenna system
DC	digital cancellation
DF	decode-and-forward
EE	energy efficiency
E/O	electrical/optical converter
FD	full duplex
FFT	fast Fourier transform
FW	Frank-Wolfe
HD	half duplex
ISI	inter-symbol interference
KKT	Karush-Kuhn-Tucker
LNA	low noise amplifier
LO	local oscillator
LOS	line-of-sight
LPF	low pass filter

LTE long term evolution
MAC media access control
MIMO multi-input multi-output
mm millimetre
MMSE minimum mean square error
MRC maximum ratio combining
NOMA non-orthogonal-multiple-access
NM nanometre
OFDM orthogonal frequency division multiplexing
OFDMA orthogonal frequency division multiple access
PA power amplifier
PHY physical layer
PL path loss
PS passive suppression
QoS quality-of-service
RF radio frequency
RMS root mean square
RRU radio remote unit
SDP semi-definite programming
SE spectral efficiency
SIC self-interference cancellation
SINR signal-to-interference-and-noise ratio
SISO single-input single-output
S-V Saleh-Valenzuela
TDD time division duplex
TDMA time division multiplex access
VCO voltage controlled oscillator
VGA variable gain amplifier
WPT wireless power transfer
ZF zero forcing

Chapter 1

Introduction

1.1 Background and Motivation

Fifth generation (5G) wireless communication systems are calling for significantly increased data rate (up to 1000 times higher than current data rate) for much richer multimedia applications, e.g. high definition video and three dimensional (3D) online games [1]. Conventional communication systems operate in half duplex (HD) mode [2], i.e. antennas receive and transmit signal in orthogonal time slots or frequencies. This leads to loss of spectral efficiency (SE). Recently, full duplex (FD) technique has attracted much attention due to its ability to achieve higher SE. FD node can receive and transmit signal simultaneously at the same frequency, which enables significant SE improvement over existing HD systems. However, strong self-interference is introduced at FD node's receiver from its transmitter and effective self-interference cancellation (SIC) is required at FD node. Thanks to recent advance in SIC, SIC amount of up to 100 dB can be achieved [3], paving the way for the commercial use of FD systems.

On the other hand, to achieve the Gbps-level data rate requirement, using the millimetre (mm)-wave band, e.g. frequencies of 28 GHz, 38 GHz and 60 GHz, is a promising solution. With the recent advance of circuit design for mm-wave band [4] [5] [6] [7] [8], there have been growing interests in standardizing its use for 5G communications. Besides, the mm level wavelength enables the creation of small-sized antennas and other radio hardware. Some advanced techniques, such as multiple-input multiple-output (MIMO) can be fabricated in the state-of-the-art small-sized terminals. The mm-wave communication systems, however, have inherent disadvantages in that the propagation loss (PL) is high at such high frequency and that the signal can be easily blocked by obstacles due to short signal wavelength (only 5 mm at a frequency of 60 GHz) [9]. To alleviate the high PL and the serious intermittent blockage effect, it is beneficial to employ relay nodes between sources and destinations to assist communications [10]. There have been active research to incorporate FD with mm-wave communications to further improve data rate and reduce latency. A 60 GHz transceiver with FD fibre-optic transmit and receive chains was developed for short-range broadband application

in [11], while FD implementation in mm/sub-mm Si-constructed chips was investigated in [12] [13]. As for the SIC design, it is shown that as much as $80 - 100$ dB of SIC can be achieved at mm-wave frequency by using passive suppression (PS), analogue cancellation (AC) and digital cancellation (DC) [14] [15].

To implement FD and mm-wave in 5G communications, however, high power consumption is a critical challenge, because additional power is triggered by SIC at FD nodes [10] and chips working at mm-wave frequency also consume much higher power than that working at a lower frequency. Moreover, the receive and transmit chains of FD node are active at all time, while only one transmit chain or one receive chain of HD node is active at each time slot [16]. To address the high power consumption issue and achieve green communication, energy efficiency (EE) is an important system performance metric proposed in 5G communication systems. However, to the best of our knowledge, there lacks investigation of EE of FD systems. This motivates the work demonstrated in this thesis.

1.2 Research Contributions

The research conducted during this PhD study has produced the following main contributions:

- The EE of FD amplify-and-forward (AF) relay systems is investigated, and a comprehensive comparison between FD AF relay and HD AF relay systems is provided. The closed form of EE gain region is given, which clearly reveals the conditions that FD outperforms HD in terms of EE. It is found that with loose transmission power constraint, FD with PS and AC of SIC techniques is even more energy efficient than the FD with PS only and HD relay systems. To improve the system EE, transmission power adaptation and opportunistic relay mode selection are developed. By adopting transmission power adaptation and opportunistic relay mode selection together, both EE and SE of FD AF relay system can be much higher than that of HD AF relay system. To rationalise the system model, a full range of power consumption and imperfect SIC are considered.

- Addressing the practical transmission problems at mm-wave frequency, such as the intermittent signal blockage and out-of-the-date channel information, the cross-layer design for FD decode-and-forward (DF) relay systems is considered in a multiuser scenario. A cross-layer EE oriented algorithm is proposed, by which subcarriers, power at source and relay, and throughput are jointly allocated. Compared to the FD DF relay system with a SE oriented algorithm, the proposed cross-layer algorithm achieves much lower outage probability, making FD DF relay system more robust against to the channel estimation errors.

Besides, a higher EE performance of the proposed EE oriented design is demonstrated over the SE oriented design, at the cost of marginal SE loss. Properties of the EE oriented resource allocation are investigated.

- In wireless power transfer (WPT)-aided FD DF relay systems, the available transmission power at relay node is much lower than that at source taking to account the PL from source to relay and low conversion efficiency at relay node. As a result, the end-to-end SE is always bounded by the relay-user hop. To better balance the SE of two hops, a novel asymmetric protocol is developed, which adaptively assigns uneven time slots for the two hops. Based on the asymmetric time slots protocol, a corresponding algorithm is proposed, by joint allocation of transmission power, subcarriers and time slot durations. Besides, we utilise self-interference rather than cancel it. It is demonstrated that more energy can be harvested by the proposed algorithm due to the enhanced of degrees of freedom. Also, higher SE is achieved compared to the symmetric time slots structure-based algorithm and time-switching-based algorithm.

- FD communications in bi-directional scenario is considered. Different from conventional FD MIMO systems, FD is incorporated with DA systems, which has natural advantages in reducing PL and blockage effect. A hybrid duplexing mode is proposed, allowing DAs work in FD, HD or sleeping modes. To maximise the system EE, a channel gain-based DA clustering algorithm is first performed to activate/deactivate transmit/receive chain of DAs, and then beamformer at DAs and transmission power at uplink user are jointly assigned. With the proposed algorithms, the hybrid duplexing FD DA systems feature higher EE, lower power consumption, and simpler SIC circuit design compared to the two benchmarks, conventional co-located FD MIMO system and sole-FD DA system.

1.3 Thesis Organisation

The rest of this thesis is organised as follows. The overview of wireless channels and systems is introduced in Chapter 2. Chapter 3 demonstrates the details of FD systems, including its classifications, SIC design and EE challenges in implementing FD systems. In Chapter 4, EE comparison between FD and HD in AF relay systems is given, revealing the conditions that FD is greener than its HD counterpart. In Chapter 5, cross-layer design in FD DF relay systems is studied, which addresses the propagation characteristic at 60 GHz. In Chapter 6, WPT-aided FD DF relay system is considered, where the relay is powered by WPT from the source. An asymmetric protocol applicable for WPT-aided FD DF relay systems is proposed. In Chapter 7, bi-directional FD DA system is considered, where DAs communicate with multiple users in both uplink and downlink simultaneously. A joint design of the status of DAs, uplink transmis-

sion power and downlink beamformer is presented. Conclusions and future work are presented in the final chapter.

1.4 Publication List

A number of publication have arisen during the course of this research, as listed below, all of which have contributed to the thesis.

Journal Papers

1. Z. Wei, X. Zhu, S. Sun, and Y. Huang, "Energy efficiency oriented cross-layer resource allocation for multiuser full-duplex decode-and-forward indoor relay systems at 60 GHz," *IEEE J. Sel. Areas Commun.*, vol. 34, no. 12, pp. 3366-3379, Dec. 2016.

2. Z. Wei, X. Zhu, S. Sun, Y. Huang, A. Al-Tahmeesschi, and Y. Jiang, "Energy efficiency of millimetre-wave full-duplex relaying systems: challenges and solutions," *IEEE Access*, vol. 4, pp. 4848-4860, Jul. 2016.

3. Z. Wei, X. Zhu, S. Sun, Y. Huang, L. Dong, and Y. Jiang, "Full-duplex vs. half-duplex amplify-and-forward relaying: which is more energy efficient in 60 GHz dual-hop indoor wireless systems? *IEEE J. Sel. Areas Commun.*, vol. 33, no. 12, pp. 2936-2947, Dec. 2015.

4. Z. Wei, X. Zhu, S. Sun, and Y. Huang, "Energy efficient hybrid duplexing strategy for millimetre-wave bi-directional distributed antenna systems, major revision in *IEEE Trans. Veh. Technol.,* Sep. 2017.

5. Z. Wei, X. Zhu, S. Sun, and Y. Huang, "Resource allocation in asymmetric full-duplex wireless-powered OFDMA decode-and-forward relay systems," submitted to *IEEE Trans. Wireless Commun.*, May. 2017.

6. Z. Wei, X. Zhu, S. Sun, Y. Jiang, A. Al-Tahmeesschi, and M. Yue, "Research issues, challenges, and opportunities of wireless power transfer-aided full-duplex relay systems," submitted to *IEEE Access*, Sep. 2017.

Conference Papers

1. Z. Wei, S. Sun, X. Zhu, Y. Huang, and J. Wang "Energy efficient hybrid duplexing and resource allocation for distributed antenna systems," in *Proc. IEEE GLOBECOM'17.*, Singapore, Dec. 2017.

2. Z. Wei, S. Sun, X. Zhu, and Y. Huang, "Wireless information and power transfer: spectral efficiency optimization for asymmetric full-duplex relay systems," in *Proc. IEEE VTC'17 SPR.*, Sydney, Australia, Jun. 2017. (invited paper)

3. Z. Wei, X. Zhu, S. Sun, Y Huang, and H. Lin, "Cross-layer energy efficiency optimization for multiuser full-duplex decode-and-forward indoor relay networks at 60 GHz," in *Proc. IEEE ICC'16.*, KL, Malaysia, Apr. 2016.

4. Y. Jiang, X. Zhu,E. G. Lin, Y. Huang, Z. Wei, and H. Lin, "Semi-blind precoding aided ML CFO estimation for ICA based MIMO OFDM systems," in *Proc. IEEE ICC'16.*, KL, Malaysia, Apr. 2016.

5. Z. Wei, X. Zhu, S. Sun, Y. Huang, T. Ma, and Y. Jiang, "Energy efficiency optimization for full-duplex relaying with hybrid self-interference cancellation in 60 GHz indoor wireless systems," in *Proc. IEEE/CIC ICCC'15.*, Shenzhen, China, Nov. 2015. (invited paper)

6. Y. Jiang, X. Zhu, E. G. Lim, Y. Huang, Z. Wei, and H. Lin, "Semi-blind full-duplex relay system with ICA based joint CFO mitigation and equalization," in *Proc. IEEE/CIC ICCC'15.*, Shenzhen, China, Nov. 2015. (invited paper)

Chapter 2

Overview of Wireless Communication Channels and Systems

This chapter outlines the evolution of wireless communication systems. The fundamentals of wireless communication channels, orthogonal frequency division multiplexing (OFDM) and mm-wave communications are also presented.

2.1 The Evolution of Wireless Communication Systems

To date, four generations of cellular communication systems have been adopted in the world with each new mobile generation emerging every 10 years or so. First generation analogue cellular systems in 1981; second generation digital technology in 1992, third generation (CDMA 2000, WiMAX) in 2001, and fourth generation (LTE, LTE-A) in 2011, as summarised in Tab. 2.1.

As the demand for data rate in mobile broadband communications increases dramatically every year, it is estimated the total mobile traffic will be increased thousand-fold

Table 2.1: Requirements and realities of 1G through 4G cellular systems [17]

Generation	Requirements	Comments
1G	No official requirements. Analogue technology.	Deployed in 1980.
2G	No official requirements. Digital technology.	First digital systems. New service such as SMS and low-rate data.
3G	ITU's IMT-2000 required 144 kbps mobiles, 2Mbps indoor	Primary technologies include CDMA2000 1×EV-DO WiMAX.
4G	ITU's IMT Advanced. Requirements include ability to operate in up to 49 MHz radio channels and with high SE ability	IEEE 802.16m LTE-Advanced

by 2020, requiring researchers to seek greater capacity to support richer multimedia service beyond the 4G standard. As 5G is developed and implemented, enhanced system metrics, e.g. higher EE and SE, longer battery life, lower outage probability, lower infrastructure costs, and higher aggregate capacity are expected, by adopting advanced techniques, e.g. FD, mm-wave, massive MIMO, highly directional beamforming antennas.

2.2 Wireless Communication Channel Models

2.2.1 Large-Scale Path Loss

The signal strength reduction caused by large distances between the transmitter and the receiver is referred to as large-scale path loss (PL), which is calculated as

$$\mathrm{PL} = l_0 + 10\tau \log_{10}(d/d_0), \tag{2.1}$$

where l_0 is the free-space PL at the reference distance and its value varies according to propagation environment and communication frequency. τ is the PL exponent. d is the distance between two communication nodes. d_0 could be set to 1 m in indoor environment or longer in outdoor environment.

2.2.2 Small-Scale Multipath Fading

Multipath fading is the rapid fluctuation of channel gain and change of phases over a short period of time or distance, caused by the constructive or destructive interference of the multiple signal paths between the transmitter and receiver. Multipath fading causes rapid small-scale variation of signals. In urban environments, transmitters and receivers are surrounded by building, trees, moving vehicles and pedestrians, which cause reflection, diffraction and scattering of the transmitted signals. Therefore, the signal undergoes different paths, and each of the paths generates a unique wave of the transmitted signal with the randomly distributed amplitude, phase and delay. The receiver vectorially combines all these waves, and this causes the signal distortion and fading [18] [19]. Letting f_i and σ_i denote the channel gain and delay for the i-th path, respectively, the root-mean-square (RMS) delay spread σ is expressed by

$$\sigma = \sqrt{\frac{\sum_i f_i^2 \sigma_i^2}{\sum_i f_i^2} - \left(\frac{\sum_i f_i^2 \sigma_i}{\sum_i f_i^2}\right)^2}. \tag{2.2}$$

The RMS delay spread interprets the multipath richness. In other words, the higher the RMS delay spread is, the larger the effect of multipath is.

In wireless communications, coherence bandwidth B_c is defined as the range of frequencies where two frequency components have a strong potential for amplitude

Table 2.2: Types of multipath fading

Flat Fading	Signal Bandwidth < Coherence Bandwidth
Frequency Selective Fading	Signal Bandwidth ≥ Coherence Bandwidth
Fast Fading	Coherence Time < Symbol Period
Slow Fading	Coherence Time ≥ Symbol Period

correlation. Coherence bandwidth B_c can be derived from the RMS delay spread σ, i.e. $B_c \approx \frac{1}{5\sigma}$.

On the other hand, the relative motion between the base station and the mobile user causes Doppler shift f_d, which is given by

$$f_d = \frac{c}{\lambda} cos\theta, \tag{2.3}$$

where c represents the velocity of a mobile user moving at. λ is wavelength and θ is the angle between the direction of the received signal wave and the direction of the mobile user's motion. Doppler spread B_d denotes the difference between Doppler shifts of signal components. The coherence time T_c is referred to as the time over which two received signal have a strong potential for amplitude correlation. It can be expressed in terms of the Doppler shift f_m, i.e. and $T_c = \frac{9}{16\pi f_m}$. Depending on the characteristics of the transmitted signal, i.e. signal bandwidth and symbol period, and the nature of the multipath channel, i.e. RMS delay spread σ and Doppler spread B_d, there are four different fading effects, which are flat fading and frequency selective fading due to multipath delay spread, and fast fading and slow fading due to Doppler spread [20]. These fading effects are summarised in Tab. 2.2.

Assume each symbol is transmitted via signal bandwidth B_s during symbol period T_s. Supposing there are N_p paths between the transmitter and the receiver, the channel impulse response (CIR) is given by:

$$f(t) = \sum_{i=0}^{N_p-1} f_i \delta(t - \sigma_i), \tag{2.4}$$

where f_i and σ_i are the channel gain and delay for the i-th path, respectively. The Rayleigh distribution is commonly used to describe the amplitude $|f_i|$, of which the probability density function is given by:

$$p(x) = \frac{x}{\tau^2} \exp(-\frac{x^2}{2\tau^2}), \tag{2.5}$$

where τ^2 denotes the time-average power of the received signal. If the received signal contains direct path and a line of sight (LOS) signal is much stronger than the others, the channel becomes into Rician fading. In Rician fading, the amplitude gain is characterised by a Rician distribution, of which the probability density function is:

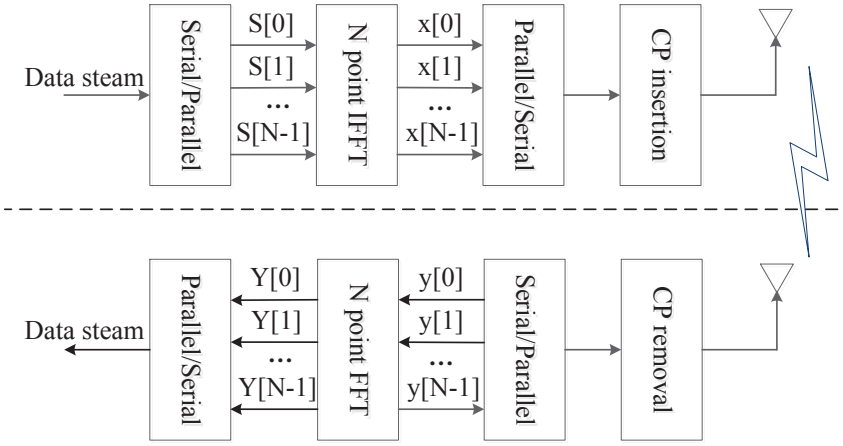

Figure 2.1: Simplified block diagram of the OFDM system.

$$p(x) = \frac{2(K+1)x}{\Omega}\exp(-K - \frac{(K+1)x^2}{\Omega})I_0(2\sqrt{\frac{K(K+1)}{\Omega}}x), \tag{2.6}$$

where K is the ratio between the power in the direct path and the power in the other scattered paths. Ω is the total power from both paths that $\Omega = v^2 + 2\tau^2$, and I_0 is the 0-th order modified Bessel function of the first kind.

2.3 Orthogonal Frequency Division Multiplexing

By employing advanced techniques, 5G wireless communication is expected to achieve Gbps-level transmission rate. However, the higher the data rate, the larger the impact of multipath fading. OFDM is one of the effective solutions to handle frequency selective fading, which converts communication over a multipath channel into communication over simpler parallel narrowband subcarriers and has natural advantages in utilizing the wide bandwidth of mm-wave communications. Therefore, OFDM has been selected as one of the key techniques in 5G standards.

The procedure of the OFDM system is presented in Fig. 2.1. Suppose there are N symbols $(S[0], ..., S[N-1])$ waiting for transmission. After the inverse fast Fourier transform (IFFT), the transmission data can be presented as:

$$x[n] = \sum_{i=0}^{N-1} S[i]e^{\frac{j2\pi}{N}in}, n \in \{0, ..., N-1\}. \tag{2.7}$$

The received signals are

$$y[n] = h(n) \otimes x[n] + z[n], n \in \{0, ..., N-1\}, \tag{2.8}$$

where $h(n)$ and $z[n]$ are the CIR and noise. The FFT is applied to the received signals after CPR, and recovered signals are

$$Y[n] = \sum_{i=0}^{N-1} y[i] e^{\frac{-j2\pi}{N} in}, n \in \{0, ..., N-1\}, \tag{2.9}$$

which is equal to

$$Y[n] = H_n S[n] + Z[n], n \in \{0, ..., N-1\}, \tag{2.10}$$

where H_n and $Z[n]$ are the CIR and noise on the n-th subcarrier in the frequency domain. It can be derived from (2.10) that each transmission data $x[n]$ consists of information from N symbols, and the information of one symbol has been spread across N transmission data. Hence, the symbol period in OFDM systems becomes NT_s, leading to a mitigated inter-symbol interference (ISI). In the frequency domain, the frequency range for each symbol is narrowed so that each transmission data carried on one subcarrier undergoes flat fading.

There are several benefits brought by the OFDM technique. First, since the bandwidth of each subcarrier is narrowed, the system is unlikely to suffer the same fading over all subcarriers in a multipath channel. Hence, there is frequency diversity in OFDM systems. Second, each subcarrier is in flat fading, and therefore the ISI problem in multipath environments is eliminated. Additionally, each subcarrier can be modulated independently in OFDM systems. It leads to a higher SE than conventional single-carrier systems under frequency selective circumstances [18]. Furthermore, as illustrated by Fig. 2.2, OFDM leads to a higher efficiency in spectrum than conventional frequency division multiplexing (FDM), where the carriers are not overlapped, and there is a guard band between two adjacent carriers. Of course, there are few disadvantages of OFDM, e.g. the CP occupies an amount of time and transmission power. Also, carrier frequency offset and peak to average power ratio are two practical issues in OFDM systems.

2.4 Millimetre Wave Communications

With the sub-3 GHz spectrum is becoming increasingly crowded and the SE of microwave links has approached its fundamental limits, it is difficult to support the exponential growth of mobile data traffic. Since, abundance of communication bandwidth at mm-wave band, 30-300 GHz, remains under utilised [21], mm-wave has been considered as one key technique in 5G communications. To pave the way for commercial use of mm-wave, several standardization activities have been conducted in recent years, e.g. IEEE 802.15.3 Task Group 3c (TG3c) [22], IEEE 802.11ad standardization task group, Wireless HD consortium, wireless gigabit alliance (WiGig), wireless personal area networks (WPANs) [23] [24] [25] and wireless local area networks (WLANs). Also, there have been active projects, e.g. FP7 EU Project METIS [26], and infield measurements

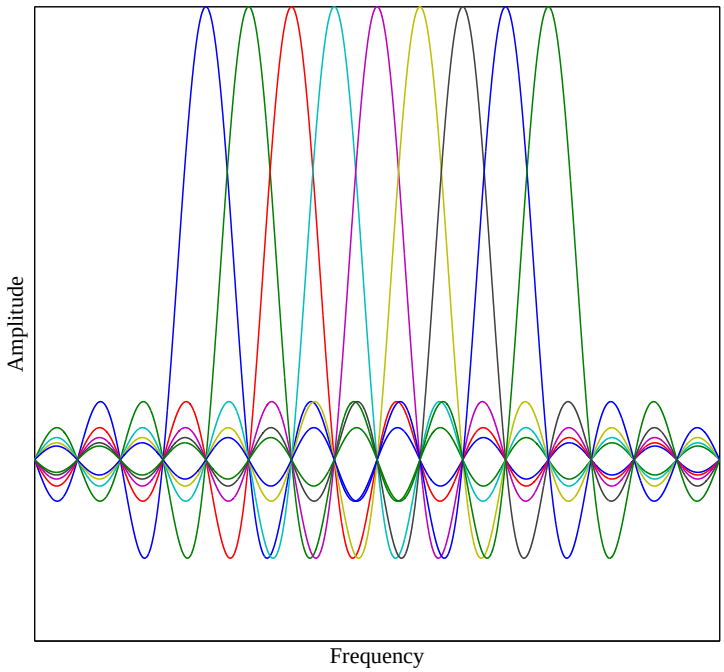

Figure 2.2: Waveform of 8 OFDM subcarriers.

[9] [17] [27]-[31] investigating how mm-wave perform in cellular systems or indoor environment. Signal propagation at 28 GHz and 38 GHz was measured in urban city, Now York and Austin by [17], proving the communication distance at mm-wave frequency can even achieve hundreds metres in a dense urban environment with highly reflective nature. In [27], 60 GHz band and E band (71-76 and 81-86 GHz) were adopted for backhaul for 5G cellular systems. The statistical parameters of 60 GHz propagation channel in various indoor environments were given by [9] [28] [29], showing the channel follow Rayleigh or Rician distribution depending on the specific communication scenario. Beamforming effects on mm-wave channel characteristics were studied by [30]. The channel parameters of narrowband and wideband direction-based beamformers was investigated in [31].

Besides, the design of mm-wave circuitry have been done by [4]-[7]. The authors in [4] designed an integrated 90 nanometre (nm) CMOS 60 GHz transceiver including radio frequency (RF), base band (BB) signal paths, local oscillator (LO) generation and distribution. A 60 GHz wideband power amplifier (PA) fabricated in a standard CMOS 65 nm processors was proposed by [5], and the maximum output saturation power achieves 14.5 dBm with peak power-added efficiency 25% when the PA is supplied by 1.8 V voltage. A 60 GHz 16 quadrature amplitude modulation transceiver including radio frequency (RF) front-end, antenna, analogue, and digital baseband circuitry was

Table 2.3: Statistical parameters in the PL models of the 60 GHz indoor channels [9]

Communication scenarios	PL in free space l_0	PL exponent
Corridor	68 dB	1.64
LOS hall		2.17
NLOS hall		3.01

designed by [7], which is able to achieve more than 7-Gb/s data rate and has potential to be extended up to 10 Gb/s.

More dedicated research at mm-wave frequency, e.g. OFDM, synchronization, random access, handover, interference management, and scheduling have been given as well. The media access control (MAC) layer design in mm-wave cellular systems was researched by [32], while multi-hop communication and cooperative diversity performance were investigated by [33]-[36].

mm-wave communications, however, have inherent disadvantages in high PL and sensitivity to blockage. Since the free space PL increases proportionally as the square of the carrier frequency, the propagation loss at mm-wave band is natural much higher than that at lower frequency bands, e.g. 2 GHz or 5 GHz. Take 60 GHz communication as an example, the PL at reference distance (1 m) is up to 68 dB, as summarised by Tab. 2.3. Also, the signal transmission at mm-wave frequency is easy to be blocked by obstacles due to short signal wavelength (only 5 mm at a frequency of 60 GHz). To alleviate the high PL and the serious intermittent blockage effect, it is beneficial to employ relay nodes between sources and destinations to assist communications. Relay-assisted communication at mm-wave frequency has been investigated by [25] [33] [35]. However, the research in [25] [33] [35] only focused HD transmission, leading to low SE. How to incorporate FD into mm-wave communications is still untouched.

Chapter 3

Overview of Full Duplex Systems

3.1 Full Duplex Classifications

FD systems can be classified in different ways as follows. Especially for FD relay systems, we take a two-hop FD relay system in the downlink as an example, which can be easily extended to a general multi-hop scenario.

3.1.1 By with or without Relay

Without the use of relay, FD systems often refers to the communication between two FD nodes, as shown by Fig. 3.1 (a). The transmission is bi-directional and thus SIC needs to be applied in both two communication nodes. On the other hand, if a FD relay is deployed to help the communication between source and destination, the system can be classified as FD relay system, where the relay can receive and transmit signal simultaneously at the same frequency. Since only relay works in FD mode, SIC is only conducted at relay node. Another more complicated FD relay application is bi-directional FD relay system, which is further clarified in subsection 3.1.5.

3.1.2 By Antenna Type

According to the type of antennas, FD systems can be classified as shared-antenna FD [37] and separate-antenna FD [2], as illustrated by Fig. 3.1 (b).

With shared-antenna, only one antenna set is adopted for both transmission and reception at relay node. A duplexer (circulator) is needed to route the received signal from antenna to the receive chain, and route the transmitted signal to the antenna from the transmit chain.

With separate-antenna, relay can use separate antennas for transmitting and receiving, respectively. In particular, separate-antenna is preferable when MIMO is applied at relay node. This is because the SIC is more complex than that in single-input single-output (SISO) systems, whereas the SIC performance with the shared-antenna configuration is not optimal since the isolation offered by the duplexer may not be sufficient.

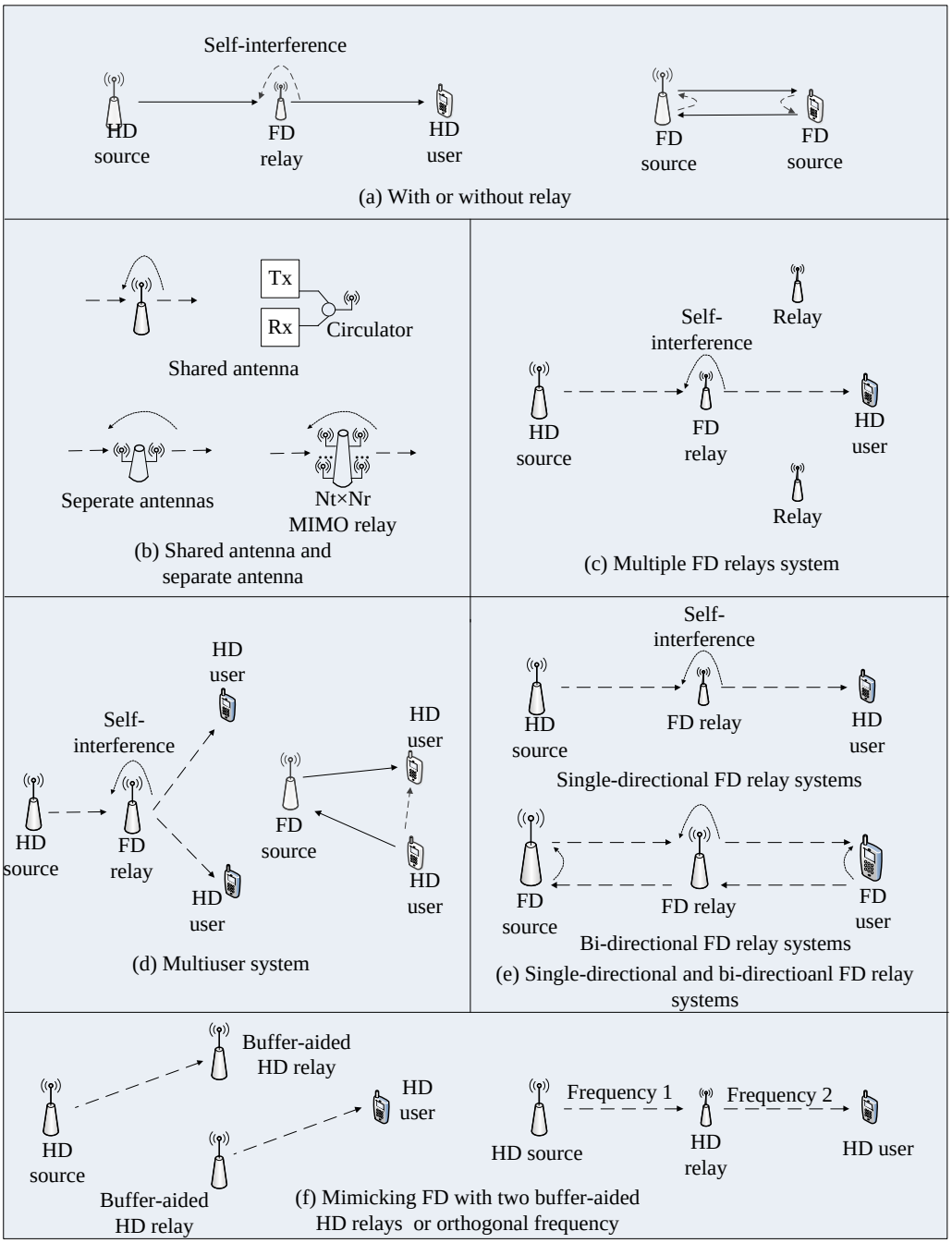

Figure 3.1: Classifications of FD systems and their mimics by HD relays.

3.1.3 By Relay Mode

Based on the relay mode, FD relay systems can be divided into AF relay systems and DF relay systems [2] [10].

An AF relay amplifies the received signal from source and forwards it, including the desired signal, noise, and residual self-interference, to destination. Therefore, AF relay systems have simpler circuit design and low power consumption. However, they introduce amplified noise and self-interference to destination.

A DF relay decodes the received signal first, and forwards the re-encoded signal to destination. Hence, the residual self-interference does not affect the link from relay to destination directly. However, a DF relay normally leads to higher power consumption and latency than an AF relay due to its complex signal processing.

3.1.4 By Numbers of Relays or Users

As illustrated by Figs. 3.1 (c) and (d), to combat the high PL and the blockage effect in mm-wave communications, a destination may be assisted by multiple relays [38]. In this case, one can apply relay selection to explore spatial diversity. Also, multiple users may be served by one relay node. In a multiuser scenario, multiple access technique, such as orthogonal frequency division duplexing access (OFDMA), can be adopted [2]. Importantly, the power of self-interference is different across subcarriers. To achieve a better SIC performance, per-subcarrier SIC [3] is desirable.

3.1.5 By Transmission Directionality

According to the transmission directionality, FD systems can be classified into single-directional FD and bi-directional FD [39], as illustrated by Fig. 3.1 (e). Single-directional FD systems are involved with an FD relay receiving and transmitting in one direction, while bi-directional FD systems consist of two communication nodes, each operating in FD mode. The two nodes send signals to each other with or without the help of the FD relay node.

3.1.6 Mimicking Full Duplex Systems by Half Duplex Nodes or Orthogonal Frequencies

There are some schemes using HD relay to mimic FD relay systems, which is given by Fig. 3.1 (f). One mimicking approach is to use two buffer-aided HD relays to corporate communication between source and destination, where one relay is used to receive the signal from source and the other is used to transmit the buffered signal to destination [40]. However, since two HD relays are needed at the same time, the associated power consumption is high.

Another mimicking approach is to let an HD relay node receive and transmit at different frequencies. However, SE is sacrificed in this case, since the frequency band

is split into two orthogonal parts for transmission and reception individually.

3.2 Self-Interference Suppression/Cancellation

Thanks to the recent advance in SIC techniques [3] [16] [41], the self-interference in FD systems can be mitigated effectively. There are three main approaches to mitigate self-interference: PS, AC and DC [3].

3.2.1 Passive Suppression

The first stage of SIC, PS, mitigates self-interference in the propagation domain, via directional antenna, antenna placement and antenna shielding. Recent research has shown that more than 70 dB of self-cancellation amount can be achieved by PS in an anechoic chamber, and more than 40 dB in a reflected room [42]. The advantage of using PS is that no additional power consumption is required. Fortunately, some features of mm-wave naturally benefit the performance of PS, e.g. the mm level wavelength and the application of directional antenna:

a) As discussed aforementioned, mm level wavelength leads to a much higher PL, which can benefit SIC in the propagation domain. For example, the distance between transmitter and receiver (separate antenna deployment) is 10 centimetre (cm) in a small-sized smart device. The resulting self-interference amount at 60 GHz is 20 dB lower than that at 5 GHz and 28 dB lower than that at 2.4 GHz, respectively, assuming the free space PL exponent [8]. Besides, for the mm level wavelength, a cm level absorptive obstacle between relay's transmitter and receiver can block the direct path of self-interference effectively.

b) Besides, applying high-gain antennas with narrow beamwidth allows relay to steer beams to concentrate radiated energy in only the desired directions, and the transmitter at relay can point to destination's receiver. The main lobe of the beam of relay's transmitter will not be routed into relay's receiver. As a result, the self-interference comes only from reflected waves, which are much weaker than the direct path. Also, the application of directional antenna is beneficial to the cross-polarization, where transmit and receive antennas in orthogonal polarization states (vertically and horizontally polarised) can achieve a SIC amount of around 20 dB. In summary, PS in mm-wave band can achieve much better performance than that in cm-wave band.

However, PS is sensitive to nearby environment, especially in reflective environment, and PS operation increases the frequency selectivity of the residual self-interference channel. To solve this problem, AC and/or DC can be used to mitigate residual self-interference further, where additional power consumption is required.

3.2.2 Analogue Cancellation

After PS, self-interference can be further mitigated by AC before signal goes through low noise amplifiers (LNAs) [16] [43] [44]. With the ready-made transmit chains and receive chains, there are two kinds of AC designs: direct-conversion architecture AC and non-direct-conversion architecture AC. The former deploys direct-conversion radio architecture to estimate self-interference and subtracts it at relay's receiver end. This kind of AC circuit design does not need additional baseband signal processing at relay node and thus consumes less power. FD node processes the transmitted signal at transmitter to form the predicted self-interference in the analogue-circuit domain. While the non-direct-conversion AC architecture generates the predicted self-interference by processing the transmit signal in digital domain, adjusts the gain/phase digitally, converts the digital signal to analogue and finally feeds it to the receive chain for AC operation. Since baseband signal processing unit, digital-to-analogue converters (DACs), mixers, low pass filters (LPFs), attenuators and adders are required. The incurred power consumption is as high as the equivalent transmit chains.

3.2.3 Digital Cancellation

DC is applied at the last stage, which subtracts the residual self-interference after PS and AC in digital domain [41]. It requires accurate estimation of the residual self-interference following PS and AC. Moreover, the transmitter and receiver distortions need to be captured by DC. Therefore, complex baseband signal processing unit is required by DC operation, which consumes non-negligible power consumption.

The summary of different SIC in FD systems is given by Tab. 3.1.

3.3 Power Consumption and Energy Efficiency Challenges in Full Duplex Systems

In this section, we discuss the power consumption and the critical EE challenges of FD systems.

3.3.1 Power Amplify Power Consumption

For wireless communication systems, the power consumed by cascaded PAs contributes a large portion to the total power consumption, which is mainly caused by the low drain efficiency. Especially for the chips working at mm-wave frequency, the drain efficiency of current 60 GHz PAs is lower than 25% [5]. This is much lower than the drain efficiency of 2.4/5 GHz PAs, which is normally 30-40% [45] [46]. As a result, chips working in mm-wave band dissipate much more power than the chips working in cm-wave band.

3.3.2 Circuit Power Consumption

Apart from PA power, circuit power also contributes a large part to the total power consumption. Generally, circuit power is the the power consumed by the signal processing parts, including LNAs, filters, DAC, analogue-to-digital converter (ADC), voltage controlled oscillator (VCO), dividers, local oscillator (LO) buffer, decoder, comparators, variable gain amplifier (VGA) etc [4]. It is worth mentioning that, limited by the start-of-the-art hardware design, circuit power consumed by a mm-wave chip is also higher than that consumed by a cm-wave chip [4].

3.3.3 Additional Power Consumption Incurred by Full Duplex Transmission

HD transmission splits the transmission into two orthogonal time slots, and only one receive chain or one transmit chain is active at each time slot. While in FD systems, both transmit chain and receive chain are active at all time. Therefore, the power consumption of FD systems is naturally higher than that of HD systems.

The other additional power consumption of FD node is incurred by SIC. Generally speaking, complex SIC scheme needs more involved components and consumes higher power. For example, the AC operation design in [3] needs DAC, transmit radio unit and adder to mitigate self-interference. The additional power consumption incurred by the SIC is even comparable with the power consumption of the equivalent transmit chains [41]. Another kind of AC design in [16] uses tunable attenuation and delay unit to route the estimated signal to the receiver for SIC. Attenuator, delay units and adders are required to adjust the delay and the amplitude, and the introduced power consumption is still non-negligible.

Besides, the power consumed by DC operation is also non-negligible. Since DC design needs to calculate the equivalent baseband signal after PS and AC operations, where digital baseband signal processing unit is required [3].

Table 3.1: Summary of different SIC schemes for FD systems in terms of EE

SIC schemes	Approaches	Additional power consumption	Features	Drawbacks
PS	Benefiting from high PL between relay's transmitter and receiver	Nil	Much higher PL than the PL with cm wave	Sensitive to environment; Increased frequency selectivity of self-interference channel
	Antenna shielding	Nil	Fully exploiting the advantage of mm level wavelength	Sensitive to environment; Increased frequency selectivity of self-interference channel
	Directional antenna	Nil	Widely used in mm-wave communications; Relay's transmitter pointing to destination with no direct self-interference	Sensitive to environment; Increased frequency selectivity of self-interference channel
AC	Direct-conversion architecture	Low	Aware to the reflected self-interference	Sensitive to wideband self-interference
	Non-Direct-conversion architecture	High	Unaware to the reflected self-interference	Not feasible in AF relay systems
DC	Digital-domain canceller	High	Inefficient given good performance by PS+AC, may degrade the EE performance	May cause negative effect to system (the introduced noise power is higher than the power of the self-interference cancelled)

Chapter 4

Energy Efficiency Comparison between Full Duplex and Half Duplex in Amplify-and-Forward Relay Systems

Nowadays, wireless communications are required to support much richer multimedia applications, such as uncompressed high definition TV and high speed video downloads. The 60 GHz frequency band, with an extremely large bandwidth of up to 7 GHz, is a promising candidate for high speed indoor wireless networks [25]. However, the 60 GHz transmission requires line-of-sight (LOS) and suffers significant propagation loss due to inherent disadvantages at such high frequency [17]. Also, it is challenging to maintain robust network connectivity at 60 GHz networks. As the wavelength at 60 GHz is only 5 mm, links are easily blocked by obstacles, such as human body and furniture. Applying relay is a leverage to extend network coverage while maintaining robust connectivity [33]. Conventional relays work in HD mode, while FD relay system [2], which allows transmitting and receiving at the same frequency and the same time, enables a significant enhancement of system throughput and has attracted much attention. Whereas, it suffers loop interference and requires effective self-interference mitigation [42].

On the other hand, 60 GHz chips generally consume much more power than the chips working at a much lower frequency [4]. Therefore, there is an urgent demand for maintaining high throughput while limiting energy consumption [47], which has attracted much attention from vendors and researchers, e.g. the IJOIN project [1]. EE, defined as the ratio of system throughput to total power consumption [47], is an important measure of green communication solutions. The EE of the relay-assisted indoor wireless network at 60 GHz should be investigated. It is also interesting to compare the EE achieved by FD relay systems with its HD counterpart.

The previous research on FD relay systems has focused on improving throughput

[48], or finding the rate gain region (the rate gain region is defined as the region where one relay mode outperforms another mode in terms of throughput) with specific self-interference mitigation technique [49]. The EEs of FD and HD relay systems have not been investigated. A power consumption model was presented in [50] for HD relay-assisted 60 GHz systems. It did not consider FD mode nor static circuit power, which is actually comparable with the transmission power in indoor environments. The total power consumption mainly includes two parts in indoor environment: PA power and circuit power. The circuit power consumption modelled in [51] is oversimplified and inaccurate due to lack of power consumption details. The circuit power modelled in [52] contains various power consumption sources including DAC, mixer, LNA, ADC, etc. However, the circuit power was assumed to be fixed, neglecting the fact that part of the circuit power is dependent on the throughput state. On the other hand, R. Bolla et al. [47] explored various perspectives of power consumption and energy saving operations, such as dynamic adaptation and sleeping/standby. In [53] and [54], the EE of direct transmission (without relay) was investigated. In [53], the EE was investigated for OFDMA networks. Li et al. [54] presented multiple transmission schemes to minimise energy consumption for wireless video transmission. [55] and [56] presented the analysis of the EE of HD relay systems. [55] showed how HD relays should be positioned to outperform direct transmission in terms of EE. In [56], a multipath routing algorithm was presented for an HD relay system, where only the transmission power is included into the power consumption model. There lacks an analysis of the EE of FD relay systems in the literature.

In this chapter, we provide a comprehensive EE analysis for a dual-hop FD AF relay-assisted OFDM system, which is one of the most important application scenario for FD wireless communication systems. Our work is different in the following aspects.

- To the best of our knowledge, this is the first work to investigate the EE of the FD relay systems and to compare it with its HD relay counterpart. It is shown that with given transmission power at the source, the FD relay systems can be more energy efficient than the HD relay systems.

- The EE gain regions between FD (PSAC), FD (PS) and HD, where one relay mode outperforms another mode in terms of EE, are clearly defined. It is shown that FD with two-stage SIC (PSAC) can be even more energy efficient than FD with one-stage interference cancellation (PS only) as well as HD, if the transmission power is relatively high and satisfies certain conditions. This enables opportunistic relay mode selection among FD (PSAC), FD (PS) and HD to optimise the EE under a maximum transmission power constraint. A low complexity algorithm is proposed to optimise the EE.

- A full range of power consumption sources is considered in our power consumption

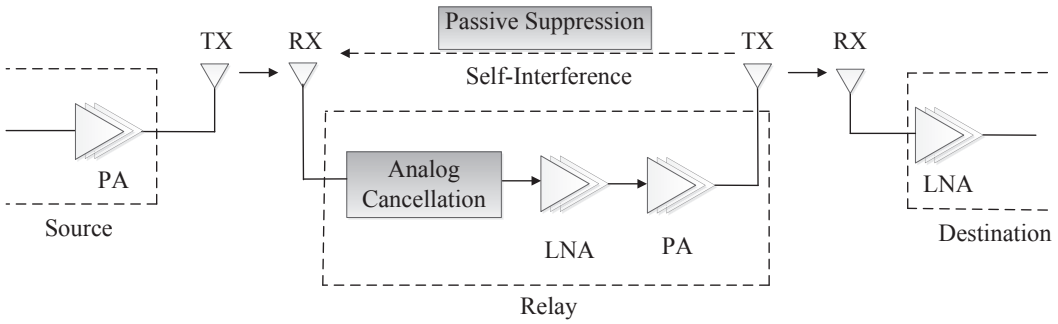

Figure 4.1: Block diagram of a simplified FD AF relay-assisted system.

model and their effects on EE are discussed. In particular, the powers consumed by the relay node and SIC are considered, which were absent from the previous work on power consumption modelling. The impact of imperfect SIC is also considered in our analysis.

4.1 System Model and Problem Formulation for Full Duplex Amplify-and-Forward Relay Systems

Assume a 3-node dual-hop AF relay system. AF relay mode is employed because it requires relatively simple signal processing and low operational power [57]. The block diagram of the FD AF relay-assisted system is illustrated in Fig. 4.1, where PAs are employed at the transmitters of the source and the relay, while cascaded LNAs are placed at the receivers of relay and the destination. It is assumed that the destination cannot hear the source directly due to high attenuation at 60 GHz [25] [33], and the relay is positioned in the middle of the source-destination link to maintain a high throughput [58]. The relay in FD mode transmits and receives at the same time and frequency, causing self-interference to the receiver from its transmitter. To reduce the self-interference, PS and AC are applied, as shown in Fig. 4.1. DC is not considered in this model due to high complexity and performance limitations (PS and AC only can be sufficiently effective for AF FD relay systems [59]). Let α denote the total amount of SIC on each subcarrier, which is defined as the ratio of the self-interference powers before and after suppression/cancellation. PS includes directional antenna and antenna shielding. An absorptive shielding (or absorber) between the relay's transmit antenna and receive antenna can block self-interference by around 10 dB in addition to directional antenna [42]. Let α_{PS} denote the total amount of self-interference cancelled by PS. The AC circuit design in [16] is adopted due to its simple implementation and no requirement for baseband signal at relay node. Its SIC amount is denoted by α_{AC}.

With a frequency-selective fading channel, the channel frequency response and the

allocated power are different across subcarriers. Ideally, the self-interference mitigation should be operated subcarrier by subcarrier. However, it is impossible for PS and also imposes extremely high complexity for AC. Therefore, for both PS and AC, SIC is frequency-flat cancellation practically: the SIC amount α is identical across all subcarriers. Thus, $\alpha = \alpha_{PS}$ in FD (PS) and $\alpha = \alpha_{PS} + \alpha_{AC}$ in FD (PSAC). In general, α_{PS} = 40 dB or more can be achieved by PS alone, and α_{AC} = 20$\sim$40 dB [43] [16].

OFDM transmission is assumed with N subcarriers. Let $h_{SR,n}$, $h_{RD,n}$ and $h_{RR,n}$ denote the channel frequency responses of links source-to-relay (S-R), relay-to-destination (R-D) and relay-to-relay (R-R) on subcarrier n, respectively. Also let l_{SR}, l_{RD} and l_{RR} denote the PLs of links S-R, R-D and R-R, respectively. The channels of the S-R and R-D links are modelled as Rician fading. It is widely used for 60 GHz channel modelling [36] [29], especially with directional antenna and beamforming, which are essential for 60 GHz frequency band to combat high PL. The Saleh-Valenzuela (S-V) model is similar to the Rician model if the direct link is not blocked and its strength is relatively high compared to other non-direct components [8]. The self-interference channel is modelled as Rayleigh fading as the LOS between the transmitter and the receiver of the relay can be easily blocked by antenna shielding due to very small wavelength at 60 GHz. Applying narrow beamwidth antenna also reduces the LOS signal strength between relay's transmitter and receiver due to the main lobe of the relay's directional transmit antenna pointing to the destination. The self-interference waves are collected from the reflected waves [8].

Assume that the PAs have equal power gain of β, and the LNAs have the same gain G and noise figure F each [50]. Let $s_n[k]$ denote the transmitted signal at the source on subcarrier n in time slot k, and $P_{s,n}$ is the allocated transmission power at the source. Similarly, define $t_n[k]$ as the transmitted signal at the relay on subcarrier n in time slot k. $z_{R,n}[k]$ and $z_{D,n}[k]$ denote complex additive white Gaussian noise (AWGN) elements on subcarrier n introduced at the relay and destination, respectively, with zero mean and variance σ^2.

With residual self-interference, the received signal at the relay node on subcarrier n in time slot k is expressed as:

$$r_n[k] = h_{SR,n}\sqrt{l_{SR}P_{s,n}}s_n[k] + h_{RR,n}\sqrt{\frac{1}{\alpha}}t_n[k-\tau] + z_{R,n}[k], \tag{4.1}$$

where τ (≥ 1) is the integer symbol processing delay, which is typically long enough to guarantee that the symbol transmitted at the relay is uncorrelated with the symbol received simultaneously [60]. The signal received at the relay passes through cascaded LNAs and PA. Thus, the transmitted signal $t_n[k]$ from the relay is given by

$$t_n[k] = \sqrt{\beta G}\Big(h_{SR,n}\sqrt{l_{SR}P_{s,n}}s_n[k] + h_{RR,n}\sqrt{\frac{1}{\alpha}}t_n[k-\tau] + \sqrt{F}z_{R,n}[k]\Big). \tag{4.2}$$

At the destination, the received signal is processed by LNAs again and is collected

as

$$\begin{aligned} y_n[k] =& h_{RD,n}\sqrt{\beta G^2 l_{RD}}\Big(h_{SR,n}\sqrt{l_{SR}P_{s,n}}s_n[k] + h_{RR,n}\sqrt{\frac{1}{\alpha}}t_n[k-\tau] + \sqrt{F^2}z_{R,n}[k]\Big) \\ &+ \sqrt{GF}z_{D,n}[k]. \end{aligned} \tag{4.3}$$

EE (bits/Joule) is calculated as the ratio of the system throughput to the total power consumption. In conventional cellular networks, circuit power dominates the power consumption and the consumed transmission power is negligible. As illustrated in [61], the circuit power of base station is dominant and could be up to 3700 W in a macro-cellular network. Thus, its EE can be approximated by $\eta = \frac{T}{P_{c,sta}+\varepsilon T+\xi P_{AC}}$. Higher EE is pursued by setting the transmission power as high as possible to achieve a high throughput. In 60 GHz indoor systems, however, higher throughput may lead to lower EE due to enhanced transmission power, which cannot be neglected in total power consumption.

Our objective is to optimise the instantaneous EE η, i.e.

$$\begin{aligned} &\underset{P_s}{\operatorname{argmax}}\ \frac{T}{P} \\ &s.t \quad P_s \le P_{max}. \end{aligned} \tag{4.4}$$

Now we discuss how to optimise EE by transmission power adaptation at source under a maximum transmission power constraint. Then the EE gain regions between FD (PSAC), FD (PS) and HD relay modes are researched. With opportunistic relay mode selection and transmission power adaptation, EE is maximised. Some parametric effects on EE gain regions are discussed as well.

4.2 Throughput and Power Consumption Analysis

4.2.1 Throughput Analysis

The received signal at the destination is rewritten as

$$\begin{aligned} y_n[k] =& \underbrace{h_{RD,n}\sqrt{\beta G^2 l_{RD}}h_{SR,n}\sqrt{l_{SR}P_{s,n}}s_n[k]}_{\text{desired signal}} + \underbrace{h_{RD,n}\sqrt{\beta G^2 l_{RD}}h_{RR,n}\sqrt{\frac{1}{\alpha}}t_n[k-\tau]}_{\text{self-interference}} \\ &+ \underbrace{h_{RD,n}\sqrt{\beta G^2 l_{RD}}\sqrt{F^2}z_{R,n}[k] + \sqrt{GF}z_{D,n}[k]}_{\text{equivalent noise}}, \end{aligned} \tag{4.5}$$

where the equivalent noise consists of the noise introduced at the relay and destination. Let Γ_n denote the signal-to-interference-and-noise ratio (SINR) on subcarrier n at the destination. Define $g_{1,n} = \beta G^2 |h_{SR,n}|^2 l_{SR} |h_{RD,n}|^2 l_{RD}$, $g_{2,n} = GF + \beta G^2 F^2 |h_{RD,n}|^2 l_{RD}$,

$g_{3,n} = \beta^2 G^3 F^3 |h_{RD,n}|^2 l_{RD} |h_{RR,n}|^2$ and $g_{4,n} = \beta^2 G^3 |h_{SR,n}|^2 l_{SR} |h_{RD,n}|^2 l_{RD} |h_{RR,n}|^2$. According to (4.5), the SINR on subcarrier n at the destination with FD relay can be derived as

$$\Gamma_{FD,n} = \frac{g_{1,n} P_{s,n}}{g_{2,n}\sigma^2 + P_{I,n}/\alpha}, \tag{4.6}$$

where $P_{I,n} = g_{3,n}\sigma^2 + g_{4,n} P_{s,n}$ represents the power of the self-interference, $g_{2,n}\sigma^2$ is the power of the equivalent noise and $g_{1,n} P_{s,n}$ is the power of the desired signal. Unlike [49] which assumed a bidirectional P-to-P FD system, in our system model, the noise introduced at the relay node and the residual self-interference after cancellation are forwarded to the destination, which can be observed from (4.5) and (4.6). The overall throughput of FD is given by

$$T_{FD} = \sum_{n=1}^{N} \frac{W}{N} \log_2(1 + \Gamma_{FD,n}), \tag{4.7}$$

where W denotes the total bandwidth while N denotes number of subcarriers. For HD relay transmission, the SINR $\Gamma_{HD,n}$ is calculated by setting the self-interference related elements in (4.6) to 0 and 1/2 is added before the log function in (4.7).

To outperform HD in terms of throughput on subcarrier n, the following equation should be satisfied by FD:

$$\frac{W}{N} \log_2(1 + \Gamma_{FD,n}) > \frac{W}{2N} \log_2(1 + \Gamma_{HD,n}). \tag{4.8}$$

Substituting (4.6) into (4.8) yields

$$\alpha > \frac{g_{3,n} p_{s,n} + g_{4,n}\sigma^2}{\sqrt{(g_{1,n} p_{s,n} + g_{2,n}\sigma^2)(g_{2,n}\sigma^2)}}. \tag{4.9}$$

Equation (4.9) indicates that the required SIC amount making FD outperform HD in terms of throughput on subcarrier n. It is obvious that a higher cancellation amount can satisfy (4.9) more easily. To increase the SIC amount, many cancellation schemes have been proposed [3] [16] [42] [43] [44]. With proper SIC design, the power of self-interference can be lower or even negligible compared to noise power. As shown from (4.9), higher power gain β at amplifier requires more SIC amount α at relay node. It is because improving power gain can improve the SINR at the second hop R-D, but corrupt the SINR at the first hop S-R. The effect of amplifier power gain β on the first hop is much more significant than its effect on the second hop because the distance between relay's transmitter and receiver is much shorter than the distance between relay's transmitter and destination's receiver. Therefore, higher SIC amount α is required for a higher value of β. Also, LNAs at relay are placed at the front-end of relay's receiver. Normally, the effect of noise from subsequent stages (e.g. noise introduced at the destination) is reduced by the gain of the relay's LNAs in a dual-hop network. Therefore, high gain LNA is preferred at the relay (the noise figure is

considered almost irrelevant to the power gain of LNA by good LNA design). However, the boosted signal by LNA is treated as self-interference to the relay's receiver when it is transmitted to the destination. Therefore, higher SIC amount α is needed to compensate for the effect of a higher valued G due to the enhanced self-interference, as can be seen from (4.9).

4.2.2 Power Consumption Analysis

Assume continuous data transmission, so that the power consumption is in active mode. The typical power consumption model for short-range or indoor communications is adopted [53], where the total power consumption contains two main parts, circuit power P_c and PA power P_{PA}. The circuit power consumption includes the power consumed by all circuit blocks along the signal path while the PA power is consumed by both source and relay. The power consumption for AC, P_{AC}, is also considered if the relay works in FD mode.

PA Power

The total PA power includes the transmission power and the dissipated power of PAs at both source and relay, given by

$$P_{PA} \approx \sum_{n=1}^{N} \frac{P_{s,n}}{\omega} \left(1 + \beta G |h_{SR,n}|^2 l_{SR}\right), \tag{4.10}$$

where ω is the drain efficiency [5]. The power allocated onto subcarrier n is a portion of the total transmission power P_s, that is, $P_{s,n} = \lambda_n P_s$, where $0 \leq \lambda_n \leq 1$ and $\sum_{n=1}^{N} \lambda_n = 1$. Defining $\tilde{\lambda}_n = \lambda_n \left(1 + \beta G |h_{SR,n}|^2 l_{SR}\right)$, (4.10) can be rewritten as

$$P_{PA} = \left(\frac{P_s}{\omega}\right) \sum_{n=1}^{N} \tilde{\lambda}_n. \tag{4.11}$$

Circuit Power

The circuit power P_c includes the power consumed by all circuit blocks along the signal path. For communication systems working at high data rate, e.g. Gbps, circuit power can be divided into static circuit power, $P_{c,sta}$, and dynamic circuit power, $P_{c,dyn}$ [53]. The former can be formulated as a fixed value [62], while the dynamic circuit power is closely related to the throughput state [63]. A well-accepted model of dynamic circuit power is $P_{c,dyn} = \varepsilon T$, where the constant ε denotes the power consumption per unit data rate [53]. Also, the relay's circuit power is non-negligible in indoor environment. Thus, the total circuit power is given by

$$P_c = P_{c,sta} + \varepsilon T. \tag{4.12}$$

Power for SIC

Applying PS actually does not consume additional power, however, the power consumed by AC is non-negligible. Besides, the power consumed by the involved chip components, such as attenuator and splitter, are not related to the throughput state [44] [16], and therefore the power consumed by AC, P_{AC}, is regarded as a constant. Using (4.11) and (4.12), the total power consumption is formulated as

$$P = \left(\frac{P_s}{\omega}\right) \sum_{n=1}^{N} \tilde{\lambda}_n + \varepsilon T + P_{c,sta} + \xi P_{AC}, \tag{4.13}$$

where $\xi = 1$ for FD (PSAC) relay systems and $\xi = 0$ for FD (PS) relay mode and HD relay mode.

4.3 Transmission Power Adaptation, Energy Efficiency Gain Regions and Opportunistic Relay Mode Selection

4.3.1 Transmission Power Adaptation

Theorem 4.1: In AF FD/HD relay-assisted OFDM systems with good SIC, EE η is strictly quasi-concave or mono-increasing with respect to transmission power $P_s \in (0, P_{max}]$.

Proof of Theorem 4.1: See Appendix A.

According to Theorem 4.1, under a transmission power constraint P_{max}, there is one and only one globally/locally optimal transmission power in terms of EE η, which can be found by calculating the gradient of η in terms of transmission power P_s. A so-called gradient calculation (GC) algorithm is proposed to optimise EE η by adjusting the total transmission power, as shown in Algorithm 1.

The proposed GC algorithm relies on $\frac{\partial \eta}{\partial P_s}$. It is hard to derive a closed-form expression of $\frac{\partial \eta}{\partial P_s}$, however, the definition of derivative can be used to get the value of $\frac{\partial \eta}{\partial P_s}$ at any given transmission power, as shown in Appendix B. With the proposed GC algorithm and feasible calculation of $\frac{\partial \eta}{\partial P_s}$, the globally/locally optimal transmission powers in the region of $P_s \in (0, P_{max}]$ can be found for FD (PSAC), FD (PS) and HD, respectively.

4.3.2 Energy Efficiency Gain Regions and Opportunistic Relay Mode Selection

In the previous subsection, the GC algorithm is proposed to optimise the EEs of FD (PSAC), FD (PS) and HD relay modes, respectively. The three modes may have different optimised EE values due to different throughputs and power consumptions. In this subsection, the EE gain regions between the three relay modes are discussed, which serve opportunistic relay mode selection. It is different from the work in [60] and [64]

Algorithm 1 GC Algorithm for Transmission Power Adaptation

if $\frac{\partial \eta}{\partial P_s}|_{P_{max}} \geq 0$ **then**
  EE is mono-increasing in the range of $P_s \in (0, P_{max}]$.
  return $\eta^* = \eta(P_{max})$.
else
  EE is quasi-concave in the range of $P_s \in (0, P_{max}]$.
  Initialise the left bound $P_L = 0$, and the right bound $P_R = P_{max}$.
  while $|\frac{\partial \eta}{\partial P_s}|_P| < \delta$ (δ is a precision factor) **do**
    $P = \frac{P_L + P_R}{2}$.
    Calculate $a = \frac{\partial \eta}{P_s}\big|_{P_L}$ and $b = \frac{\partial \eta}{P_s}\big|_{P}$.
    if $a \cdot b \geq 0$ **then**
      $P_L = P$.
    else
      $P_R = P$.
    end if
  end while
  return $\eta^* = \eta(P)$.
end if

on opportunistic relay mode selection, which were based on system throughput. Then opportunistic relay mode selection and transmission power adaptation are combined to obtain the maximum system EE.

Substituting (4.7) and (4.13) into (4.4) yields the EE of FD (PSAC) as:

$$\eta_{FD(PSAC)} = \frac{T_{FD(PSAC)}}{\left(\frac{P_s}{\omega}\right)\sum_{n=1}^{N}\tilde{\lambda}_n + \varepsilon T_{FD(PSAC)} + P_{c,sta} + P_{AC}}. \tag{4.14}$$

The EE of FD (PS) is given by

$$\eta_{FD(PS)} = \frac{T_{FD(PS)}}{\left(\frac{P_s}{\omega}\right)\sum_{n=1}^{N}\tilde{\lambda}_n + \varepsilon T_{FD(PS)} + P_{c,sta}}. \tag{4.15}$$

Similarly, the EE of HD is given by

$$\eta_{HD} = \frac{T_{HD}}{\left(\frac{P_s}{\omega}\right)\sum_{n=1}^{N}\tilde{\lambda}_n + \varepsilon T_{HD} + P_{c,sta}}. \tag{4.16}$$

$$P_s^{\dagger,1} = \begin{cases} \dfrac{\omega}{\sum_{n=1}^{N}\tilde{\lambda}_n}\left(\dfrac{P_{AC}}{\frac{T_{FD(PSAC)}}{T_{FD(PS)}} - 1} - P_{c,sta}\right), & \frac{T_{FD(PSAC)}}{T_{FD(PS)}} < \frac{P_{AC}}{P_{c,sta}} + 1 \\ 0, & \frac{T_{FD(PSAC)}}{T_{FD(PS)}} \geq \frac{P_{AC}}{P_{c,sta}} + 1. \end{cases} \tag{4.17}$$

$$P_s^{\dagger,2} = \begin{cases} \dfrac{\omega}{\sum_{n=1}^{N}\tilde{\lambda}_n}\left(\dfrac{P_{AC}}{\frac{T_{FD(PSAC)}}{T_{HD}} - 1} - P_{c,sta}\right), & 1 < \frac{T_{FD(PSAC)}}{T_{HD}} < \frac{P_{AC}}{P_{c,sta}} + 1 \\ 0, & \frac{T_{FD(PSAC)}}{T_{HD}} \geq \frac{P_{AC}}{P_{c,sta}} + 1. \end{cases} \tag{4.18}$$

Similarly to the rate gain region defined in [48], the EE gain region is defined as the region in which one relay mode outperforms another mode in terms of EE. In the following, the EEs of FD (PSAC), FD (PS) and HD relay modes are compared with given transmission power P_s, which is constrained by a maximum transmission power P_{max}. The differences between the EEs of the three relay modes are provided in Appendix C.

FD (PSAC) vs. FD (PS)

It is obvious that the system throughput of FD (PSAC) is always higher than that of FD (PS), i.e. $T_{FD(PS)} < T_{FD(PSAC)}$, at the cost of additional power consumption on AC operation. According to (C.1) in Appendix C, if the value of $(\frac{P_s}{\omega}\sum_{n=1}^{N}\tilde{\lambda}_n + P_{c,sta})(\frac{T_{FD(PSAC)}}{T_{FD(PS)}} - 1) < P_{AC}$, then $\eta_{FD(PSAC)} - \eta_{FD(PS)} < 0$, i.e. FD (PS) is more energy efficient than FD (PSAC). If the transmission power P_s keeps increasing, the value of $\left(\frac{P_s}{\omega}\sum_{n=1}^{N}\tilde{\lambda}_n + P_{c,sta}\right)\cdot\left(\frac{T_{FD(PSAC)}}{T_{FD(PS)}} - 1\right)$ may exceed the value of P_{AC}, leading to $\eta_{FD(PSAC)} - \eta_{FD(PS)} > 0$. This implies that FD (PSAC) becomes more energy efficient than FD (PS) when the transmission power is higher than a crossing power $P_s^{\dagger,1}$, which is calculated as (4.17).

Remark 4.1: Under a maximum transmission power constraint P_{max}, any transmission power P_s in the range of $P_s \in (P_s^{\dagger,1}, P_{max}]$ enables FD (PSAC) to outperform FD (PS) in terms of EE.

By considering (4.17) and Remark 4.1 together, the EE gain region for FD (PSAC) outperforming FD (PS) is given as $P_s \in (P_s^{\dagger,1}, P_{max}]$, and the EE gain region for FD (PS) outperforming FD (PSAC) is $P_s \in (0, P_s^{\dagger,1})$. If $P_{max} < P_s^{\dagger,1}$, FD (PS) is always more energy efficient than FD (PSAC) in the range of $P_s \in (0, P_{max}]$.

FD (PSAC) vs. HD

According to (C.2) in Appendix C, the sign of $\eta_{FD(PSAC)} - \eta_{HD}$ is the same as the sign of $\left(\frac{P_s}{\omega}\sum_{n=1}^{N}\tilde{\lambda}_n + P_{c,sta}\right)\left(\frac{T_{FD(PSAC)}}{T_{HD}} - 1\right) - P_{AC}$. If $T_{HD} \geq T_{FD(PSAC)}$ holds within the feasible range of $P_s \in (0, P_{max}]$, $\eta_{FD(PSAC)} < \eta_{HD}$ is readily derived. If $T_{HD} < T_{FD(PSAC)}$, which occurs commonly, the value of $(\frac{P_s}{\omega}\sum_{n=1}^{N}\tilde{\lambda}_n + P_{c,sta})(\frac{T_{FD(PSAC)}}{T_{HD}} - 1)$ may be smaller than that of P_{AC}. Thus, the crossing transmission power for FD (PSAC) outperforming HD is calculated as (4.18).

Remark 4.2: Under a maximum transmission power constraint P_{max}, any transmission power P_s in the range of $P_s \in (P_s^{\dagger,2}, P_{max}]$ enables FD (PSAC) to outperform HD in terms of EE.

By considering (4.18) and Remark 4.2 together, the EE gain region for FD (PSAC) outperforming HD is given by $P_s \in (P_s^{\dagger,2}, P_{max}]$, and the EE gain region for HD outperforming FD (PSAC) is $P_s \in (0, P_s^{\dagger,2})$. If $P_{max} < P_s^{\dagger,2}$, HD is always more energy efficient than FD (PSAC) in the range $P_s \in (0, P_{max}]$.

Specially, with near-perfect SIC, the throughput of FD (PSAC) approximately doubles that of HD, i.e. $T_{FD(PSAC)} \approx 2T_{HD}$ [59]. Hence, (4.18) reduces to

$$P_s^{\dagger,2} = \frac{\omega}{\sum_{n=1}^{N} \tilde{\lambda}_n} \left(P_{AC} - P_{c,sta}\right). \tag{4.19}$$

In general, the power consumed by AC is lower than the static circuit power consumption by proper design of the AC circuit. That is, $P_{AC} < P_{c,sta}$ [4][16] and $P_s^{\dagger,2} = 0$. Thus, Remark 4.3 is derived.

Remark 4.3: With near-perfect SIC at the relay and $T_{FD(PSAC)} \approx 2T_{HD}$, FD (PSAC) outperforms HD in terms of EE, given any transmission power P_s in the range of $P_s \in (0, P_{max}]$.

FD (PS) vs. HD

According to (C.4) in Appendix C, FD (PS) outperforms HD in terms of EE if $T_{FD(PS)} > T_{HD}$. By (4.17) and (4.18), $T_{FD(PS)} > T_{HD}$ is readily obtained if $P_s^{\dagger,1} > P_s^{\dagger,2}$ holds.

The EE gain regions and the corresponding conditions analysed above are summarised in Tab. 4.1. It provides clear guidance on opportunistic relay selection, that is, the relay mode achieving the highest EE is selected given transmission power and channel gains. The combination of opportunistic relay mode selection and transmission power adaptation is described in Algorithm 2.

Algorithm 2 EE Optimisation with Opportunistic Relay Mode Selection and Transmission Power Adaptation

Calculate $T_{FD(PSAC)}, T_{FD(PS)}$ and T_{HD} with transmission power $P_s = P_{max}$.
if $T_{HD} > T_{FD(PSAC)}$ **then**
  Call the GC algorithm for HD.
  return $\eta^* = \eta^*_{FD(HD)}$.
else
  Calculate $P_s^{\dagger,1}$ and $P_s^{\dagger,2}$ according to (4.17) and (5.13), respectively.
  In case: $P_{max} > P_s^{\dagger,1} > P_s^{\dagger,2}$
    Call the GC algorithm for FD (PSAC) and FD (PS).
    Return $\eta^* = max\{\eta^*_{FD(PSAC)}, \eta^*_{FD(PS)}\}$.
  In case: $P_s^{\dagger,2} > P_s^{\dagger,1} > P_{max}$ or $P_s^{\dagger,2} > P_{max} > P_s^{\dagger,1}$
    Call the GC algorithm for HD only.
    Return $\eta^* = \eta^*_{HD}$.
  In case: $P_{max} > P_s^{\dagger,2} > P_s^{\dagger,1}$
    Call the GC algorithm for FD (PSAC) and HD.
    Return $\eta^* = max\{\eta^*_{FD(PSAC)}, \eta^*_{HD}\}$.
  In case: $P_s^{\dagger,1} > P_{max} > P_s^{\dagger,2}$ or $P_s^{\dagger,1} > P_s^{\dagger,2} > P_{max}$
    Call the GC algorithm for FD (PS) only.
    Return $\eta^* = \eta^*_{FD(PS)}$.
end if

Table 4.1: Summary of EE Gain Regions and the Corresponding Conditions

	EE Comparison	Conditions
Case 1	$\eta_{HD} < \eta_{FD(PS)} < \eta_{FD(PSAC)}$	$P_s^{\dagger,2} < P_s^{\dagger,1}$ and $P_s \in (P_s^{\dagger,1}, P_{max}]$
Case 2	$\eta_{HD} < \eta_{FD(PSAC)} < \eta_{FD(PS)}$	$P_s^{\dagger,2} < P_s^{\dagger,1}$ and $P_s \in (P_s^{\dagger,2}, min\{P_s^{\dagger,1}, P_{max}\})$
Case 3	$\eta_{FD(PS)} < \eta_{HD} < \eta_{FD(PSAC)}$	$P_s^{\dagger,1} < P_s^{\dagger,2}$ and $P_s \in (P_s^{\dagger,2}, P_{max}]$
Case 4	$\eta_{FD(PS)} < \eta_{FD(PSAC)} < \eta_{HD}$	$P_s^{\dagger,1} < P_s^{\dagger,2}$ and $P_s \in (P_s^{\dagger,1}, min\{P_s^{\dagger,2}, P_{max}\})$
Case 5	$\eta_{FD(PSAC)} < \eta_{FD(PS)} < \eta_{HD}$	$P_s^{\dagger,1} < P_s^{\dagger,2}$ and $P_s \in (0, P_s^{\dagger,1})$
Case 6	$\eta_{FD(PSAC)} < \eta_{HD} < \eta_{FD(PS)}$	$P_s^{\dagger,2} < P_s^{\dagger,1}$ and $P_s \in (0, P_s^{\dagger,2})$

4.4 Parametric Effects on Energy Efficiency Gain Regions

4.4.1 Impact of Drain Efficiency on the Energy Efficiency Gain Regions

At 60 GHz, a maximum PA drain efficiency of $\omega = 25\%$ can be achieved [5], which is lower than the drain efficiency at a lower frequency, e.g. $\omega = 50\%$ at 2.4 GHz. According to Lemmas 1 and 2, low drain efficiency ω results in $P_s^{\dagger,1}$ and $P_s^{\dagger,2}$ approaching 0. Also, a higher static circuit power is required for 60 GHz than a lower frequency [4]. If the circuit static power is so large that $P_{c,sta} > \frac{P_{AC}}{T_{FD(PSAC)}/T_{FD(PS),HD}-1}$, $P_s^{\dagger,1} = 0$ or $P_s^{\dagger,2} = 0$ is obtained, which means that the static circuit power dominates the total power consumption, and that FD (PSAC) outperforms FD (PS) or HD in terms of EE with any transmission power. Therefore, a conclusion is drawn:

Remark 4.4: Low PA drain efficiency or high static circuit power enables a large range of transmission power, over which FD (PSAC) relay systems achieve a higher EE than FD (PS) or HD relay systems.

4.4.2 Impact of the Self-Interference Cancellation Amount of Passive Suppression on the Energy Efficiency Gain Regions

Existing PS schemes do not consume additional power. Therefore, improving its SIC amount α_{PS} can improve the EEs of both FD (PS) and FD (PSAC). For the cancellation operation at the second stage, generally, better AC performance needs more accurate and complex circuit design, which consumes higher power P_{AC} and could reduce the EE of FD (PSAC) over FD (PS). By proper design, such as effective antenna shielding or highly directional antenna, the performance of PS could be sufficient enough [42]. In this case, applying AC does not improve the throughput significantly as the residual self-interference after PS is already little. Thus, Remark 4.5 is obtained:

Remark 4.5: If the SIC amount of PS is sufficient, applying additional AC may reduce EE.

Table 4.2: Simulation Setup

Central carrier frequency f_c	60 GHz
Bandwidth W	2640 MHz
Number of subcarriers	512
AWGN power spectral density	-174 dBm/Hz
Distance between source and relay	5 m
Distance between relay and destination	5 m
Distance between source and destination	10 m
Power gain of each LNA G	10.5 dB
Noise figure of each LNA F	5.5 dB
Number of cascaded LNAs at relay and destination	3
Power gain of PA	16 dB
PL exponent θ	3
The ratio of LOS to NLOS for Rician channel	10 dB
Static power consumption $P_{c,sta}$	200 mW
Dynamic circuit factor ε	50 mW/Gbps
Drain efficiency of PA ω	25%
Cancellation amount α	α_{PS} = 40 dB, α_{AC} = 20 dB
Analogue SIC power P_{AC}	50 mW
Linear gains of all antennas	10 dBi

4.5 Numerical Results

Numerical results are used to verify our analysis. The simulation setup [9] [50] is shown in Tab. 4.2. The PL model measured in [9] is adopted, as $l = 68 + 10\theta log_{10}(d/d_0)$, where θ is the PL exponent, d is the distance between two nodes, and d_0 is reference distance, which is normally set to 1 m in indoor environment. The total SIC amounts of FD (PSAC), FD (PS) are set to $\alpha = 60$ dB and 40 dB, respectively, which are within the reasonable range of cancellation amount as discussed.

Fig. 4.2 demonstrates the average system throughput achieved with different transmission powers. The throughputs achieved by two FDs are much higher than the throughput achieved by the HD relay systems. With a transmission power of 40 mW, the throughputs achieved by FD (with perfect interference cancellation), FD (PSAC, $\alpha = 60$ dB), FD (PS, $\alpha = 40$ dB), and HD are approximately 1.92 Gbps, 1.9 Gbps, 1.3 Gbps and 0.96 Gbps, respectively. As expected, with good interference cancellation, FD (PSAC) achieves a throughput that is approximately twice as high as that of HD. The ratio between the throughputs of FD (PSAC) and FD (PS) is around 1.4.

Fig. 4.3 shows the average optimal EE performances of FD (PSAC, $\alpha = 60$ dB), FD (PS, $\alpha = 40$ dB) and HD under the proposed GC algorithm with given maximum transmission power constraint P_{max}. With given transmission power which is under the maximum transmission power constraint of $P_{max} > 12$ mW, FD (PSAC) achieves the highest optimised EE among the three relay modes, while FD (PS) is the most energy efficient if $P_{max} \leq 12$ mW. By applying the GC algorithm and opportunistic relay mode selection together, the optimised EE by FD relay can be up to 1.4 Gb/Joule higher

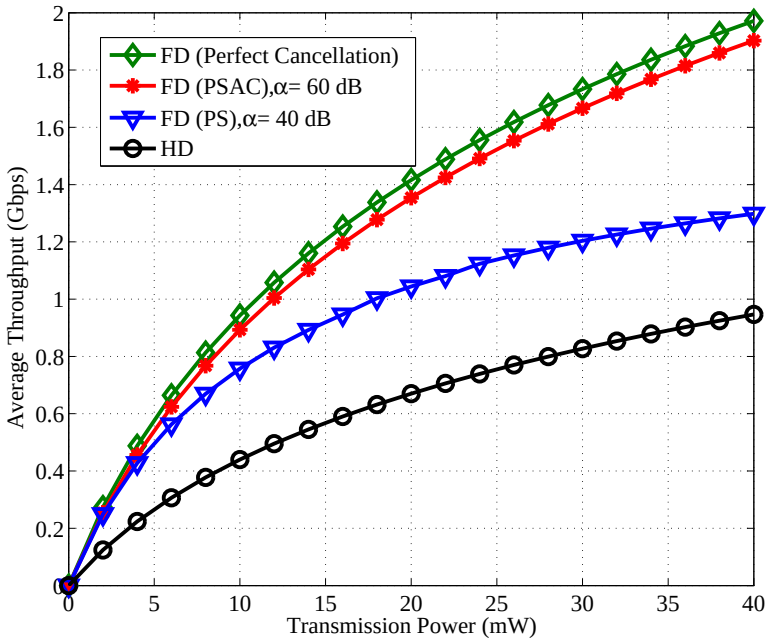

Figure 4.2: The average throughputs of the FD (with perfect interference cancellation), FD (PSAC, $\alpha = 60$ dB), FD (PS, $\alpha = 40$ dB) and HD relay systems.

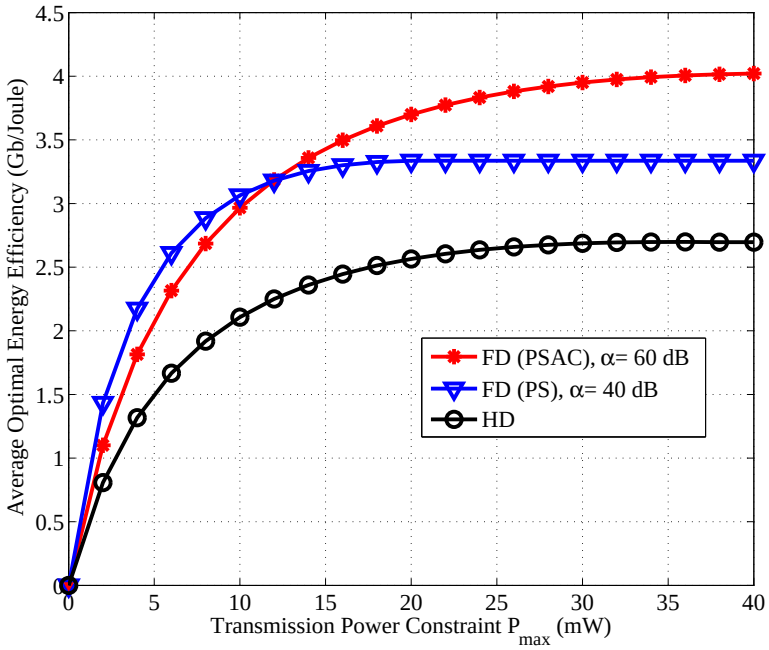

Figure 4.3: Average optimal EE performances of FD (PSAC, $\alpha = 60$ dB), FD (PS, $\alpha = 40$ dB) and HD relay systems.

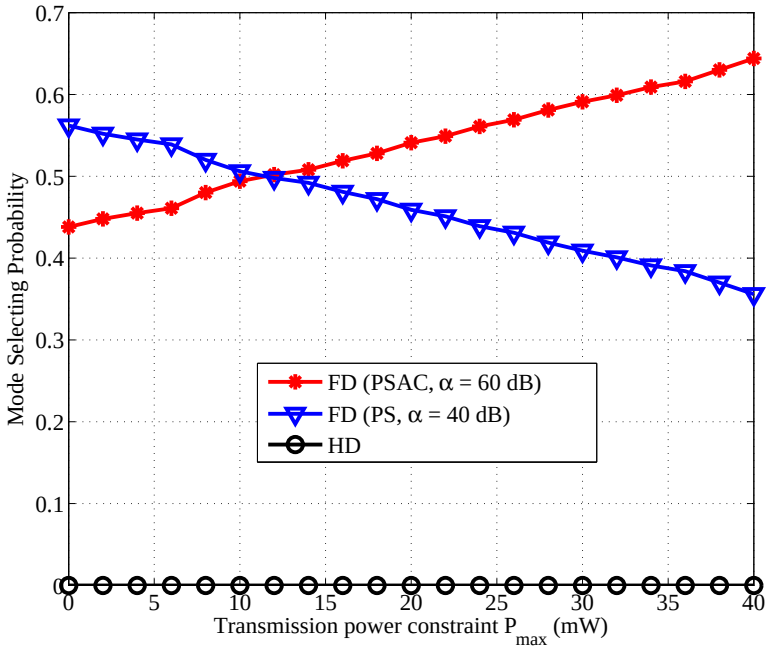

Figure 4.4: Probabilities of selecting FD (PSAC, $\alpha = 60$ dB), FD (PS, $\alpha = 40$ dB) and HD relay systems.

than that of HD relay. Also, FD (PSAC, $\alpha = 60$ dB) demonstrates higher average EE than HD across all transmission powers, which verifies the special case in Remark 1. Besides, the value of the average optimal EE of FD (PSAC) is mono-increasing under the transmission power constraint P_{max}, because its EE is a mono-increasing function of the transmission power under the P_{max} constraint. While the EE of FD (PS) is strictly quasi-concave within the given range of transmission power. Therefore, its average optimal EE is unchanged when P_{max} is higher than 22 mW.

Fig. 4.4 shows the probabilities of selecting FD (PSAC, $\alpha = 60$ dB), FD (PS, $\alpha = 40$ dB) and HD, respectively, by applying Algorithm 2. The result is consistent with the result in Fig. (4.3), that is, FD (PS) is preferable with a relatively low transmission power constraint P_{max}, while FD (PSAC) is preferable with a relatively high P_{max}, in terms of the optimised EE. When P_{max} is low, the critical transmission power $P_s^{\dagger,1}$ in (4.17) easily exceeds P_{max}. Thus, FD (PS) easily outperforms FD (PSAC) in terms of the optimised EE by the GC algorithm. With the increase of P_{max}, the probability of $P_s^{\dagger,1} < P_{max}$ becomes higher, implying that FD (PSAC) has a higher chance of achieving a higher EE than FD (PS) does. Also, the probability of selecting HD is 0 across all values of P_{max}, showing that FD relay is always more energy efficient than HD relay with the simulation setup.

Fig. 4.5 shows the effect of SIC by PS on the probabilities of selecting among the FD (PSAC), FD (PS) and HD modes, by using Algorithm 2. The amount of self-

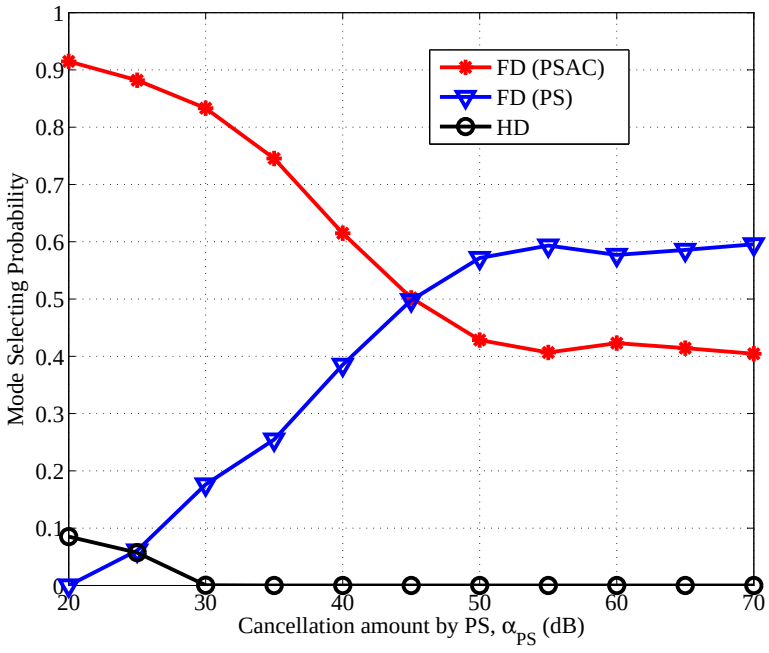

Figure 4.5: Probabilities of selecting FD (PSAC), FD (PS) and HD, with the amount of self-interference cancelled by AC $\alpha_{AC} = 20$ dB and the transmission power $P_s = 20$ mW.

interference cancelled by PS, α_{PS}, varies from 20∼70 dB, as the performance of PS is sensitive to nearby environment, while the amount of SIC by AC is set to $\alpha_{AC} = 20$ dB. With the increase of the value of α_{PS}, FD (PS) has a higher chance of achieving a higher optimal EE than FD (PSAC) and HD. In this case, applying AC leads to the decrease of EE, which verifies Remark 3. Only with $\alpha_{PS} < 30$ dB, which occurs rarely [42], HD mode may be selected with a probability of up to 10%, due to highest EE achievable. This is because the throughput of HD is higher than those of FD (PS) and FD (PSAC), or the throughput of HD is lower than that of FD (PSAC) while the crossing transmission power $P_s^{\dagger,2}$ is not achievable under the P_{max} constraint.

Fig. 4.6 shows the EEs of FDs and HD with drain efficiency set to $\omega = 25\%$ and 15%, respectively. It is obvious that lower drain efficiency results in lower EEs for all modes. The maximum EE reduction is 1 Gb/Joule when the drain efficiency decreases from 25% to 15%. This is because lower drain efficiency leads to more power being dissipated by PAs. Besides, it can be seen that lower drain efficiency makes FD (PSAC) outperform FD (PS) more easily. With ω=25%, FD (PSAC) outperforms FD (PS) when the transmission power is beyond a threshold of 12 mW, while it is 8 mW with ω=15%. This confirms our finding in Remark 4.4. High static circuit power has similar effects on EE to low drain efficiency. The results are not shown due to space limit.

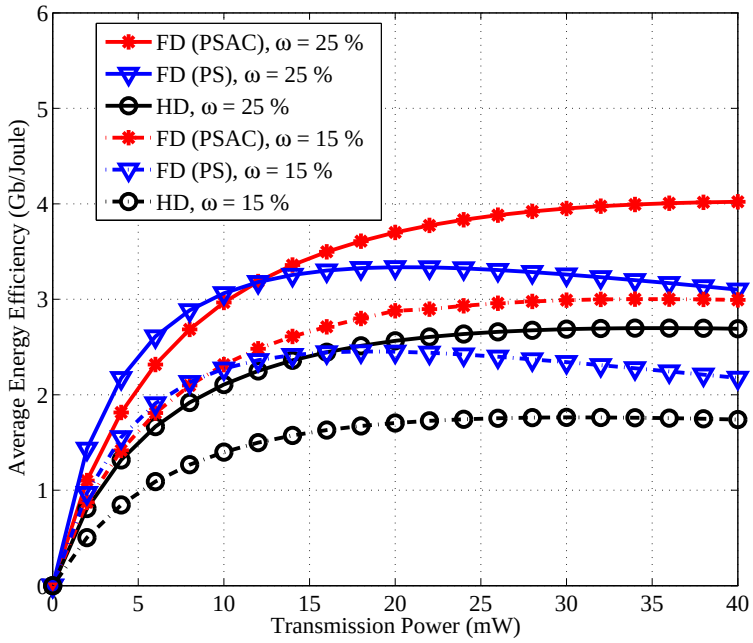

Figure 4.6: EE performances of FD (PSAC) and FD (PS), with drain efficiency ω = 25% and 15%.

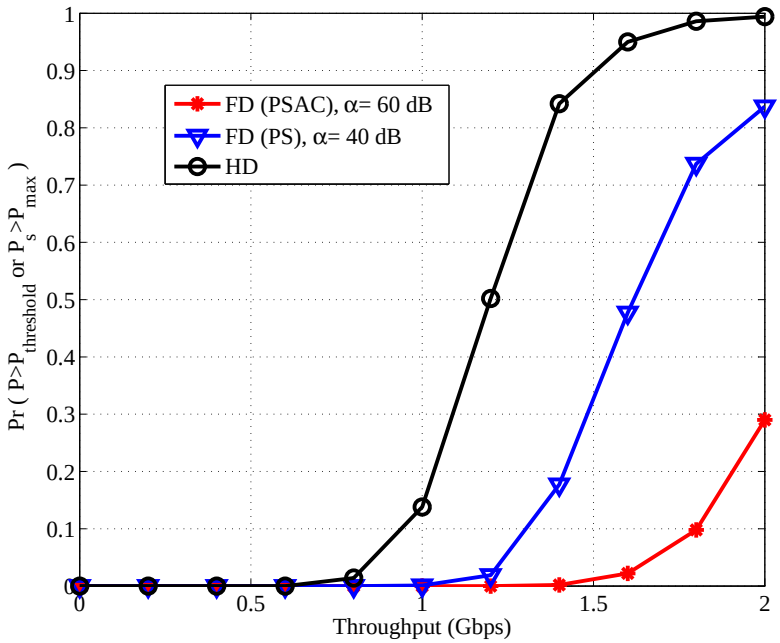

Figure 4.7: Outage probabilities of FD (PSAC, α= 60 dB), FD (PS, α= 40 dB) and HD, with total power threshold $P_{threshold}$= 500 mW and transmission power constraint P_{max}= 40 mW.

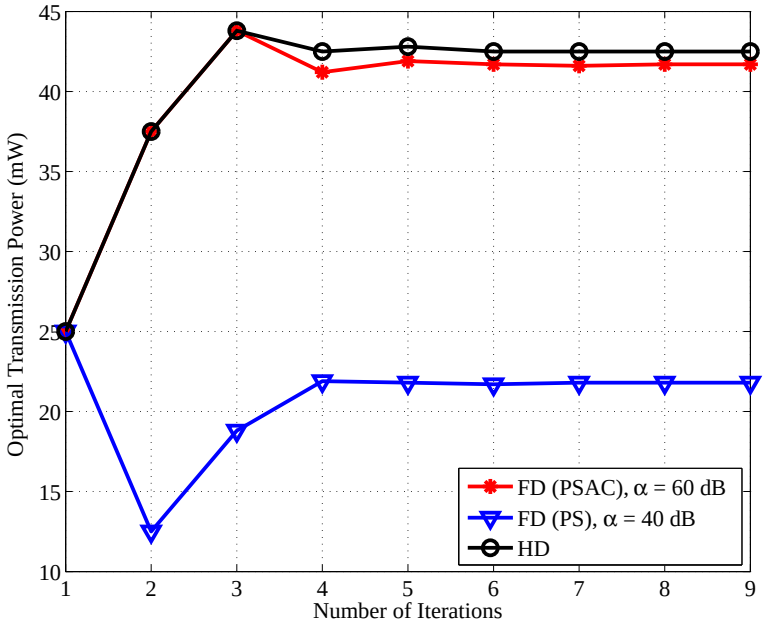

Figure 4.8: Convergence behaviours of the proposed GC algorithm for FD (PSAC, α = 60 dB), FD (PS, α = 40 dB) and HD, with maximum transmission power P_{max} = 100 mW.

Fig. 4.7 shows the outage probabilities that the total power consumption exceeds a threshold $P_{threshold}$= 500 mW or the transmission power exceeds an upper limit P_{max}= 40 mW. When the throughput is lower than 0.6 Gbps, the outage probabilities of all three relay modes are 0, implying that low throughput can be easily achieved by all three relay modes, with low carbon footprint. With the increase of the throughput, the outage probability of HD boosts fast, because HD needs much higher transmission power to pursue high throughput. Therefore, its transmission power or total power consumption easily exceeds the threshold. In particular, for a throughput higher than 1.8 Gbps, the outage probability of HD is nearly 1, implying that HD requires much higher transmission power and total power to achieve a high throughput. For FD (PSAC, α= 60 dB) and FD (PS, α= 40 dB), however, the outage probabilities are lower, which are only 0.1 and 0.75 at 1.8 Gbps, respectively. This confirms that FD relay is a greener solution for higher speed communication, with more carbon footprint savings.

Fig. 4.8 shows the convergence behaviours of FD (PSAC), FD (PS) and HD by the GC algorithm under the maximum transmission power constraint P_{max} = 100 mW. Only around 6 iterations are needed in all three cases to achieve the steady states. The optimal transmission power corresponding to the maximised EE is around 42 mW for FD (PSAC) and 43 mW for HD , while it is only around 22 mW for FD (PS). It is because the optimal transmission power is around the value that makes the sum

of the PA power and dynamic circuit power comparable with the static circuit power. FD (PSAC) consumes the highest circuit power among three relay modes, therefore its optimal transmission power needs to be high enough to compensate for the highest circuit power. For HD, its optimal transmission power is also high due to its low achievable throughput resulting in a low dynamic circuit power. Note that if P_{max} is relatively small, e.g. $P_{max} \leq 40$ mW, the EEs may be mono-increasing in the range of $P_s \in (0, P_{max}]$ as analysed in Theorem 4.1. In this case, the transmission power corresponding to the maximum EE is simply equal to P_{max}, and no iteration is needed.

4.6 Summary

In this chapter, with a full range of power consumption sources considered, the EE gain regions of FD (PSAC), FD (PS) and HD relay modes have been compared in dual-hop OFDM systems at 60 GHz. It is found that FD (PS) can outperform HD in terms of EE, while FD (PSAC) is even more energy efficient than FD (PS) if the transmission power is higher than a threshold in the feasible range. It is proved that EE is strictly quasi-concave or mono-increasing with respect to the transmission power under a maximum transmission power constraint. A low-complexity algorithm is proposed to optimise EE by calculating the gradient of EE with respect to the transmission power. Based on the EE optimization and opportunistic relay mode selection, the average optimal EE of FD relay is up to 1.4 Gb/Joule higher than that of HD relay with given transmission power. It is shown that with the same transmission power, the throughput achieved by FD relay is 1.3-2 times of that of HD relay, when the SIC amount varies from 40$\sim$60 dB (40 dB can be achieved by PS only with relative ease). It is also shown that with low drain efficiency or high static circuit power, FD (PSAC) is preferable over FD (PS) in terms of EE. This work is general and is applicable to a short-range wireless relay system at any frequency band.

Chapter 5

Energy Efficiency Oriented Cross-Layer Resource Allocation in Full Duplex Decode-and-Forward Relay Multiuser Systems

Much research has been conducted on optimal resource allocation for FD transmission in physical (PHY) layer. In [65], [66] and [67], SE maximisation was investigated in bi-directional FD networks. In [65], the optimal transmission power policies at two communicating nodes were proposed to maximise ergodic capacity in a FD MIMO communication system. In [66], a beamforming scheme was proposed to maximise SE in small cell networks, where a FD base station (BS) communicates with multiple HD users in the uplink and downlink channels simultaneously. In [67], the authors considered a single cell FD OFDMA network, which consists of one FD BS and multiple FD users. The subcarrier and power allocation were jointly optimised in terms of sum-capacity, while in [2], [39], [60] and [68], SE maximisation of FD relay-assisted networks was investigated. In [39], a joint relay selection and power allocation method for maximising SINR was proposed in a multiple AF FD relay system. In [68], a joint precoding/decoding design was presented to maximise end-to-end SINR in an AF FD relay network. In [60], the combination of opportunistic relay mode selection and transmit power adaptation at source was proposed to maximise SE, while in [2], resource allocation issue in multiuser MIMO networks was investigated in terms of SE. FD transmission in cognitive radio (CR) networks was researched in [69] and [70], respectively. Based on time division multiplex access (TDMA) (therefore HD transmission), the authors in [24] [25] studied the SE maximisation in 60 GHz wireless personal area networks.

In terms of EE oriented resource allocation, all existing work has focused on HD

relay systems [50] [55] [71] [72] or direct transmission (without relay) [53] [73]-[75]. In [71], maximising EE was investigated for MIMO OFDMA based LTE cellular systems. While in [50], a power consumption model was presented for HD relay-assisted 60 GHz systems. However, it did not consider FD mode nor static circuit power, which is actually comparable with the transmission power in indoor environments. The authors of [72] studied the EE-SE trade-off in a multiuser cellular virtual-MIMO system with DF type protocols, however, only transmission power was considered as power consumption. In [55], the position of HD relay was investigated to outperform direct (without relay) transmission in terms of EE. In [73], EE issue was researched for MIMO OFDM systems with statistical quality-of-service (QoS) constraints, where only transmission power was considered. EE oriented resource allocation of OFDMA networks in downlink was considered in [53] [74] [75]. The authors indicated that transmission power and circuit power need to be considered together to rationalise the power consumption model. Besides, EE oriented designs in CR networks were given in [70] and [76]. In [77], the authors investigated the EE balance between downlink and uplink transmission in a single cell system, where a base station can communicate with users via time division duplex (TDD) transmission mode. Since uplink and downlink transmission were decoupled in orthogonal time slots, the self-interference can be avoided at the expense of SE. In [78], the EE oriented resource allocation was investigated in heterogeneous networks with multiple access points, in which the multi-objective optimisation problem was transformed into an equivalent single objective optimisation problem by the weighted Tchebycheff method to find the Pareto optimal solution. Resource allocation for uplink in LTE networks was investigated in [79]. However, the authors took maximisation of total uplink SE as objective function. Therefore, the EE may not be optimal due to the fully utilised transmission power. In [80], the EE oriented resource allocation was investigated for uplink of LTE networks under QoS requirements. However, only transmission power was taken into account to trace the total power consumption. In [81], the power consumption model was investigated for LTE based marco/pico cell, revealing that MIMO may not lead to energy saving due to the increased circuit power consumption. Also, EE issues in 5G systems were extensively reviewed in [82], and a variety of EE optimisation methods in uplink and downlink were discussed.

The aforementioned EE oriented resource allocation methods designed for HD relay systems or direct transmission may not be directly applied to FD relay systems due to the presence of residual self-interference, while most existing work on resource allocation for FD relay systems was presented to maximise SE. On the other hand, due to the significant PL of mm-wave communications, ultra-dense small cell network and WiFi access points are promising solutions for local-area connectivity, which act as front/back haul to provide seamless coverage in 5G systems [83]. The application of small cell network was presented in [84] [85] for indoor/outdoor use. It was also

indicated that relay-assisted optimal resource allocation in mm-wave small cell is still challenging. The EE issue of FD transmission was investigated in our previous work [10]. However, it focused on the comparison between HD and FD with different SIC schemes in a single user AF relay system, and also did not consider cross-layer design and multiuser scenarios. In [86], EE oriented resource allocation in cellular networks with FD relay was investigated. However, only PHY resource allocation was considered. Besides, the FD relay power consumption model in [86] is not accurate since the power consumption for SIC at FD relay was ignored. There lacks investigation of cross-layer EE oriented resource allocation for multiuser FD relay systems in the literature, which is the motivation of our work.

In this chapter, cross-layer EE oriented resource allocation is investigated for multiuser FD DF relay-assisted indoor systems, which is the first work to the best of our knowledge. Our work is different in the following aspects.

- To address cross-layer design for FD relay system at 60 GHz, throughput outage probability, a MAC layer performance metric, is considered, while only PHY layer performance metrics were considered in our previous work [10]. This makes the proposed work more practical at 60 GHz than existing resource allocation works [2] [41] [86] [87], since throughput outage easily occurs in the presence of channel estimation errors and out-of-date channel state information (CSI), caused by mobility of users and intermittent blockage effects at 60 GHz.

- A low-complexity resource allocation algorithm, referred to as the Q-FERA algorithm, is proposed, by which the transmission power, subcarrier and throughput are allocated jointly across multiple users to maximise system EE. Based on the proposed EE oriented resource allocation algorithm, FD relay systems can achieve a higher EE than FD relay systems with an SE oriented approach in [2], while offering a comparable SE. In addition, the throughput outage probability is much lower by the proposed Q-FERA algorithm, showing its robustness against the channel estimation errors.

- Properties of the EE oriented resource allocation are investigated: 1) Impact of transmission power on EE is investigated, revealing that utilising higher transmission power does not ensure a higher EE. Especially, higher transmission power at relay node may degrade both EE and SE, with poor SIC performance. 2) EE oriented water-filling for two-hop FD relay systems is presented, which indicates that more power will be allocated to the subcarriers with lower residual self-interference. 3) By trading off SE and EE in FD relay systems, FD relay with the proposed Q-FERA algorithm can outperform FD relay with SE oriented algorithms in terms of EE, at the expense of SE. 4) With a higher Rician factor (indoor 60 GHz channel can be modelled by Rician fading with a typical Rician

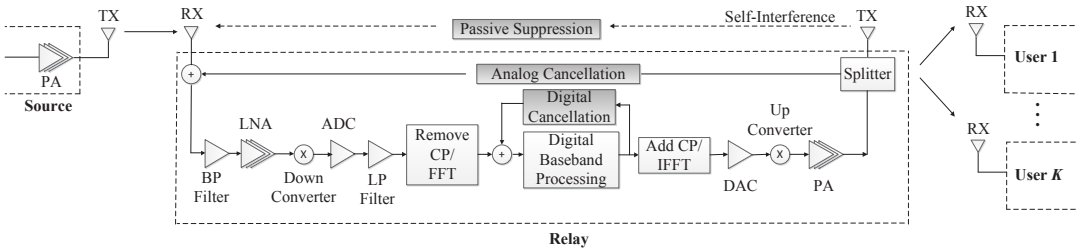

Figure 5.1: Simplified FD DF relay assisted system in the downlink, with PS, AC and DC of SIC.

factor of 5−15 dB), more aggressive throughput can be assigned while satisfying the target outage probability, which reflects the suitability of the proposed algorithm for 60 GHz. 5) Impact of outage probability constraint on EE is researched, showing that adopting stringent outage probability constraint does not necessarily guarantee a higher EE.

5.1 System Model and Problem Formulation for Full Duplex Decode-and-Forward Relay Multiuser Systems

In this section, system model is described in subsection 5.1.1, and then present the optimisation problem in subsection 5.1.2.

5.1.1 System Model

A K-user FD DF relay-assisted system is considered in the downlink, as illustrated in Fig. 5.1. It is assumed that the users can not hear the source directly [25]. This typical assumption corresponds to coverage extension scenarios due to high attenuation at 60 GHz [10]. The relay works in FD mode, causing self-interference to the receiver from its transmitter. SIC schemes, PS, AC and DC are applied at the relay.

OFDMA transmission is assumed with N subcarriers. Let $h_{SR,k,n}$, $h_{RD,k,n}$ and $h_{RR,k,n}$ denote the channel frequency responses of links source-to-relay (S-R), relay-to-user (R-D) and relay-to-relay (R-R) on subcarrier n for user k, respectively. Also let $l_{SR,k}$, $l_{RD,k}$ and $l_{RR,k}$ denote the PLs of links S-R, R-D and R-R for user k, respectively. The channels of the S-R and R-D links are modelled as Rician fading [9], which is widely used for 60 GHz channel modelling [36] [29]. Without loss of generality, it is assumed that the Rician factor $\hat{k}$ is equal at the two links, i.e. $h_{SR,k,n} \sim CN(\sqrt{\hat{k}/(1+\hat{k})}, 1/(1+\hat{k}))$ and $h_{RD,k,n} \sim CN(\sqrt{\hat{k}/(1+\hat{k})}, 1/(1+\hat{k}))$. Normally, the Rician factor $\hat{k}$ varies between 5 dB and 15 dB in 60 GHz indoor environment [9]. The self-interference channel is modelled as Rayleigh fading channel as the LOS between the transmitter and the receiver of the relay can be effectively blocked by antenna shielding and placement due to the very small wavelength at 60 GHz [10]. The self-interference waves are

collected from reflected waves [8]. It is assumed that perfect CSI of link S-R can be obtained. Since both the BS and relay are static and fixed high in indoor environment and is immune to the blockage effect, the fading gain can be reliably estimated with negligible estimation error [88], whereas the channel estimation error of the link R-D is presented with imperfect channel estimate $\hat{h_{RD,k,n}}$ and estimation error $\Delta h_{RD,k,n} \sim CN(0, \sigma^2_{error})$, where σ^2_{error} is the variance of the estimation error and is independent of k and n. It is because the wavelength at 60 GHz is only 5 mm, any obstacles whose size is significant larger than the wavelength will cause serious blockage effect [34], e.g. mobility of human or small-size furniture can even eliminate the LOS transmission and penalise the link by $20-30$ dB, resulting in time-varying channel state and out-of-date CSI of link R-D. Besides, the channel estimation error of link R-R is absorbed into the effect of cancellation amount α [10], i.e. higher value of α means more accurate estimation of link R-R and lower circuit distortion of the SIC operation [1].

For OFDMA usage in multiuser scenario, define power allocation matrices $\boldsymbol{P_s} = [p_{s,k,n}]_{K\times N}$, $\boldsymbol{P_r} = [p_{r,k,n}]_{K\times N}$, whose elements $p_{s,k,n}$ and $p_{r,k,n}$ denote the transmission powers allocated at the resource and the relay node for user k on subcarrier n, respectively. Define subcarrier allocation matrix $\boldsymbol{\rho} = [\rho_{k,n}]_{K\times N}$, whose element $\rho_{k,n} = \{1, 0\}$ denotes whether subcarrier n is assigned to user k (by 1) or not (by 0). Subcarrier mapping is not considered due to high complexity. $z_{R,k,n}[i]$ and $z_{D,k,n}[i]$ denote complex AWGN on subcarrier n introduced at the relay and user k in time slot i, respectively, with zero mean and variance σ^2. Define end-to-end instantaneous capacity matrix $\boldsymbol{C} = [c_{k,n}]_{K\times N}$, whose element $c_{k,n}$ denotes end-to-end capacity of user k achieved on subcarrier n, and overall capacity is calculated as $C = \sum_{k=1}^{K}\sum_{n=1}^{N} c_{k,n}$. In most cross-layer designs, capacity is a meaningful measure when the schedulers have perfect CSI. However, in practice, outage occurs whenever throughput exceeds the instantaneous capacity, which is caused by the channel estimation error [88]. Therefore, the per-subcarrier outage constraint is needed to ensure low frame error rate applications [89] and to avoid network congestion caused by the retransmission of lost message. Therefore, the instantaneous throughput $t_{k,n}$ of user k on subcarrier n can be given by

$$t_{k,n} = \begin{cases} t_{k,n}, t_{k,n} \leq c_{k,n} \\ 0\ , t_{k,n} > c_{k,n}. \end{cases} \tag{5.1}$$

Denote $\boldsymbol{T} = [t_{k,n}]_{K\times N}$ as the throughput assignment policy and the overall throughput of system is calculated as $T = \sum_{k=1}^{K}\sum_{n=1}^{N} t_{k,n}$.

[1] There are other models which assume that the residual self-interference is proportional to the transmission power [87], or the residual self-interference increases the noise power by a coefficient σ regardless of the transmission power [67]. The first modelling of self-interference actually is the same method as we formulated, since the self-interference is the transmitted signal from the relay node itself and the power of residual self-interference is directly determined by the relay's transmission power and the SIC amount α. While the second one simplifies the self-interference model by ignoring the transmission power at the transmitter.

5.1.2 Problem Formulation

Define $\eta(\boldsymbol{\rho}, \boldsymbol{P_s}, \boldsymbol{P_r}, \boldsymbol{T})$ as the EE (in bits/Joule), which is the ratio of the system throughput T to the incurred total power consumption P_{total}. Accordingly, the optimal EE resource allocation problem of the FD DF relay system is formulated as

$$P5.1: \quad \underset{\boldsymbol{\rho}, \boldsymbol{P_s}, \boldsymbol{P_r}, \boldsymbol{T}}{\text{argmax}} \ \eta(\boldsymbol{\rho}, \boldsymbol{P_s}, \boldsymbol{P_r}, \boldsymbol{T}) = \frac{T}{P_{total}}, \tag{5.2}$$

$s.t.$ $(C1): \sum_{k=1}^{K} \sum_{n=1}^{N} (p_{s,k,n} + p_{r,k,n}) \leq P_{max}$, $(C2): p_{s,k,n} \geq 0$, $p_{r,k,n} \geq 0$, $(C3): \sum_{k=1}^{K} \rho_{k,n} = 1$, $(C4): \rho_{k,n} \in \{0, 1\}$, and $(C5): Pr[t_{k,n} > c_{k,n} \mid \hat{h_{RD,k,n}}] \leq \theta^k$ for $\forall k \in K$ and $n \in N$, where $(C1)$ is a joint power constraint for the source and relay with a maximum total transmission power P_{max}, which provides useful insight into the power usage of the whole system rather than the per-hop required power [88]; $(C2)$ implies non-negative transmission power allocation at the source and relay; $(C3)$ and $(C4)$ are imposed to guarantee that each subcarrier is only used by one user; $(C5)$ represents a per-subcarrier throughput outage probability constraint for user k on subcarrier n with the estimated channel $\hat{h_{RD,k,n}}$, i.e. the probability that the assigned throughput $t_{k,n}$ on subcarrier n exceeds its channel capacity $c_{k,n}$ is upper bounded by θ^k. $(C1) - (C4)$ are PHY constraints while $(C5)$ is a MAC layer constraint.

5.2 Throughput and Power Consumption Analysis

The problem formulation in (5.2) includes the system throughput and total power consumption. Hereby, the throughput and power consumption are analysed in Section 5.2. At the relay node, the received signal for user k on subcarrier n in time slot i is

$$r_{k,n}[i] = h_{SR,k,n} \sqrt{l_{SR,k} p_{s,k,n}} x_{k,n}[i] + h_{RR,k,n} \sqrt{\frac{l_{RR,k}}{\alpha}} q_{k,n}[i] + z_{R,k,n}[i], \tag{5.3}$$

where $x_{k,n}[i]$ is the transmitted signal from the source on subcarrier n for user k in time slot i. The DF relay decodes the received signal and re-encodes and forwards it to user k. Therefore, the transmitted signal $q_{k,n}[i]$ from the relay for user k on subcarrier n is given by

$$q_{k,n}[i] = \sqrt{p_{r,k,n}} x_{k,n}[i - \tau], \tag{5.4}$$

where the integer $\tau \geq 1$ is the symbol delay. At the user end, the received signal is

$$y_{k,n}[i] = h_{RD,k,n} \sqrt{l_{RD,k} p_{r,k,n}} x_{k,n}[i - \tau] + z_{D,k,n}[i]. \tag{5.5}$$

Therefore, the SINRs at the first hop S-R and the second hop R-D are given by (5.6) and (5.7), respectively.

$$\Gamma_{1,k,n}^{FD} = \frac{p_{s,k,n}\gamma_{SR,k,n}}{1 + p_{r,k,n}\gamma_{RR,k,n}}, \tag{5.6}$$

$$\Gamma_{2,k,n}^{FD} = p_{r,k,n}\gamma_{RD,k,n}, \tag{5.7}$$

where $\gamma_{SR,k,n} = \frac{h_{SR,k,n}^2 l_{SR,k}}{\sigma^2}$, $\gamma_{RD,k,n} = \frac{h_{RD,k,n}^2 l_{RD,k}}{\sigma^2}$ and $\gamma_{RR,k,n} = \frac{h_{RR,k,n}^2 l_{RR,k}}{\alpha\sigma^2}$ are channel-to-noise ratios (CNRs) of links S-R, R-D and R-R, respectively. For simplicity, the bandwidth of each subcarrier is normalized in the mathematical derivation. Hence, the end-to-end capacity on subcarrier n for user k is given by

$$c_{k,n} = \rho_{k,n}\min\{log_2(1 + \Gamma_{1,k,n}^{FD}), log_2(1 + \Gamma_{2,k,n}^{FD})\}, \tag{5.8}$$

On the other hand, for short-range communications, the power amplifier (PA) power is comparable with the circuit power [53] due to the small chip size in indoor environment and the low drain efficiency of 60 GHz chips [6], and is given by

$$P_{PA} = \frac{1}{\omega}\sum_{k=1}^{K}\sum_{n=1}^{N}(p_{s,k,n} + p_{r,k,n}), \tag{5.9}$$

where ω is the drain efficiency. The circuit power includes the power consumed by all circuit blocks along the signal path, which can be divided into static circuit power, $P_{c,sta}$, and dynamic circuit power, $P_{c,dyn}$ [53]. A well-accepted model of dynamic circuit power is $P_{c,dyn} = \varepsilon T$, where the constant ε denotes the power consumption per unit data rate.

For FD relay, applying PS actually does not consume additional power, however, the power consumed by AC and DC is non-negligible. Besides, the power consumed by the involved chip components, such as attenuator, splitter and adder are not related to the throughput state [3], and therefore the power consumed by AC and DC, P_{AD}, is regarded as a constant. The total power consumption of FD relay system is formulated as

$$P_{total} = \underbrace{\frac{1}{\omega}\sum_{k=1}^{K}\sum_{n=1}^{N}(p_{s,k,n} + p_{r,k,n})}_{\text{PA power}} + \underbrace{P_{c,sta} + \varepsilon T}_{\text{circuit power}} + P_{AD}. \tag{5.10}$$

5.3 Energy Efficiency Oriented Cross-Layer Resource Allocation

Based on the derived throughput and total power consumption, substituting (5.1), (5.8) and (5.10) into (5.2) yields the EE oriented resource allocation problem of the FD DF

relay system:

$$P5.2: \underset{\boldsymbol{\rho},\boldsymbol{P_s},\boldsymbol{P_r},\boldsymbol{T}}{\text{argmax}} \frac{T}{\frac{\sum_{k=1}^{K}\sum_{n=1}^{N}(p_{s,k,n}+p_{r,k,n})}{\omega} + P_{c,sta} + \varepsilon T + P_{AD}}, \tag{5.11}$$

$s.t.\ (C1)-(C5)$.

The policies of subcarrier allocation $\boldsymbol{\rho}$, transmission power allocation $\boldsymbol{P_s}$ and $\boldsymbol{P_r}$ and throughput assignment $\boldsymbol{T}$ need to be optimised jointly, subject to the cross-layer constraints. To solve the non-convex problem P5.2 in a polynomial time, a series of transformations are needed, i.e. solving the original P5.2 is transformed into solving P5.3 and P5.4, as presented in subsection 5.3.1. Final solution is demonstrated in subsection 5.3.2.

5.3.1 Transformations of the Optimisation Problem

A new variable is introduced first to combine $\boldsymbol{P_s} = [p_{s,k,n}]_{K\times N}$ and $\boldsymbol{P_r} = [p_{r,k,n}]_{K\times N}$ without the loss of optimality [2]. Let matrix $\boldsymbol{P} = [p_{k,n}]_{K\times N}$ denote end-to-end transmission power policy, whose element $p_{k,n} = p_{s,k,n} + p_{r,k,n}$ represents end-to-end transmission power for user k on subcarrier n via hops S-R and R-D. For DF relay systems, the maximum EE for user k on subcarrier n is achieved when $\Gamma_{1,k,n}^{FD} = \Gamma_{2,k,n}^{FD}$ (which is easy to prove by a counter example). Let $p_{r,k,n} = p_{k,n} - p_{s,k,n}$ and substitute it into $\Gamma_{1,k,n}^{FD} = \Gamma_{2,k,n}^{FD}$. The quadratic function of $p_{r,k,n}$ can be solved and equivalent end-to-end capacity $c_{k,n}$ of FD DF relay systems on subcarrier n for user k is given by Lemma 5.1.

Lemma 5.1: The equivalent end-to-end capacity of FD DF relay systems for user k on subcarrier n is given by (5.12).

$$c_{k,n} = \rho_{k,n} log_2\big(1 + \frac{\sqrt{4p_{k,n}\gamma_{RD,k,n}\gamma_{SR,k,n}\gamma_{RR,k,n} + (\gamma_{RD,k,n}+\gamma_{SR,k,n})^2} - (\gamma_{RD,k,n}+\gamma_{SR,k,n})}{2\gamma_{RR,k,n}}\big). \tag{5.12}$$

Next, the MAC layer constraint in $(C5)$ and the PHY layer parameters can be incorporated. The "$\leq$" sign in $(C5)$ is replaced with an "$=$" sign, which is reasonable in low outage probability applications (e.g. $\theta^k \leq 0.01$) [88]. The equivalent outage probability constraint is given by Lemma 5.2.

Lemma 5.2: The outage probability constraint in $(C5)$: $Pr[t_{k,n} > c_{k,n} \mid \hat{h_{RD,k,n}}] = \theta^k$ for $\forall k \in K$ and $n \in N$, is equivalent to allocating throughput as

$$t_{k,n} = log_2(1 + \Lambda_{k,n}), \tag{5.13}$$

where $\Lambda_{k,n} = \frac{\sqrt{4p_{k,n}\Phi_{k,n} + \Psi^2} - \Psi}{2\gamma_{RR,k,n}}$, $\Psi_{k,n} = \gamma_{\hat{RD},k,n} + \gamma_{SR,k,n}$, $\Phi_{k,n} = \gamma_{\hat{RD},k,n}\gamma_{SR,k,n}\gamma_{RR,k,n}$ and $\gamma_{\hat{RD},k,n} = \frac{F_{k,n}^{-1}(\theta^k)\sigma_{error}^2 l_{RD,k}}{2\sigma^2}$. $F_{k,n}(\cdot)$ denotes the cumulative distribution function

(cdf) of the non-central chi-square random variable, with 2 degrees of freedom, and non-central parameter $\frac{2|\hat{h_{RD,k,n}}|^2}{\sigma^2_{error}}$. $F^{-1}_{k,n}(\cdot)$ denotes the inverse function of $F_{k,n}(\cdot)$.

Proof: See Appendix D.

Then the combinational constraint $(C4)$ caused by the subcarrier assignment is relaxed. The binary variable $\rho_{k.n}$ is relaxed to a real number within the interval [0,1], indicating the time sharing factor of subcarrier n among K users. The relaxation of $(C4)$ does not affect the optimality when the number of subcarriers goes to infinity $(N \to \infty)$. Given a large number of subcarriers, the loss of optimality is negligible and the solution after relaxation is near-optimal [90] [91]. Hence, the transformed problem P5.3 is given by (5.14).

$$P5.3 : \underset{\boldsymbol{\rho},\boldsymbol{P}}{\operatorname{argmax}} \frac{\sum_{k=1}^{K}(1-\theta^k)\sum_{n=1}^{N}\rho_{k,n}log_2(1+\frac{\Lambda_{k,n}}{\rho_{k,n}})}{\frac{\sum_{k=1}^{K}\sum_{n=1}^{N}p_{k,n}}{\omega}+P_{c,sta}+\varepsilon\sum_{k=1}^{K}(1-\theta^k)\sum_{n=1}^{N}\rho_{k,n}log_2(1+\frac{\Lambda_{k,n}}{\rho_{k,n}})+P_{AD}}, \tag{5.14}$$

s.t. $(C2)$, $(C3)$, $(C6)$: $\rho_{k,n} \in [0,1]$ and $(C7)$: $\sum_{k=1}^{K}\sum_{n=1}^{N}p_{k,n} \leq P_{max}$.

Notice that $(C1)$ and $(C4)$ are transformed to $(C7)$ and $(C6)$, respectively, whereas $(C5)$ can be omitted after the transform through Lemma 5.2. Therefore, optimising $\eta(\boldsymbol{\rho}, \boldsymbol{P_s}, \boldsymbol{P_r}, \boldsymbol{T})$ under constraints $(C1)-(C5)$ is transformed into optimising $\eta(\boldsymbol{\rho}, \boldsymbol{P})$ under new constraints $(C2)$ $(C3)$ $(C6)$ and $(C7)$ through Lemmas 5.1 and 5.2. Theorem 5.1 is introduced to help solve the problem P5.3.

Theorem 5.1: EE $\eta(\boldsymbol{\rho}, \boldsymbol{P})$ is strictly quasi-concave or mono-increasing with respect to the total end-to-end transmission power P, under a maximum transmission power constraint P_{max}.

The proof of theorem 5.1 is similar to that of theorem 4.1, and therefore is omitted.

Theorem 5.1 confirms the existence and uniqueness of the global maximum $\eta(\boldsymbol{\rho}, \boldsymbol{P})$. Obviously, the target function EE $\eta(\boldsymbol{\rho}, \boldsymbol{P})$ is mono-increasing with respect to the total end-to-end throughput T with a fixed end-to-end transmission power P. According to Theorem 5.1, if there is a globally optimal end-to-end transmission power P^*, maximising $\eta(\boldsymbol{\rho}, \boldsymbol{P})$ is equal to maximising the total end-to-end throughput with this P^* rather than P_{max}. Then the optimisation problem P5.3 in (5.14) can be transformed into

$$P5.4 : \underset{\boldsymbol{\rho},\boldsymbol{P}}{\operatorname{argmax}} \sum_{k=1}^{K}(1-\theta^k)\sum_{n=1}^{N}\rho_{k,n}log_2(1+\frac{\Lambda_{k,n}}{\rho_{k,n}}), \tag{5.15}$$

s.t. $(C2)$, $(C3)$, $(C6)$ and $(C8)$: $\sum_{k=1}^{K}\sum_{n=1}^{N}p_{k,n} = P^*$, where $(C8)$ is a transform of $(C7)$ according to Theorem 1. Notice that P_{max} is replaced by P^* in $(C8)$.

5.3.2 Solution to the Cross-Layer Resource Allocation Algorithm

After a series of transformations in subsection 5.3.1, the problem P5.4 in (5.15) is jointly-concave in terms of $p_{k,n}$ and $\rho_{k,n}$, which is proved in Appendix E. To solve the problem P5.4, Lagrange multiplier method [92] is applied. The Lagrange function of (5.15) is given by

$$\begin{aligned} L = \sum_{k=1}^{K}(1-\theta^k)\sum_{n=1}^{N}\rho_{k,n}log_2(1+\frac{\Lambda_{k,n}}{\rho_{k,n}})+ \\ \mu(P^* - \sum_{k=1}^{K}\sum_{n=1}^{N}p_{k,n}) + \beta_n(1-\sum_{k=1}^{K}\rho_{k,n}), \end{aligned} \tag{5.16}$$

where μ and $\beta_n, \forall n \in N$ are Lagrange multipliers corresponding to the transmission power constraint and the subcarrier constraints, respectively. Let $\mu^*, \beta_n^*, \forall n \in N$ denote the corresponding optimal Lagrange multipliers. Using the Karush-Kuhn-Tucker (KKT) conditions, (5.16) is differentiated with respect to $p_{k,n}$ and $\rho_{k,n}$, respectively. By setting each derivative to 0, (5.17) and (5.18) are obtained.

$$\begin{aligned} &\frac{\partial L}{\partial p_{k,n}}\bigg|_{\rho_{k,n}=\rho_{k,n}^*} = (1-\theta^k)\frac{\Phi_{k,n}}{ln(2)\sqrt{4p_{k,n}^*\Phi+\Psi_{k,n}^2}}\frac{2\rho_{k,n}^*}{2\rho_{k,n}^*\gamma_{RR,k,n}+\sqrt{4p_{k,n}^*\Phi+\Psi_{k,n}^2}-\Psi_{k,n}} \\ &-\mu^* = \begin{cases} <0, p_{k,n}^* = 0 \\ =0, 0 < p_{k,n}^*. \end{cases} \end{aligned} \tag{5.17}$$

$$\begin{aligned} &\frac{\partial L}{\partial \rho_{k,n}}\bigg|_{p_{k,n}=p_{k,n}^*} = (1-\theta^k)log_2(1+\frac{\sqrt{4p_{k,n}^*\Phi+\Psi_{k,n}^2}-\Psi_{k,n}}{2\rho_{k,n}^*\gamma_{RR,k,n}})- \\ &\frac{(1-\theta^k)}{ln(2)}\frac{4p_{k,n}\Phi_{k,n}}{(2\rho_{k,n}^*\gamma_{RR,k,n}+\sqrt{4p_{k,n}^*\Phi+\Psi_{k,n}^2}-\Psi_{k,n})(\sqrt{4p_{k,n}^*\Phi+\Psi_{k,n}^2}+\Psi_{k,n})} - \beta_{k,n}^* \\ &= \begin{cases} <0, \rho_{k,n}^* = 0 \\ \geq 0, \rho_{k,n}^* = 1. \end{cases} \end{aligned} \tag{5.18}$$

The optimal end-to-end transmission power $p_{k,n}^*$ on subcarrier n for user k can be derived from (5.17):

$$p_{k,n}^* = \left[\frac{4\Phi_{k,n}(1-\theta^k)^2}{(\mu^* ln2(\sqrt{\Xi_{k,n}^2+\frac{8\Phi_{k,n}(1-\theta^k)}{\mu^* ln2}}-\Xi_{k,n}))^2} - \frac{\Psi_{k,n}^2}{4\Phi_{k,n}}\right]^+, \tag{5.19}$$

where operation $[\cdot]^+$ denotes $[x]^+ = max(0,x)$, $\Xi_{k,n} = \Psi_{k,n} - 2\gamma_{RR,k,n}$. Accordingly, the optimal transmission power $p_{s,k,n}^*$ at the source and $p_{r,k,n}^*$ at the relay node are

obtained by Lemma 5.1, and the optimal throughput $t^*_{k,n}$ is obtained by substituting $p^*_{k,n}$ into (5.13).

Also, the optimal subcarrier allocation indicator $\rho^*_{k,n}$ is obtained from (5.18). It can be known that subcarrier n should be assigned to user k satisfying

$$\rho^*_{k,n} = \begin{cases} 1, k = k^* \\ 0, k \neq k^*, \end{cases} \tag{5.20}$$

where $k^* = \underset{k}{\operatorname{argmax}}(1-\theta^k)\big[log_2(1+\Lambda^*_{k,n}) - \frac{p^*_{k,n}\gamma_{SR,k,n}\gamma_{R\hat{D},k,n}}{ln(2)(1+\Lambda^*_{k,n})}\frac{1}{\gamma_{RR,k,n}\Lambda^*_{k,n}+\Psi_{k,n}}\big]$, and $\Lambda^*_{k,n}$ is obtained by substituting $p^*_{k,n}$ into $\Lambda^*_{k,n} = \dfrac{\sqrt{4p^*_{k,n}\Phi_{k,n}+\Psi^2}-\Psi}{2\gamma_{RR,k,n}}$. Notice that multiplier $\beta_n, \forall n \in N$ is omitted due to subcarrier constraints being naturally satisfied by (5.20). Hence, the next aim is to determine the optimal Lagrange multiplier μ^* satisfying

$$f(\mu) = P^* - \sum_{k=1}^{K}\sum_{n=1}^{N}\left[\frac{4\Phi_{k,n}(1-\theta^k)^2}{(\mu ln2(\sqrt{\Xi^2_{k,n}+\frac{8\Phi_{k,n}(1-\theta^k)}{\mu ln2}}-\Xi_{k,n}))^2} - \frac{\Psi^2_{k,n}}{4\Phi_{k,n}}\right]^+ = 0. \tag{5.21}$$

It can be found that (5.21) is a mono-increasing function for $\mu > 0$, and $f(\mu) < 0|_{\mu\to 0}$ and $f(\mu) > 0|_{\mu\to+\infty}$. The searching upper bound can be set as $\mu_{upper} = max\{\frac{8\Phi_{k,n}}{ln(2)(\Psi_{k,n}-4\Xi_{k,n})}\}, \forall k \in k, n \in N$.

Based on the theoretic analysis, a so-called quasi-concave based FD EE oriented resource allocation (Q-FERA) algorithm is proposed, as summarised in Algorithm 3, to optimise the EE of the multiuser FD DF relay systems, under cross-layer constraints. The proposed Q-FERA algorithm presented in subsection 5.3.1 relies on finding P^*, which helps us transform the problem P3 into the problem P4. According to the characteristic of derivative, i.e. $\dfrac{\partial\eta}{\partial P}\big|_{P^*} = \lim\limits_{\Delta P\to 0}\dfrac{\eta(P^*+\Delta P)-\eta(P^*)}{\Delta P}$, P^* is readily obtained.

5.4 Properties of the Energy Efficiency Oriented Resource Allocation

Based on the theoretic analysis above, some useful properties of the EE oriented resource allocation are discovered.

5.4.1 Impact of Transmission Power on Energy Efficiency

In FD DF relay systems, EE shows a mono-increasing or quasi-concave shape with respect to the transmission power, as indicated by Theorem 5.1. Therefore higher transmission power does not ensure a higher EE. For the transmission power at the source $P_s = \sum_{k=1}^{K}\sum_{n=1}^{N} p_{s,k,n}$, the end-to-end capacity is non-decreasing with respect to P_s, and thus the assigned throughput is also non-decreasing with respect to P_s.

Algorithm 3 Quasi-concave based Full-Duplex Energy Efficient Resource Allocation (Q-FERA) Algorithm

Input: $P_{max}, P_{c,sta}, P_{AD}, \omega, \varepsilon, \theta^k, h_{SR,k,n}, h_{RR,k,n}, l_{SR,k}$, $l_{RD,k}$ and $l_{RR,k}$, $\forall k \in K, n \in N$.

Output: Optimal subcarrier and end-to-end transmission power allocation policy $\boldsymbol{\rho^*}, \boldsymbol{P^*}$, and optimal throughput assignment policy $\boldsymbol{T^*}$.

Set $P = P_{max}$
for $n = 1 : N$ **do**
  for $k = 1 : K$ **do**
    Allocate subcarrier n the user k satisfying (6.21), calculate end-to-end transmission power $p_{k,n}$ according to (5.19) and assign throughput $t_{k,n}$ according to (5.13).
  end for
end for
Calculate $\frac{\partial \eta}{\partial P}$ at $P = P_{max}$.
if $\frac{\partial \eta}{\partial P}|_{P_{max}} \geq 0$ **then**
  return $P^* = P_{max}$, $\eta^* = \eta(\boldsymbol{\rho^*}, \boldsymbol{P^*}, \boldsymbol{T^*})$
else
  Initialise the left bound $P_L = 0$, and the right bound $P_R = P_{max}$.
  while $|\frac{\partial \eta}{\partial P}|_{P_M}| < \delta$ (δ is a precision factor) **do**
    $P_M = \frac{P_L + P_R}{2}$.
    Do subcarrier and transmission power allocation policy and throughput assignment policy as did in steps $2-6$, with total end-to-end transmission power $P = P_M$ and $P = P_L$, respectively.
    if $\frac{\partial \eta}{\partial P}|_{P_L} \cdot \frac{\partial \eta}{\partial P}|_{P_M} \geq 0$ **then**
      $P_L = P_M$
    else
      $P_R = P_M$
    end if
  end while
  return $P^* = P_M$, $\eta^* = \eta(\boldsymbol{\rho^*}, \boldsymbol{P^*}, \boldsymbol{T^*})$
end if

However, EE may be degraded by the raised total power consumption. Differently, improving the transmission power at the relay $P_r = \sum_{k=1}^{K} \sum_{n=1}^{N} p_{r,k,n}$ may decrease both throughput and EE given a poor SIC configuration. As can be seen from (5.8), the signal transmitted from the relay is treated as self-interference to the relay's receiver. Therefore, higher transmission power P_r improves the power of self-interference with a poor SIC. As a result, both throughput and EE are deteriorated.

There are other models that assume the residual self-interference only increases the noise power by a coefficient [67] or treat the residual self-interference as a noise-like constant (which are special cases of our generalised model). The residual self-interference in these models is independent of transmission power. Therefore, increasing transmission power P_r in this case guarantees a non-decreasing end-to-end throughput. However, EE may be degraded due to the increased transmission power. By replacing the residual self-interference in (5.13) as a noise-like constant, it is easy to prove that the EE is still mono-increasing or quasi-concave with respect to the transmission power.

5.4.2 Energy Efficiency Oriented Water-Filling for Two-Hop FD Relay Systems

By (5.20), it can be found that user k with lower $\gamma_{RR,k,n}$ has a higher opportunity to get subcarrier n, implying that it is preferable that a subcarrier be allocated to a user with less self-interference on that subcarrier. Similarly, it is obvious that more power will be allocated to subcarrier n with lower $\gamma_{RR,k,n}$ as shown in (5.19). It is different to the conventional water-filling algorithm in HD networks by taking the presence of residual self-interference and the channel conditions of links R-R, S-R and R-D into account, which can be classified as EE oriented two-hop FD relay systems water-filling policy.

5.4.3 Trade-off between Energy Efficiency and Spectral Efficiency for Two-Hop Full Duplex Relay Systems

For FD relay systems with SE oriented algorithms, the transmission power is fully utilised in the case of effective SIC, where the power of the residual self-interference can be much lower than that of noise. However, the EE of SE oriented FD relay systems may be hindered by the incurred high total power consumption. Different from SE oriented algorithms, FD relay systems with EE oriented algorithm make trade-off between EE and SE, where the utilised transmission power may be lower than the available transmission power constraint. As a result, the total power consumption is lower than that of SE oriented FD relay systems, and higher EE can be obtained at the expense of SE.

5.4.4 Suitability of the Proposed Algorithm for 60 GHz Applications

With a fixed outage probability requirement, more aggressive throughput assignment matrix $\boldsymbol{T} = [t_{k,n}]_{K\times N}$ can be achieved with a higher Rician factor $\hat{k}$. Since cdf of chi-square function $F(\cdot)$ is mono-decreasing with respect to its non-centrality parameter. Inversely, the inverse function $F^{-1}(\cdot)$ is mono-increasing with respect to its non-central parameter, which is $\frac{2|\hat{h_{RD,k,n}}|^2}{\sigma^2_{error}}$ as derived. Higher Rician factor $\hat{k}$ leads to higher value of $\mathbb{E}\{|h_{RD,k,n}|^2\} = \mathbb{E}\{|\hat{h_{RD,k,n}}|^2\}$ (assume the estimator is unbiased) and higher non-central parameter. As a result, higher throughput can be assigned while satisfying the target outage probability, and therefore higher EE is obtained.

The analysis above accords with intuition that, applying directional or narrow beam-width antenna provides strong LOS transmission and a higher Rician factor, e.g. $\hat{k}$ ranges from $5-15$ dB in a typical 60 GHz indoor environment, where the channel is more flat with strong LOS components and poor NLOS components. In this case, more aggressive throughput assignment can be obtained while satisfying the outage probability naturally.

In some special scenarios, the channels at 60 GHz may follow Rayleigh distribution with the utilization of omnidirectional low gain antenna and long distance between transmitter and receiver [93]. By setting the Rician factor $\hat{k} = 0$, our algorithm is easily extended to a Rayleigh scenario. Also, the S-V and two wave with diffuse power (TWDP) channels were modelled at 60 GHz in [8], which can actually be approximated as Rician distribution when $\hat{k} > 0$ and does not approach $+\infty$.

5.4.5 Impact of Outage Probability Constraint on Energy Efficiency

Since capacity analysis does not capture the effect of outage with imperfect channel estimation, the definition of throughput and outage probability is introduced first, which is constrained by θ^k. According to the theoretic analysis, the total average bits per second per Hz successfully delivered to users is given by $\sum_{k=1}^{K}(1-\theta^k)\sum_{n=1}^{N} t_{k,n}$ [94]. With a coarse outage constraint θ^k, the throughput arrangement $t_{k,n}$ can be aggressive. However, the term $(1-\theta^k)$ is degraded, indicating outage is more likely to occur. Inversely, with a stringent outage constraint θ^k, the term $(1-\theta^k)$ is improved and it is likely more data can be delivered to users successfully. However, a stringent outage constraint θ^k leads to a smaller value of $F^{-1}(\theta^k)$ and hence a conservative value of $t_{k,n}$ (see. (5.13)). Considering an extreme case that outage probability θ^k is an infinitely small value that approaches 0 ($\theta^k \to 0$). The first term $(1-\theta^k)$ is equal to 1, indicating all encoded information can be readily delivered to users without outage. However, the second term $t_{k,n}$ approaches 0 since the value of $\lim_{\theta^k\to 0} F^{-1}(\theta^k)$ is equal to 0. Therefore, a stringent outage probability constraint does not necessarily guarantee higher EE or SE. Also, a coarse constraint may lead to poor EE.

Table 5.1: ANALYTICAL COMPUTATIONAL COMPLEXITY (N: NUMBER OF SUBCARRIERS; K: NUMBER OF USERS; δ: REQUIRED PRECISION FACTOR IN ITERATIVE SEARCH; l_{ite}: NUMBER OF ITERATIONS[2])

Designs	Algorithms	Complexities
EE. Max	Q-FERA	$\mathcal{O}(2NKl_{ite1}) + l_{ite2}\mathcal{O}(4NKl_{ite1})$ $\approx \mathcal{O}(2NKl_{ite1})$.
	[3] QA-ERA in [71]	$\mathcal{O}(N(K+1)^3)log_2(\frac{1}{\delta})$
SE. Max	[4] FRAA in [67]	$\mathcal{O}(NKl_{ite3})log_2(\frac{1}{\delta})$
	[5] FDRA in [2]	$\mathcal{O}(NKl_{ite4})$

5.5 Complexity Analysis

In this section, the complexity of the proposed algorithm is analysed in terms of number of multiplications.

The Q-FERA algorithm is proposed to perform subcarrier allocation, transmission power allocation and throughput assignment jointly. At first, the gradient of EE is calculated at the maximum transmission power P_{max}, and the complexity of this step is $\mathcal{O}(2NKl_{ite1})$, where l_{ite1} is the number of iterations required to obtain the optimal Lagrange multiplier μ^* with given total transmission power P_{max}, and is upper bounded by $l_{ite1} \leq log_2(\frac{\mu_{upper}-\mu^*}{\delta})$ by bisection searching algorithm. The coefficient 2 is induced by the twice computation at the transmission power P_{max} and $P_{max} + \Delta P$, respectively. If $\frac{\partial \eta}{\partial P}|_{P_{max}} \geq 0$, $P_{max} = P^*$ is readily obtained and the algorithm terminates. Otherwise, the globally optimal transmission power P^* needs to be iteratively searched between (0, P_{max}], within at most $l_{ite2} \leq log_2(\frac{P_{max}-P^*}{\delta})$ iterations by bisection searching algorithm. Once the globally optimal transmission power P^* is found, the subcarrier and power allocation are allocated at the complexity $\mathcal{O}(4NKl_{ite1})$. Hence the total complexity of the whole algorithm is $\mathcal{O}(2NKl_{ite1}) + l_{ite2} \times \mathcal{O}(4NKl_{ite1})$.

Practically, the optimal transmission power always exists at the value that the transmission power related power consumptions (PA power P_{PA}, dynamic circuit power $P_{c,dyn}$) are comparable with the power consumption of the static power $P_{c,sta}$. Since the static power of 60 GHz chip is high while the feasible transmission power range is limited, i.e. $P_{max} \leq 16$ dBm [4], P^* could be close to or even equal to P_{max}. Therefore, very few or no iteration l_{ite2} is needed in finding the optimal total transmission power P^*, and the whole complexity can be reduced to $\mathcal{O}(2NKl_{ite1})$ in this case. As a result, the complexity of the proposed Q-FERA is comparable with that of the SE oriented algorithms in [67] and [2], and is lower than that of the EE oriented algorithm in [71], which is for direct transmission rather than for relay systems.

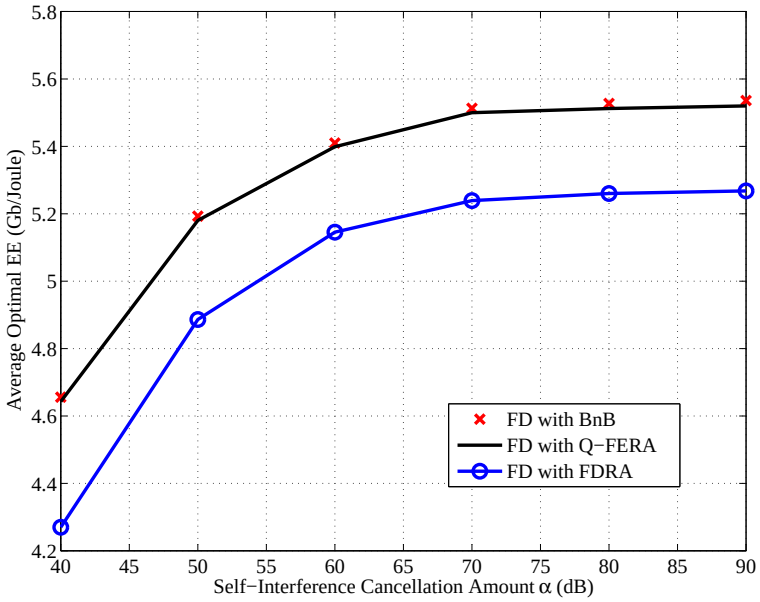

Figure 5.2: The average EEs of FD with the BnB approach, FD with the Q-FERA and FD with the FDRA vs. different SIC amounts.

5.6 Simulation Results

Numerical results are used to verify our analysis. In all figures, Q-FERA is used to denote the proposed cross-layer EE oriented resource allocation, and FD dynamic resource allocation (FDRA) to denote the SE oriented resource allocation by the algorithm in [2]. The PL model in [10] is adopted, as $l = 68 + 10\nu log_{10}(d/d_0)$, where $\nu = 3$ is the PL exponent, d is the distance between two nodes, and $d_0 = 1$ m is the reference distance. The Rician factor $\hat{k}$ is 15 dB except in Fig. 5.7. The total bandwidth is 2640 MHz with 512 subcarriers [95]. The AWGN power spectral density is -174 dBm/Hz. The S-R and R-D (all users and $K = 5$) distances are all 5 m. The drain efficiency ω of the PA is 25%. The static circuit power is 300 mW and the dynamic circuit factor $\varepsilon = 50$ mW/Gbps. The SIC power is $P_{AD} = 40$ mW. The maximum transmission power constraint is set to $P_{max} = 50$ mW. The throughput outage constraint is $\theta^k = 0.01$ for all users, and the channel estimation error variance is set to $\sigma^2_{error} = 10^{-3}$ except in

[2]The number of iteration l_{ite} depends on the number of multiplier variables in Lagrange function and the applied search algorithm, i.e. ellipsoid searching is used in [71] while subgradient searching is used in [2].

[3]The QA-ERA algorithm in [71] is applied in LTE-based MIMO-OFDMA systems, which considers individual minimum throughput requirement for different users, which means more K multipliers needs to be found during iterations by the ellipsoid searching method.

[4]The FRAA algorithm in [67] is applied in FD OFDMA systems, and the local Pareto optimality is used to solve the optimisation problem.

[5]For fair comparison, the complexity of the algorithm in [2] is calculated in a simplified two-antenna infrastructure relay (one transmit antenna and one receive antenna at relay node) and single relay configuration.

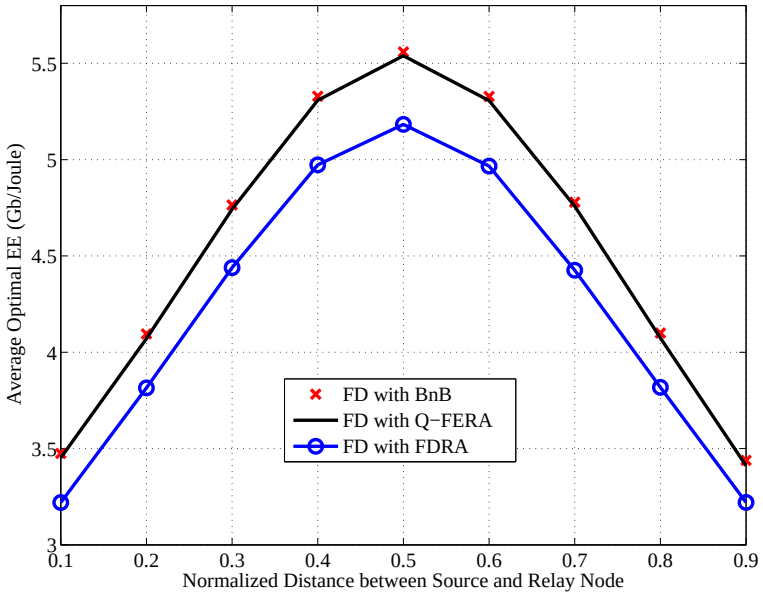

Figure 5.3: The average EEs of FD with the BnB approach, FD with the Q-FERA and FD with the FDRA vs. different normalised distances between S-R, with SIC amount $\alpha = 80$ dB.

Fig. 5.6. To evaluate the optimality of the proposed Q-FERA algorithm, the branch-and-bound (BnB) approach [96] is adopted as a benchmark, which yields a theoretic optimum on subcarrier allocation. The application of BnB in OFDMA systems is given by Appendix F.

Fig. 5.2 shows the average optimal EE performances of FD with different algorithms. It can be observed that FD with the Q-FERA algorithm shows higher EE than FD with the SE oriented FDRA algorithm across a wide range of SIC amount. The Q-FERA algorithm has nearly the same performance as the BnB approach, which certificates that our Q-FERA algorithm is near-optimal. Also, all the EEs of the FD systems increase with the SIC amount, since less residual self-interference is left.

Fig. 5.3 demonstrates the average EEs of FD with different values of the normalised relay's position, which is defined as the ratio of the distance of S-R to the distance of S-D. Obviously, for all FD relay curves, the optimal position of the FD relay is around in the middle between source and destinations. It is because with 80 dB of SIC amount, the power of residual self-interference can be much smaller than the power of noise. The optimal EE performance is achieved when the throughputs of two links are equal. Besides, it can be seen that FD with the Q-FERA always outperforms FD with the FDRA in terms of EE at all distances. It indicates that FD relay systems with the proposed Q-FERA algorithm maintains a high EE level. Last but not least, all the EE curves change rapidly with different relay's position, since the high PL at 60 GHz

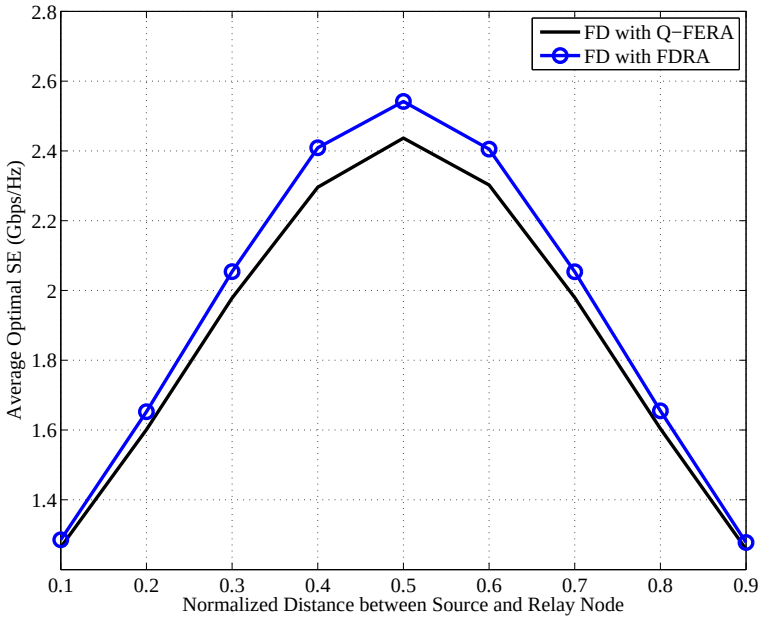

Figure 5.4: The average SEs of FD with the Q-FERA and FD with the FDRA vs. different normalised distances between S-R, with SIC amount $\alpha = 80$ dB.

results in a significant impact on system throughput.

Fig. 5.4 demonstrates the average SEs of FD with different values of the normalised relay's position. It shows that the EE oriented Q-FERA algorithm offers a comparable SE to the SE oriented FDRA algorithm. It means that FD with the proposed Q-FERA algorithm makes a proper trade-off between EE and SE, with marginal loss of SE.

Fig. 5.5 shows the probabilities that the total power consumption of FD relay systems exceeds a threshold $P_{threshold}$. When P_{max} is lower than 25 mW, the probabilities of both the FD systems are equal to 0. With the increase of P_{max}, the outage probability of FD with the FDRA boosts fast, because the FDRA algorithm utilises all available transmission power to maximise SE. Hence, its total power consumption easily exceeds the threshold of 500 mW (a reasonable power consumption of 60 GHz chips). While the probability of FD with the Q-FERA maintains low, which is only 0.1 with threshold 500 mW and $P_{max} \geq 30$ mW. This indicates that to obtain higher EE performance, the utilised transmission power may be lower than the available transmission power constraint P_{max} and its EE may be quasi-concave with respect to the transmission power. Fig. 5.5 confirms that the proposed EE oriented algorithm is a greener solution, with more carbon footprint savings.

Fig. 5.6 shows the average throughput outage probabilities of FD with the Q-FERA and FD with the FDRA. It can be observed that FD with the Q-FERA is robust against channel estimation errors, even though the system has no accurate channel information of the small-fading of the R-D link when $\sigma^2_{error} \to 1$ (which represents

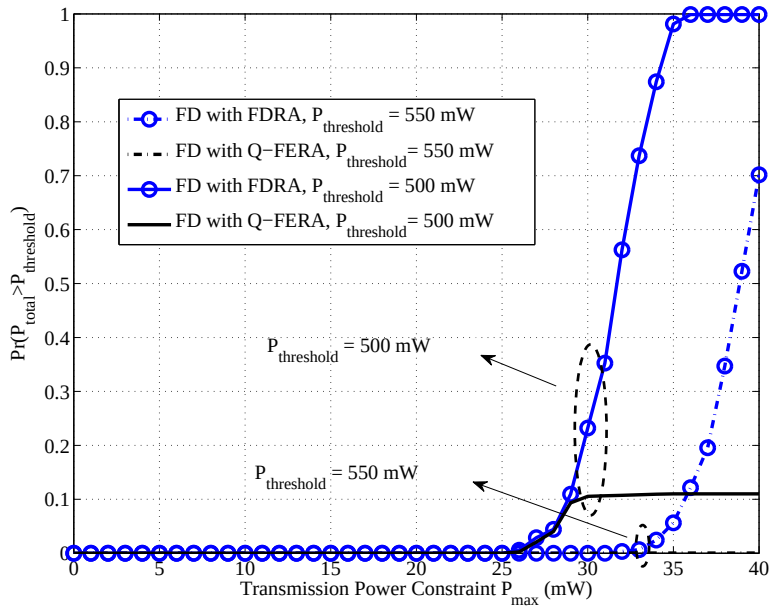

Figure 5.5: The average probabilities that total power consumptions of FD with the Q-FERA and FD with the FDRA exceeds the thresholds $P_{threshold} = 500$ mW and 550 mW, with SIC amount $\alpha = 80$ dB.

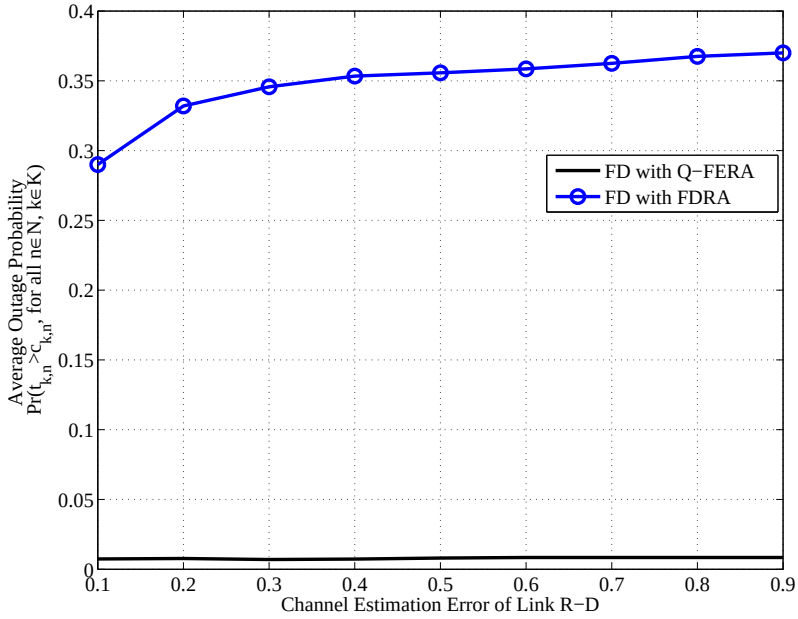

Figure 5.6: The average outage probabilities that the assigned throughput is higher than channel capacity, i.e. $\Pr(t_{k,n} > c_{k,n})$ for $\forall k \in K, n \in N$, under different channel estimation error, with SIC amount $\alpha = 80$ dB.

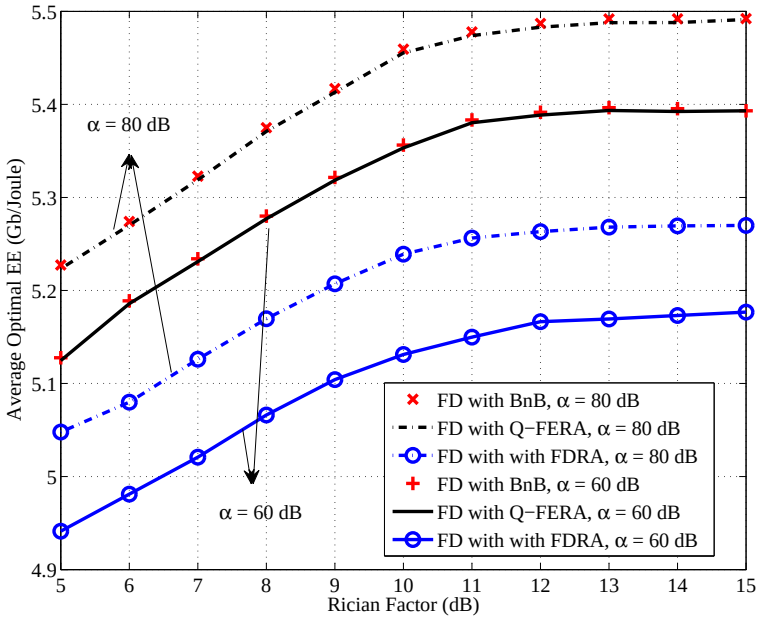

Figure 5.7: The average EEs of FD with the BnB approach, FD with the Q-FERA and FD with the FDRA vs. different Rician factor $\hat{k}$, with SIC amount α= 60 dB and 80 dB, respectively.

a noisy estimation in [19] [88]). This is because the channel condition of link R-D is adopted in a probabilistic manner in the proposed Q-FERA algorithm. Therefore, the throughput outage probability is satisfied naturally in our cross-layer design. It is worth mentioning that the outage probability was not considered in the SE oriented algorithm in [2], the throughput outage probabilities boosts with the increase of channel estimation error σ^2_{error}.

Fig. 5.7 shows the optimal average EEs of FD with the BnB approach, FD with the Q-FERA and FD with the FDRA under different Rician factors $\hat{k}$, whose value ranges from 5 dB to 15 dB in a typical indoor environment at 60 GHz. It is observed that higher Rician factor can improve the EEs of all FDs, since higher Rician factor means the R-D channel more flat with less fluctuation, and throughput can be assigned more aggressively while satisfying the pre-set outage probability. However, the EEs keep unchanged when the Rician factor is higher than 12 dB, this is because the LOS components almost overwhelm the NLOS components, and thus the channel is approximately a constant. Besides, it can be seen that FD with the Q-FERA (with $\alpha = 60$ dB) even shows higher EE than FD with the FDRA (with $\alpha = 80$ dB), which reflects that FD with the Q-FERA can maintain a considerable EE value when SIC performance is not very high, especially in a typically high Rician factor scenario at 60 GHz indoor environment.

Figs. 5.8 and 5.9 present the convergence behaviours of the Q-FERA algorithm

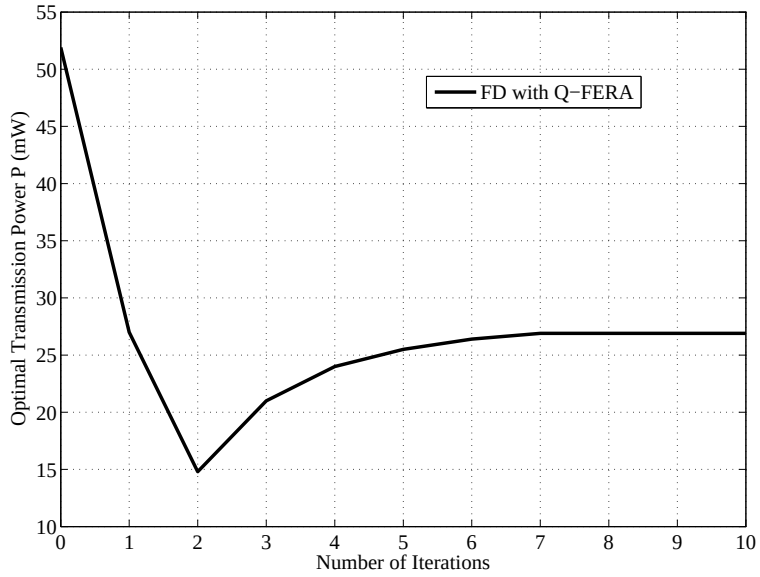

Figure 5.8: The convergence behaviours of the proposed Q-FERA algorithm.

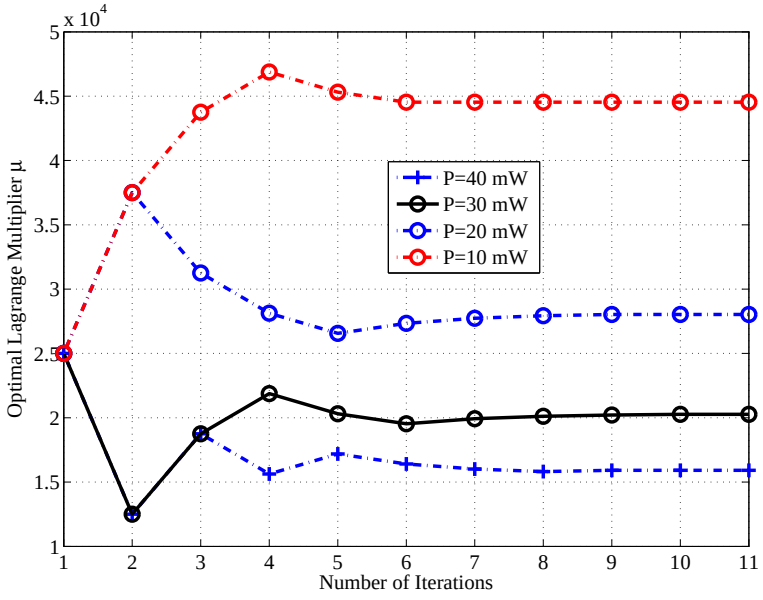

Figure 5.9: The convergence behaviours of the proposed Q-FERA algorithm.

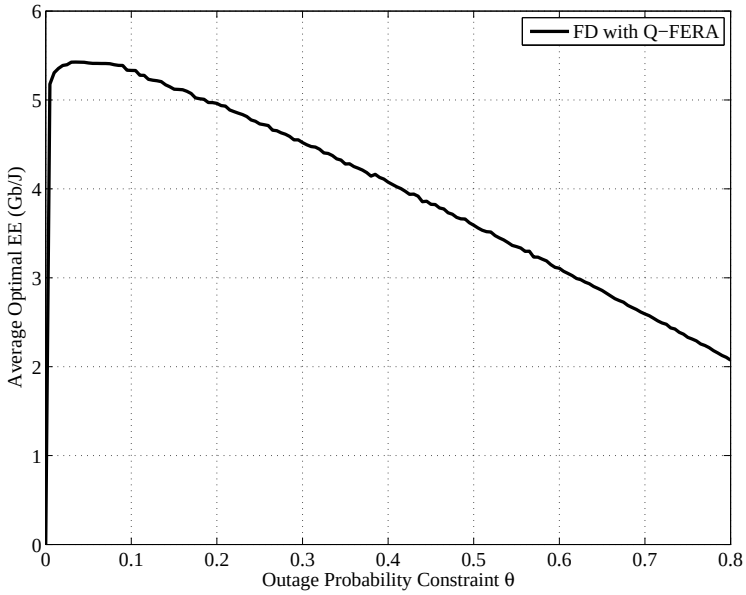

Figure 5.10: The average EEs with different outage probability constraints, with cancellation amount $\alpha = 80$ dB.

under the maximum transmission power constraint $P_{max} = 50$ mW. Fig. 5.8 shows the convergence behaviour of finding optimal transmission power P^*, while Fig. 5.9 shows the convergence behaviour of finding the optimal multiplier μ^* with different values of given transmission power. It can be seen that the at most around 10 iterations are needed in both figures. Especially, if P_{max} is relatively small, EE may be mono-increasing in the range of $P_s \in (0, P_{max}]$, as analysed in Theorem 5.1. In this case, the optimal transmission power P^* corresponding to the maximum EE is simply equal to P_{max}, and no iteration is needed in finding the optimal transmission power P^* in Fig. 5.8.

Fig. 5.10 presents the average EE performance with different outage probability constraints. It can be seen that EE approaches 0 given an infinitely small outage probability constraint, indicating a stringent outage probability constraint does not necessarily lead to better EE performance. Inversely, EE degrades significantly when constraint θ^k exceeds 0.1, which reveals that a coarse constraint may lead to poor EE and verifies the analysis in subsection 5.4.5.

5.7 Summary

In this chapter, EE oriented resource allocation for indoor multiuser FD DF relay systems has been investigated with cross-layer constraints. A novel low-complexity algorithm, referred to as Q-FERA, is proposed to perform transmission power allocation, subcarrier allocation and throughput assignment jointly to maximise system EE.

Simulation results show a higher EE performance of the proposed EE oriented design over SE oriented design, at the cost of marginal SE loss. Also, the throughput outage probability of the proposed algorithm is much lower than that of the algorithm in [2] and is robust against channel estimation errors, addressing the intermittent blockage problem at mm-wave communications. Besides, some useful properties of the EE oriented resource allocation are discussed, such as the impact of transmission power on EE, EE oriented water-filling power allocation, EE-SE trade-off for two-hop FD relay systems, the suitability of the Q-FERA algorithm for 60 GHz applications and the impact of outage probability constraint on EE. This work is extend-able to a short-range wireless relay system at a lower frequency.

Chapter 6

Energy Efficiency Oriented Resource Allocation for Wireless Power Transfer-Aided Full Duplex Decode-and-Forward Relay Multiuser Systems

WPT-aided relay communications have become an attractive technique due to recent advances in radio frequency-based WPT technique [97], especially in scenarios where regular battery replacement or recharging is inconvenient or even impossible (e.g. in a toxic environment) [98] [99]. By harvesting energy from the source node, WPT-aided relays are able to continuously assist communication between sources and users, and thus network connectivity can be maintained and its lifetime prolonged [100].

The early research on WPT-aided relay systems mainly focused on the three-time-slots HD transmission [101] [102]. One time slot is dedicated for energy harvesting at the relay node and another two time slots are required for a two-hop information transmission from the source to the user through the relay node. By making use of the power splitting architecture [103], another WPT-aided HD relay system needs only two time slots, where the source transmits to the relay in the first time slot, and only a part of the received signal at the relay node is decoded and forwarded to the destination while the rest of the received signal is stored to support the relay's operation in the second time slot. In summary, the aforementioned WPT-aided HD relay systems either need extra time slots [101] [102] or only decode and forward a part of the desired signal to the destination [103], incurring significant SE loss due to the low resource utilization efficiency.

In an effort to overcome the SE loss by HD, FD relay systems have attracted extensive attention. With signal transmitted and received simultaneously over the same frequency, FD has approximately doubled the SE over HD relay systems [10]. This has

also led to growing interest in integrating FD and WPT-aided relay techniques to obtain higher SE [104]. In [105] and [106], SE maximisation in FD WPT-aided relay systems was investigated, where the energy harvesting and the information transmission are decoupled into two orthogonal time slots, one for energy harvesting and the other for information transmission in FD mode. Joint design of source and relay beamformers was given in [107] for FD MIMO AF relay systems, where the multiple users are powered by WPT from the relay node. With the FD mode relay for information transfer, only two time slots are required in [105]-[107], improving SE over the HD counterparts.

In the aforementioned WPT-aided FD relay systems, however, self-interference is treated as noise and hence needs to be cancelled as much as possible. On the contrary, a WPT-aided FD relay system were investigated in [108] [109] to utilise self-interference for energy harvesting. The relay receives signal-bearing information in the first time slot, and forwards signal to the destination and concurrently harvests wireless transferred energy from the source and the relay's self-interference in the second time slot. As a result, the relay can harvest energy from both its transmitter and the source node. However, uniform time slot durations were assumed for the two hops in [108] and [109], ignoring the fact that the received SINR of the source-relay and the relay-users links can hardly be equivalent in WPT-aided relay systems. It is because the relay's transmission power could be much lower than that at the source, due to the wireless channel attenuation from the source to the relay and the energy harvesting efficiency at the relay node (smaller than 1). As a result, the end-to-end SE is bounded by the relay-users link while a large proportion of the SE in the source-relay link is wasted in the symmetric transmission system. Besides, the system models proposed in [105]-[109] only consider a signal-user and single-carrier scenario, which is not applicable to a multiuser scenario.

In this chapter, a novel protocol is proposed for the downlink OFDMA system with a WPT-aided relay working in FD and DF mode. Our work is different in the following aspects:

- An asymmetric time slot protocol is developed for the two hops, which enhances the degree of freedom and hence the system SE, and the system is more robust against the relay node's locations and the number of users than the work in [105]-[109].
- Unlike the previous work [105]-[107], where the self-interference at the FD relay is cancelled, the self-interference is utilised for energy harvesting. With the enhanced degree of freedom due to asymmetric time slots, much more energy can be harvested on every subcarrier, leading to a higher EE than the work in [105] and [108].
- A multiuser scenario is investigated, which is more general in communication

networks, such as sensor networks, while only single user was considered in the previous work [105]-[109].

- Based on the developed asymmetric protocol, a corresponding algorithm is proposed to maximise the overall system SE by performing joint allocation of time slot durations, transmission power at source and relay, and subcarriers for multiple users. The closed-forms of the optimal results are given. By optimising multiple variables concurrently, significant SE enhancement is achieved over the symmetric WPT-aided FD relay (Sym-WPT-FR) system [108] and the time-switching WPT-aided FD relay (TS-WPT-FR) system [105], where only one variable (transmission power [108] or time splitting factor [105]) is involved in optimisation.

- An intensive performance analysis of WPT-aided FD relay systems is presented, including the relative time slots durations of the two hops, and the effect of self-interference utilisation at the relay on power allocation, revealing some implicit characteristics of WPT-aided FD relay systems.

6.1 System Model and Problem Formulation for Wireless Power Transfer-Aided Full Duplex Decode-and-Forward Relay Multiuser Systems

6.1.1 System Model

A downlink OFDMA system is considered with K users and N subcarriers, and the communication between the source and the users is assisted by a relay in between. The relay relies on external charging through WPT from the source [101]. It is assumed that the users can not hear the source directly due to the blockage and the channel attenuation [105]. The channel state information is available at the source and the relay node, obtained by the pilot assisted reciprocal channel estimation [110]. The relay is equipped with two antennas, one for receiving information and harvesting energy and the other for transmitting signal to multiple users, while the source and the users are equipped with one antenna, respectively, as depicted by Fig. 6.1. In the first time slot of duration T_1, the source sends information-bearing signal to the relay. In the second time slot of duration T_2, the received signal at the relay is decoded, re-coded and forwarded to the user, and wireless energy is sent from the source to the relay's receiver for energy harvesting concurrently.

Define power allocation matrices at the source $\boldsymbol{p_s} = [p_{s,k,n}]_{K\times N}$ and at the relay $\boldsymbol{p_r} = [p_{r,k,n}]_{K\times N}$, whose elements $p_{s,k,n}$ and $p_{r,k,n}$ denote the transmission power allocated at the resource and the relay node for user k on subcarrier n, respectively. Define subcarrier allocation matrix $\boldsymbol{\beta} = [\beta_{k,n}]_{K\times N}$, whose element $\beta_{k,n} = \{1, 0\}$ denotes whether subcarrier n is assigned to user k (by 1) or not (by 0).

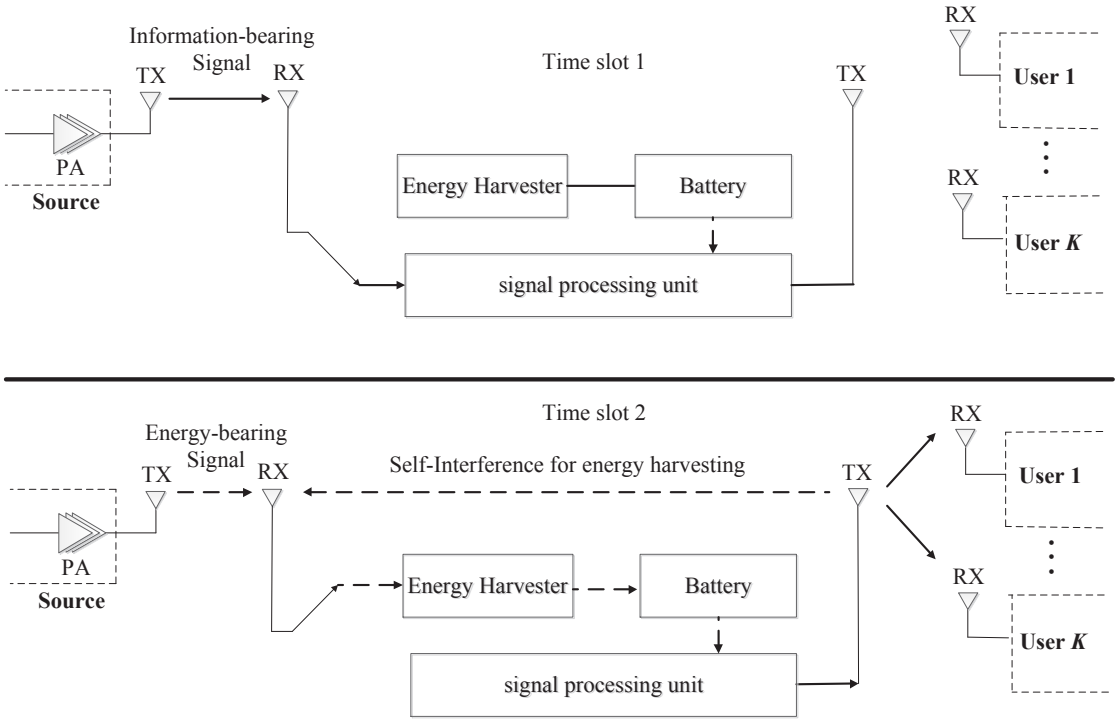

Figure 6.1: Illustration of asymmetric WPT-aided FD DF relay multiuser system, where dashed and solid lines denote energy-bearing and information-bearing signals, respectively.

The received signal on subcarrier n for user k at the relay in the first time slot is expressed as

$$r_{k,n,1}[i] = \sqrt{p_{k,n} l_{sr}} h_{sr,n} x_{k,n}[i] + n_{r,n}[i] \tag{6.1}$$

where i denotes the symbol index. $x_{k,n}[i]$ is the information-bearing symbol for user k on subcarrier n with unit power $\mathbb{E}\{|x_{k,n}[i]|^2\} = 1$. $p_{s,k,n}$ is the transmission power allocated at the source for user k on subcarrier n. $h_{sr,n}$ denotes the channel response of the source-relay link on subcarrier n, and l_{sr} captures the large-scale fading of the source-relay link. $n_{r,n}[i]$ is the noise introduced on subcarrier n at the relay. Therefore, the overall SE of the source-relay link in the first time slot T_1 is calculated as

$$C_{SR} = \frac{T_1}{T} \sum_{k=1}^{K} \sum_{n=1}^{N} \beta_{k,n} \log_2(1 + p_{s,k,n} \gamma_{sr,k,n}), \tag{6.2}$$

where $\beta_{k,n}$ denotes subcarrier n is assigned for user k, $\forall k \in K, n \in N$. $\gamma_{sr,k,n} = \frac{|h_{sr,n}|^2 l_{sr}}{N_0 B}$ denotes the CNR of the source-relay link on subcarrier n for user k. N_0 is the single-sided power spectral density and B is the bandwidth of each subcarrier. In the second time slot of duration T_2, the received signal at the relay is forwarded to the user. For

simplicity, subcarrier mapping is not considered. The received signal by user k on subcarrier n is given by

$$y_{k,n}[i] = \sqrt{p_{r,k,n} l_{rd,k}} h_{rd,k,n} x_{k,n}[i] + z_{k,n}[i], \tag{6.3}$$

where $p_{r,k,n}$ denotes the transmission power for user k on subcarrier n at the relay. $h_{rd,k,n}$ is the channel response of the link between the relay and user k on subcarrier n for user k, and $l_{rd,k}$ captures the effects of large-scale fading of the relay-user k. $z_{k,n}[i]$ is the noise introduced at user k. Therefore, the overall SE in the second time slot is calculated as

$$C_{RD} = \frac{T_2}{T} \sum_{k=1}^{K} \sum_{n=1}^{N} \beta_{k,n} \log_2(1 + p_{r,k,n} \gamma_{rd,k,n}) \tag{6.4}$$

where $\gamma_{rd,k,n} = \frac{|h_{rd,n}|^2 l_{rd,k}}{N_0 B}$ denotes the CNR of the relay-user k on subcarrier n. Finally, the end-to-end SE in the whole time $T = T_1 + T_2$ is expressed as

$$C = \min\{C_{SR}, C_{RD}\} \tag{6.5}$$

Concurrently with information transmission by the relay in the second time slot T_2, wireless energy is sent from the source to the relay's receiver for energy harvesting. Since information signal is being transmitted by the relay at the same time, the relay also receives the self-interference from its own transmitter, which can be collected by WPT [108]. Therefore, the received signal at the relay's receiver in the second time slot T_2 for user k on subcarrier n is

$$r_{k,n,2}[i] = \sqrt{p_{s,k,n} l_{sr}} h_{sr,n} x^{(e)}_{k,n}[i] + \sqrt{p_{r,k,n} l_{rr}} h_{rr,n} x_{k,n}[i - \tau] + n_{r,n}[i] \tag{6.6}$$

where $x^{(e)}_{k,n}[i]$ is the energy-bearing symbol sent from the source to the relay during the second time slot T_2 with normalised energy $\mathbb{E}\{|x^{(e)}_{k,n}[i]|^2\} = 1$. τ is the processing delay at relay node. $h_{rr,n}$ is the self-interference channel from the relay's transmitter to its receiver on subcarrier n and l_{rr} is large-scale fading. In summary, the overall harvested energy at the relay during the second time slot T_2 is

$$E_r = \frac{T_2}{T} \omega \sum_{k=1}^{K} \sum_{n=1}^{N} \beta_{k,n} E\{\left| \sqrt{p_{s,k,n} l_{sr}} h_{sr,n} x^{(e)}_{k,n}[i] + \sqrt{p_{r,k,n} l_{rr}} h_{rr,n} x_{k,n}[i - \tau] \right|^2\}, \tag{6.7}$$

where ω is the energy harvesting efficiency [1].

Since the channel condition and the transmitted signal $x^{(e)}_{s,k,n}[i]$ and $x_{s,k,n}[i-\tau]$ are known by the system, it is natural to set the state of $x^{(e)}_{s,k,n}[i]$ as $x_{s,k,n}[i]e^{j\angle h_{sr,n}} = x_{s,k,n}[i-\tau]e^{j\angle h_{rr,n}}$, ($\angle h_{sr,n}$ and $\angle h_{rr,n}$ denotes the phase of the complex number $h_{sr,n}$ and $h_{rr,n}$, respectively) to make the harvested energy maximised [108], which is summarised in Lemma 6.1.

Lemma 6.1: In the asymmetric WPT-aided FD relay OFDMA system, the maximal energy harvested at the relay is given by $E_r = \frac{T_2}{T}\omega \sum_{k=1}^{K}\sum_{n=1}^{N} \beta_{k,n}(p_{s,k,n}|h_{sr,n}|^2 l_{sr} + p_{r,k,n}|h_{rr,n}|^2 l_{rr})$.

6.1.2 Problem Formulation

Now define $C(T_1, T_2, \boldsymbol{p_s}, \boldsymbol{p_r}, \boldsymbol{\beta})$ as the SE (in bps/Hz) [2]. Accordingly, the SE oriented resource allocation optimisation problem is formulated as

$$\begin{aligned} P6.1: \quad & \underset{T_1,T_2,\boldsymbol{p_s},\boldsymbol{p_r},\boldsymbol{\beta}}{\operatorname{argmax}} \; C(T_1, T_2, \boldsymbol{p_s}, \boldsymbol{p_r}, \boldsymbol{\beta}) \\ & = \min\{\frac{T_1}{T}\sum_{k=1}^{K}\sum_{n=1}^{N}\beta_{k,n}\log_2(1+p_{s,k,n}\gamma_{sr,n}), \frac{T_2}{T}\sum_{k=1}^{K}\sum_{n=1}^{N}\beta_{k,n}\log_2(1+p_{r,k,n}\gamma_{rd,k,n})\}, \end{aligned} \tag{6.8}$$

s.t. $(C1): 0 \le p_{s,k,n}$, for $\forall n \in N, k \in K$. $(C2): \sum_{k=1}^{K}\sum_{n=1}^{N}\beta_{k,n}p_{s,k,n} \le p_{max}$, $(C3): 0 \le p_{r,k,n}$, for $\forall n \in N, k \in K$. $(C4): \sum_{k=1}^{K}\sum_{n=1}^{N}\beta_{k,n}p_{r,k,n} \le \omega\sum_{k=1}^{K}\sum_{n=1}^{N}\beta_{k,n}(p_{s,k,n}|h_{sr,n}|^2 l_{sr} + p_{r,k,n}|h_{rr,n}|^2 l_{rr})$, $(C5): T_1 + T_2 = T$. $(C6): \sum_{k=1}^{K}\beta_{k,n} = 1$, for $\forall n \in N$, $(C7): \beta_{k,n} \in \{0,1\}$, for $\forall n \in N, k \in K$. $(C1)$ and $(C2)$ imply the transmission power at the source should be non-negative and lower than a threshold p_{max}. $(C3)$ and $(C4)$ are the constraints imposed on transmission power at the relay, which should be non-negative and lower than the overall harvested power. $(C5)$ indicates that the summation of two time slots T_1 and T_2 should be equivalent to T. $(C6)$ and $(C7)$ guarantee that each subcarrier is only used by one user.

The allocation of time slots T_1 and T_2, subcarrier $\boldsymbol{\beta}$, transmission power $\boldsymbol{p_s}$ and $\boldsymbol{p_r}$ need to be optimised jointly, subject to multiple constraints $(C1) - (C7)$. The joint optimisation algorithm is detailed in the next section.

[1] There are some methods to improve the harvesting efficiency ω by hardware design at relay node, such as improving mutual coupling between relay's two antennas [109] or directing the self-interference power from relay's transmit antenna into the relay's battery [111]. More information can be referred from [109] [111].

[2] It has been assumed that the transmission power at the relay relies on WPT from the source, while the circuit power consumed by the relay is negligible as compared to the radiation power, which could be the case for low-complexity wireless devices (such as wireless sensors and tags) with simple electronics and low signal processing requirement [108] [112].

6.2 Asymmetric Resource Allocation for Wireless Power Transfer-Aided Full Duplex Decode-and-Forward Relay Multiuser Systems

6.2.1 Transformation of the Optimisation Problem

To solve the non-convex problem P6.1, the minimum function in the objective function should be handled first. It can be deduced that P6.1 is maximised only when $\frac{T_1}{T}\sum_{k=1}^{K}\sum_{n=1}^{N}\beta_{k,n}\log_2(1+p_{s,k,n}\gamma_{sr,k,n}) = \frac{T_2}{T}\sum_{k=1}^{K}\sum_{n=1}^{N}\beta_{k,n}\log_2(1+p_{r,k,n}\gamma_{rd,k,n})$, which is easy to prove by a counter example. Therefore, the original optimisation problem $\min\{\frac{T_1}{T}\sum_{k=1}^{K}\sum_{n=1}^{N}\beta_{k,n}\log_2(1+p_{s,k,n}\gamma_{sr,n}), \frac{T_2}{T}\sum_{k=1}^{K}\sum_{n=1}^{N}\beta_{k,n}\log_2(1+p_{r,k,n}\gamma_{rd,k,n})\}$ is equivalent to maximising the summation of SE of the two hops, with an additional constraint $\frac{T_1}{T}\sum_{k=1}^{K}\sum_{n=1}^{N}\beta_{k,n}\log_2(1+p_{s,k,n}\gamma_{sr,k,n}) = \frac{T_2}{T}\sum_{k=1}^{K}\sum_{n=1}^{N}\beta_{k,n}\log_2(1+p_{r,k,n}\gamma_{rd,k,n})$.

Then the combinational constraint $(C7)$ caused by the subcarrier assignment is relaxed. The binary variable $\beta_{k.n}$, for $\forall k \in K, n \in N$, is relaxed to a real number within the interval [0,1], indicating the time sharing factor of subcarrier n among K users. Given a large number of subcarriers, the loss of optimality is negligible and the solution after relaxation is near-optimal [91]. Hence, the transformed problem P6.2 is given by (6.9).

$$
\begin{aligned}
&P6.2: \quad \underset{T_1,T_2,\boldsymbol{p_s},\boldsymbol{p_r},\boldsymbol{\beta}}{\operatorname{argmax}} \; C(T_1,T_2,\boldsymbol{p_s},\boldsymbol{p_r},\boldsymbol{\beta}) = \\
&\frac{T_1}{T}\sum_{k=1}^{K}\sum_{n=1}^{N}\beta_{k,n}\log_2\left(1+\frac{p_{s,k,n}\gamma_{sr,k,n}}{\beta_{k,n}}\right)+\frac{T_2}{T}\sum_{k=1}^{K}\sum_{n=1}^{N}\beta_{k,n}\log_2\left(1+\frac{p_{r,k,n}\gamma_{rd,k,n}}{\beta_{k,n}}\right),
\end{aligned}
\tag{6.9}
$$

$s.t.$ $(C1), \widetilde{(C2)}: \sum_{k=1}^{K}\sum_{n=1}^{N}p_{s,k,n} \le p_{max}, (C3), \widetilde{(C4)}: \sum_{k=1}^{K}\sum_{n=1}^{N}p_{r,k,n} \le \omega\sum_{k=1}^{K}\sum_{n=1}^{N}(p_{s,k,n}|h_{sr,n}|^2 l_{sr}+p_{r,k,n}|h_{rr,n}|^2 l_{rr}), (C5), (C6), \widetilde{(C7)}: \beta_{k,n} \in [0,1]$, for $\forall n \in N, k \in K$, and $(C8): \frac{T_1}{T}\sum_{k=1}^{K}\sum_{n=1}^{N}\beta_{k,n}\log_2(1+\frac{p_{s,k,n}\gamma_{sr,k,n}}{\beta_{k,n}}) = \frac{T_2}{T}\sum_{k=1}^{K}\sum_{n=1}^{N}\beta_{k,n}\log_2(1+\frac{p_{r,k,n}\gamma_{rd,k,n}}{\beta_{k,n}})$.

The transformation from $P6.1$ to $P6.2$ is straightforward, and it should be noticed that P6.2 is subject to a new constraint (C8). Now Theorem 6.1 is given to solve the optimisation problem P6.2.

Theorem 6.1: The equivalent end-to-end SE $\frac{T_1}{T}\sum_{k=1}^{K}\sum_{n=1}^{N}\beta_{k,n}\log_2(1+\frac{p_{s,k,n}\gamma_{sr,k,n}}{\beta_{k,n}})+\frac{T_2}{T}\sum_{k=1}^{K}\sum_{n=1}^{N}\beta_{k,n}\log_2(1+\frac{p_{r,k,n}\gamma_{rd,k,n}}{\beta_{k,n}})$ is jointly-concave with respect to all variables T_1, T_2, $p_{s,k,n}$, $p_{r,k,n}$, $\beta_{k,n}$, for $\forall n \in N, k \in K$ in the feasible domain.

The proof of theorem 6.1 is provided in Appendix G.

6.2.2 Solution to the Asymmetric Resource Allocation for Wireless Power Transfer-Aided Full Duplex Decode-and-Forward Relay Multiuser Systems

Because P6.2 is a standard concave optimisation problem, it can be solved by using the KKT conditions. Its Lagrangian function is given by

$$\begin{aligned} L = & \frac{T_1}{T}\sum_{k=1}^{K}\sum_{n=1}^{N}\beta_{k,n}\log_2(1+\frac{p_{s,k,n}\gamma_{sr,k,n}}{\beta_{k,n}}) + \frac{T_2}{T}\sum_{k=1}^{K}\sum_{n=1}^{N}\beta_{k,n}\log_2(1+\frac{p_{r,k,n}\gamma_{rd,k,n}}{\beta_{k,n}}) \\ & - \mu(\sum_{k=1}^{K}\sum_{n=1}^{N}p_{s,k,n} - p_{max}) - \phi\big(\sum_{k=1}^{K}\sum_{n=1}^{N}p_{r,k,n}(1-\omega|h_{rr,n}|^2 l_{rr}) - \rho(T_1+T_2-T) \\ & - \lambda\big(\frac{T_1}{T}\sum_{k=1}^{K}\sum_{n=1}^{N}\beta_{k,n}\log_2(1+\frac{p_{s,k,n}\gamma_{sr,k,n}}{\beta_{k,n}}) - \frac{T_2}{T}\sum_{k=1}^{K}\sum_{n=1}^{N}\beta_{k,n}\log_2(1+\frac{p_{r,k,n}\gamma_{rd,k,n}}{\beta_{k,n}})\big) \\ & - \omega(\sum_{k=1}^{K}\sum_{n=1}^{N}p_{s,k,n}|h_{sr,n}|^2 l_{sr})\big) - \sum_{n=1}^{N}\psi_n(\sum_{k=1}^{K}\beta_{k,n}-1), \end{aligned} \tag{6.10}$$

where μ, ϕ, ρ, λ and ψ_n (for $\forall n \in N$) are Lagrange multipliers. It can be derived from the KKT conditions that $\mu \geq 0, \phi \geq 0, \rho \geq 0$, $\lambda \in (-1, 1)$ and $\psi_n \geq 0$ (for $\forall n \in N$). Let μ^*, ϕ^*, ρ^*, λ^* and ψ_n^* (for $\forall n \in N$) denote the optimal Lagrange multipliers, it has

$$\frac{\partial L}{\partial T_1} = \frac{(1-\lambda^*)}{T}\sum_{k=1}^{K}\sum_{n=1}^{N}\beta_{k,n}^*\log_2(\frac{1+p_{s,k,n}^*\gamma_{sr,k,n}}{\beta_{k,n}^*}) - \rho^*\begin{cases} <0, T_1^*=0 \\ =0, T_1^*>0 \end{cases} \tag{6.11}$$

$$\frac{\partial L}{\partial T_2} = \frac{(1+\lambda^*)}{T}\sum_{k=1}^{K}\sum_{n=1}^{N}\beta_{k,n}^*\log_2(1+\frac{p_{r,k,n}^*\gamma_{rd,k,n}}{\beta_{k,n}^*}) - \rho^*\begin{cases} <0, T_2^*=0 \\ =0, T_2^*>0 \end{cases} \tag{6.12}$$

From (6.11), (6.12) and constraint (C8), an equality can be obtained as

$$\frac{T_1^*}{1-\lambda^*} = \frac{T_2^*}{1+\lambda^*}, \tag{6.13}$$

According to (6.13) and constraint (C5), it can be derived that the optimal time slot T_1 is given by

$$T_1^* = \frac{1-\lambda^*}{2}T. \tag{6.14}$$

and the optimal time slot T_2^* is

$$T_2^* = \frac{1+\lambda^*}{2}T. \tag{6.15}$$

Similarly, taking the derivative of L with respect to $p_{s,k,n}$ and $p_{r,k,n}$ yields

$$\frac{\partial L}{\partial p_{s,k,n}} = \frac{(1-\lambda^*)T_1^*\gamma_{sr,k,n}\beta_{k,n}^*}{T(\beta_{k,n}^* + p_{s,k,n}^*\gamma_{sr,k,n})} - \mu^* + \phi^*\omega|h_{sr,k,n}|^2 l_{sr} \begin{cases} < 0, p_s^* = 0 \\ = 0, p_s^* > 0 \end{cases} \tag{6.16}$$

$$\frac{\partial L}{\partial p_{r,k,n}} = \frac{(1+\lambda^*)T_2^*\gamma_{rd,k,n}\beta_{k,n}^*}{T(\beta_{k,n}^* + p_{r,k,n}^*\gamma_{rd,k,n})} - \phi^*(1-\omega|h_{rr,n}|^2 l_{rr}) = \begin{cases} < 0, p_r^* = 0 \\ = 0, p_r^* > 0 \end{cases} \tag{6.17}$$

By substituting (6.14) and (6.15) into (6.16) and (6.17), the optimal power allocation at the source is given by

$$p_{s,k,n}^* = [\frac{(1-\lambda^*)^2\beta_{k,n}^*}{2(\mu^* - \phi^*\omega|h_{sr,n}|^2 l_{sr})} - \frac{\beta_{k,n}^*}{\gamma_{sr,k,n}}]^+, \tag{6.18}$$

where $[x]^+ = max\{0, x\}$. Also, the optimal power allocation at the relay is expressed as

$$p_{r,k,n}^* = [\frac{(1+\lambda^*)^2\beta_{k,n}^*}{2\phi^*(1-\omega|h_{rr,n}|^2 l_{rr})} - \frac{\beta_{k,n}^*}{\gamma_{rd,k,n}}]^+, \tag{6.19}$$

By taking derivative L with respect to $\beta_{k,n}$, we have

$$\begin{aligned} \frac{\partial L}{\partial \beta_{k,n}} &= \frac{(1-\lambda^*)T_1}{T}\log_2(1 + \frac{p_{s,k,n}^*\gamma_{sr,k,n}}{\beta_{k,n}^*}) - \frac{(1-\lambda^*)T_1^* p_{s,k,n}^*\gamma_{sr,k,n}}{T(\beta_{k,n}^* + p_{s,k,n}^*\gamma_{sr,k,n})} \\ &+ \frac{(1+\lambda^*)T_2^*}{T}\log_2(1 + \frac{p_{r,k,n}^*\gamma_{rd,k,n}}{\beta_{k,n}^*}) - \frac{(1+\lambda^*)T_2^* p_{r,k,n}^*\gamma_{rd,k,n}}{T(\beta_{k,n}^* + p_{r,k,n}^*\gamma_{rd,k,n})} - \psi_n^* = \begin{cases} < 0, \beta_{k,n}^* = 0 \\ \geq 0, \beta_{k,n}^* = 1. \end{cases} \end{aligned} \tag{6.20}$$

Since $\beta_{k,n}$ is either 0 or 1, by substituting (6.14), (6.15), (6.18) and (6.19) into (6.20), it can be derived that the subcarrier n will be assigned to the user k satisfying

$$\beta_{k,n}^* = \begin{cases} 1, k = k^* \\ 0, k \neq k^*, \end{cases} \tag{6.21}$$

$$\begin{aligned} k^* = \underset{k}{\text{argmax}} \; &\frac{(1-\lambda^*)^2}{2}[\log_2(\frac{(1-\lambda^*)^2}{2}\frac{\gamma_{sr,k,n}}{(\mu^* - \phi^*\omega|h_{sr,n}|^2 l_{sr})})]^+ + \frac{(1+\lambda^*)^2}{2}[\log_2(\frac{(1+\lambda^*)^2}{2}\frac{\gamma_{rd,k,n}}{\phi^*(1-\omega|h_{rr,n}|^2 l_{rr})})]^+ \\ &-[\frac{(1-\lambda^*)^2\gamma_{sr,k,n} - 2(\mu^* - \phi^*\omega|h_{sr,n}|^2 l_{sr})}{2\gamma_{sr,k,n}}]^+ - [\frac{(1+\lambda^*)^2\gamma_{rd,k,n} - 2\phi^*(1-\omega|h_{rr,n}|^2 l_{rr})}{2\gamma_{rd,k,n}}]^+. \end{aligned}$$

Hence, the optimal value of $p_{s,k,n}$ and $p_{r,k,n}$ is finally given by

$$p_{s,k,n}^* = [\frac{(1-\lambda^*)^2}{2(\mu^* - \phi^*\omega|h_{sr,n}|^2 l_{sr})} - \frac{1}{\gamma_{sr,k,n}}]^+. \tag{6.22}$$

$$p^*_{r,k,n} = [\frac{(1+\lambda^*)^2}{2\phi^*(1-\omega|h_{rr,n}|^2 l_{rr})} - \frac{1}{\gamma_{rd,k,n}}]^+. \tag{6.23}$$

After obtaining the optimal results $T_1^*, T_2^*, p^*_{s,k,n}, p^*_{r,k,n}$ and $\beta^*_{k,n}$ (for $\forall k \in K$ and $\forall n \in N$), the next aim is to determine the optimal Lagrange multipliers. The gradient method is used to update the multipliers μ, ϕ, λ and ρ, while multiplier ψ_n (for $\forall n \in N$) has been omitted naturally in deriving (6.21). According to the gradient method, the updating rules can be given as

$$\begin{aligned}
\mu(j+1) &= \mu(j) + \epsilon_1(\sum_{k=1}^{K}\sum_{n=1}^{N} p_{s,k,n} - p_{max});\\
\phi(j+1) &= \phi(j) + \epsilon_2\big(\sum_{k=1}^{K}\sum_{n=1}^{N} p_{r,k,n}(1-\omega|h_{rr,n}|^2 l_{rr}) - \omega\sum_{k=1}^{K}\sum_{n=1}^{N} p_{s,k,n}|h_{sr,n}|^2 l_{sr}\big);\\
\lambda(j+1) &= \lambda(j) + \epsilon_3\big(\sum_{k=1}^{K}\sum_{n=1}^{N} \beta_{k,n}\log_2(1+\frac{p_{s,k,n}\gamma_{sr,k,n}}{\beta_{k,n}}) -\\
&\qquad \sum_{k=1}^{K}\sum_{n=1}^{N} \beta_{k,n}\log_2(1+\frac{p_{r,k,n}\gamma_{rd,k,n}}{\beta_{k,n}})\big);\\
\rho(j+1) &= \rho(j) + \epsilon_4(T_1+T_2-T);
\end{aligned} \tag{6.24}$$

where ϵ_1, ϵ_2 ϵ_3, and ϵ_4 are the corresponding step sizes [91]. Now the optimisation problem P6.2 is readily solved. Based on our theoretic analysis, a so-called asymmetric WPT-aided FD relay (Asym-WPT-FR) algorithm is proposed, which is detailed in Algorithm 4.

6.3 Complexity Analysis

With N subcarriers and K users, the complexity of the algorithm is $\mathcal{O}(NK \times l_{ite})$, where l_{ite} is the number of iterations for updating multipliers until convergence. By properly selecting the step size and initial values of the multipliers, the subgradient based algorithm leads to convergence within polynomial time [113]. More insight of the complexity is given by numerical results in section 6.5.

6.4 Properties Discussion for Wireless Power Transfer-Aided Full Duplex Relay Multiuser Systems

Some useful properties on resource allocation in asymmetric WPT-aided FD relay systems are discovered.

Algorithm 4 Asymmetric WPT-aided FD relay (Asym-WPT-FR) Algorithm

Input: Initial value of multipliers $\mu(0)$, $\phi(0)$, $\lambda(0)$ and $\rho(0)$, channel condition $h_{sr,n}, h_{rd,k,n}, h_{rr,n}, l_{sr}, l_{rd,k}$, and l_{rr}, power related parameters p_{max} and ω.

Output: Optimal Lagrange multipliers λ^*, ϕ^*, μ^* and ρ^*, optimal results T_1^*, T_2^*, $p_{s,k,n}^*$, $p_{r,k,n}^*$ and $\beta_{k,n}^*$, for $\forall n \in N, k \in K$.

repeat

  Allocate subcarrier n to user k satisfying (21).

  Allocate T_1, T_2, p_s, p_r as

  $T_1 = \frac{1-\lambda}{2}T$;

  $T_2 = \frac{1+\lambda}{2}T$;

  $p_{s,k,n} = [\frac{(1-\lambda)^2}{2(\mu-\phi\omega|h_{sr,n}|^2 l_{sr})} - \frac{1}{\gamma_{sr,k,n}}]^+$;

  $p_{r,k,n} = [\frac{(1+\lambda)^2}{2\phi(1-\omega|h_{rr,n}|^2 l_{rr})} - \frac{1}{\gamma_{rd,k,n}}]^+$;

  Update multipliers

  $\mu(j+1) = \mu(j) + \epsilon_1(\sum_{k=1}^{K}\sum_{n=1}^{N} p_{s,k,n} - p_{max})$;

  $\phi(j+1) = \phi(j) + \epsilon_2\big(\sum_{k=1}^{K}\sum_{n=1}^{N} p_{r,k,n}(1 - \omega|h_{rr,n}|^2 l_{rr}) - \omega\sum_{k=1}^{K}\sum_{n=1}^{N} p_{s,k,n}|h_{sr,n}|^2 l_{sr}\big)$;

  $\lambda(j+1) = \lambda(j) + \epsilon_3\big(\sum_{k=1}^{K}\sum_{n=1}^{N} \beta_{k,n}\log_2(1 + \frac{p_{s,k,n}\gamma_{sr,k,n}}{\beta_{k,n}}) - \sum_{k=1}^{K}\sum_{n=1}^{N} \beta_{k,n}\log_2(1 + \frac{p_{r,k,n}\gamma_{rd,k,n}}{\beta_{k,n}})\big)$;

  $\rho(j+1) = \rho(j) + \epsilon_4(T_1 + T_2 - T)$;

until Convergence

6.4.1 Relative Length of Time Slots in Wireless Power Transfer-Aided Full Duplex Decode-and-Forward Relay Systems

In asymmetric WPT-aided FD relay systems, the length of time slot T_2 is normally longer than that of time slot T_1.

In WPT relay systems, the relay's transmission power is harvested from the source, which is much lower than that at the source due to the channel attenuation from the source to the relay and harvesting efficiency (smaller than 1). As a result, the SINR of the source-relay link overwhelms the SINR of the relay-users link, which confines the value of λ into (0,1), as can be seen from (6.24). Therefore, the value $T_2 = \frac{1+\lambda}{2}T$ is higher than that of $T_1 = \frac{1-\lambda}{2}T$. In some extreme cases that the distance of the relay-destination is much shorter than that of the source-relay, the SINR of the relay-user link may be higher than that of the source-relay link. The multiplier λ in this case may fall into the domain (-1,0) and thus T_1 may be higher than T_2 in order to balance the SE of the two links. In summary, according to the relative SINR of the two links, the proposed asymmetric system can adaptively adjust the value of T_1 and T_2 to maximise the overall end-to-end SE.

6.4.2 Transmission Power Allocation Policy in Wireless Power Transfer-Aided Full Duplex Decode-and-Forward Relay Systems

By the proposed Asym-WPT-FR system, transmission power allocation at the relay is completely different from that in conventional grid-powered FD relay systems.

As can be seen from (6.23), the transmission power at the relay node $p_{r,k,n}$, for $\forall n \in N, k \in K$, is jointly decided by the channel frequency responses $|h_{rr,k,n}|$ and $|h_{rd,k,n}|$. Now, how channel $|h_{rr,k,n}|$ affects the power allocation is investigated. With the same channel response on $|h_{rd,k,n}|$, it can be seen that the proposed Asym-WPT-FR system prefers to assign more power on the subcarrier with a higher value of $|h_{rr,k,n}|$. On the contrary, more transmission power is allocated on the subcarrier with a lower value of $|h_{rr,k,n}|$ in conventional FD grid-powered relay systems [114]. It is because in the proposed algorithm, self-interference is adopted for energy harvesting and more energy can be harvested with a higher value of $|h_{rr,k,n}|$, while self-interference is treated as noise in [114] [115], and therefore the channel frequency response of the self-interference channel should be as low as possible.

6.5 Simulation Results

The performance of the proposed Asym-WPT-FR system is demonstrated in this section, compared with the performance of the following systems:

1) Sym-WPT-FR system [108], where the two time slots are of equal length.

2) TS-WPT-FR system [105], where the relay only harvests energy from the source in the first time slot. In the second time slot, the source transmits signal to the destinations with the help of a FD relay. The self-interference is mitigated as noise at the relay node, and amount of the self-interference cancelled in [105] is set to 80 dB. The values of the time slot durations, T_1 and T_2, are calculated according to ([105], Eq.(16)).

The number of subcarrier is set to $N = 128$ with bandwidth $B = 156$ kHz on each subcarrier. The number of users K is set to 3 except for Fig. (6.4). The single-sided AWGN power spectral density is $N_0 = -174$ dBm/Hz. The PL model for a practical scenario at 900 MHz [112] is adopted as $\text{PL} = 31.7 + 10\theta\log_{10}(d/d_0)$, where $\theta = 2.5$ is the PL exponent, d is the distance between two nodes, and $d_0 = 1$ m is the reference distance. Without loss of generality, it is set that $d_{SD} = d_{SR} + d_{RD} = 100$ m, where d_{SD}, d_{SR} and d_{RD} are the distances of the source-users, the source-relay and the relay-users links. A six-path Rayleigh fading channel with an exponential delay profile and a RMS delay spread of 0.022 us are assumed. The energy harvesting efficiency ω is set to 0.8.

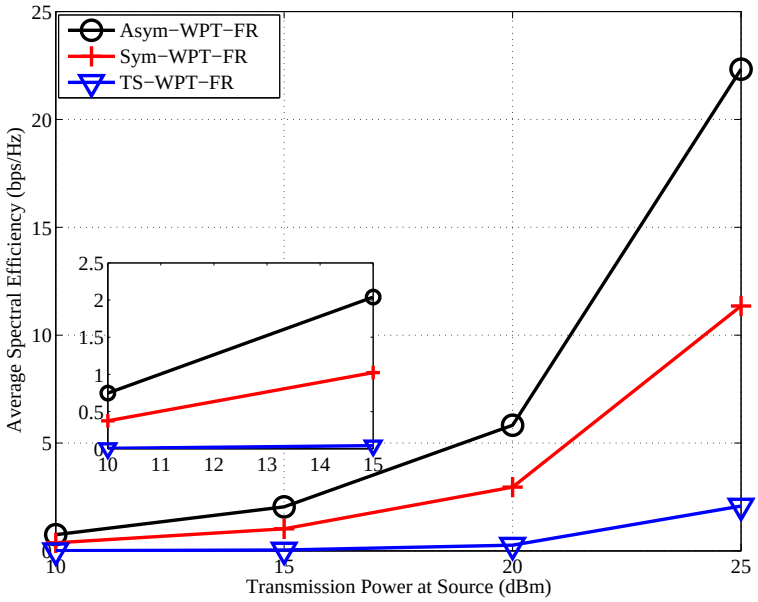

Figure 6.2: Impact of the transmission power at the source on SE performance with $d_{SR} = d_{RD} = 50$ m.

6.5.1 Spectral Efficiency Performance

Fig. 6.2 shows the SE performance of three systems with different transmission power at the source. It can be seen that the proposed Asym-WPT-FR achieves around twice higher SE than the Sym-WPT-FR system. It is because the SE of the two links can be well balanced by the Asym-WPT-FR system, benefiting from the higher degree of freedom. As a comparison, the Sym-WPT-FR system allocates uniform time slots for its source and relay, whereas the effective SINR of the relay-user link is much lower than that of the source-relay link. As a result, the end-to-end SE is bounded by the relay-user link, and the SE of the source-relay link is wasted partially. The TS-WPT-FR shows the poorest SE performance among the three systems. It is because its relay's transmission power is only harvested from the source in the first time slot, and self-interference is not effectively utilised, leading to a low available transmission power at the relay node. Therefore, the SE of the TS-WPT-FR system is limited by its weak transmission power.

Fig. 6.3 demonstrates the SE performance with different relay's position. The proposed Asym-WPT-FR system shows the highest SE among the three systems, showing the robustness on the relay's position. With different relay's position, the SINRs of the source-relay and the relay-user vary, and the Asym-WPT-FR system can adjust the lengths of two time slots to equate the SE of the two hops. Besides, higher SE can be achieved when the relay moves to the middle point between the source and the users, which is because the relay can harvest reasonable energy from source and is

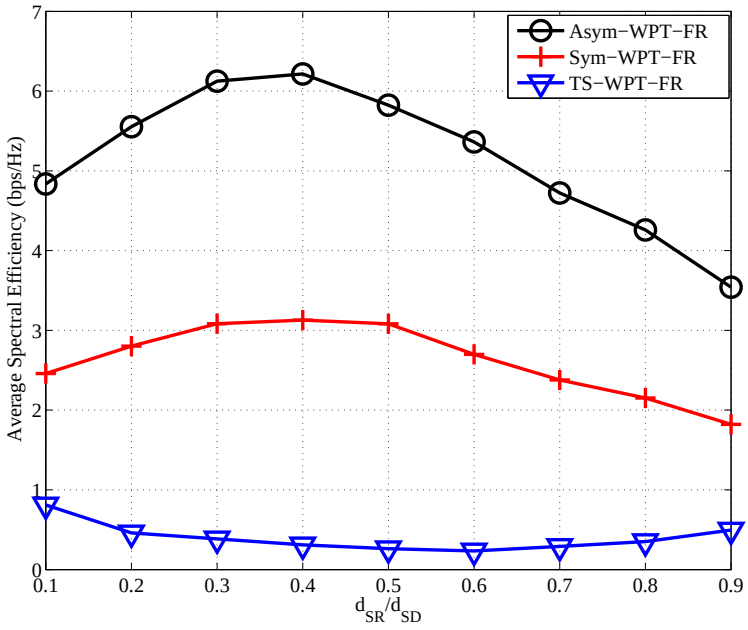

Figure 6.3: Impact of the normalised source-relay distance on SE performance with $d_{SD} = 100$ m and $p_s = 20$ dBm.

not so far from the users around the middle point. While the SE of the TS-WPT-FR system is maximised when the relay is either close to the source or close to the users. It is because in the TS-WPT-FR system, T_2 (used for information transmission only) approaches 40% in the aforementioned two cases and a higher SE is obtained. More insight of time allocation is given in the subsection 6.5.3.

Fig. 6.4 shows the SE performance of three systems with different numbers of users. It can be seen that the SE of the proposed Asym-WPT-FR system increases much faster than others. It is because the diversity of the relay-multiuser link increases with more users, which helps our algorithm maximise the system SE, by adjusting the lengths of the two time slots, and allocating subcarrier and power for multiple users. While the TS-WPT-FR and the Sym-WPT-FR have little increase in SE with the increase of the number of users.

6.5.2 Harvested Energy

Fig. 6.5 demonstrates the harvested energy by the three systems with different transmission power. It can be observed that the proposed Asym-WPT-FR system harvests the most energy, achieving at least 30% improvement than the Sym-WPT-FR system. Since the asymmetric system can allocate more time for the second time slot T_2 to compensate the weak SINR at user end, allowing the relay to have more time to harvest energy concurrently. Besides, in the Asym-WPT-FR system, wireless energy comes

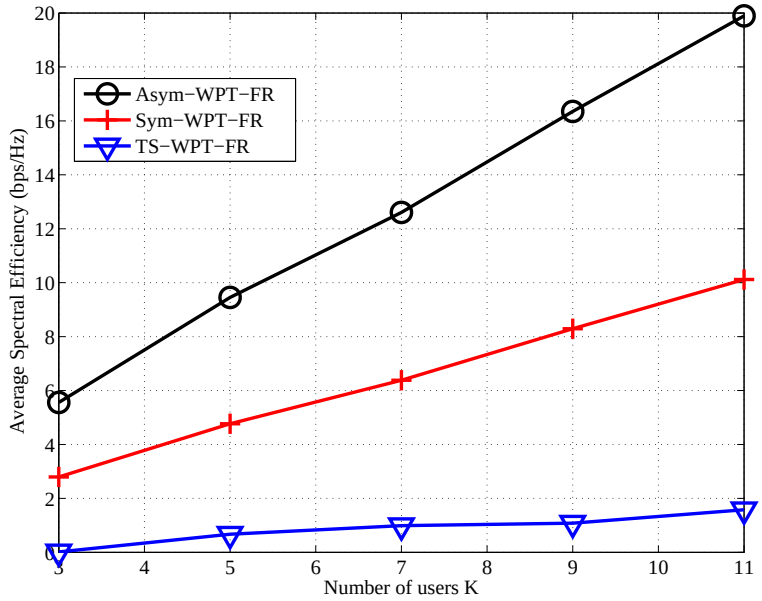

Figure 6.4: Impact of the number of users on SE performance with $d_{SD} = d_{RD} = 50$ m and $p_s = 20$ dBm.

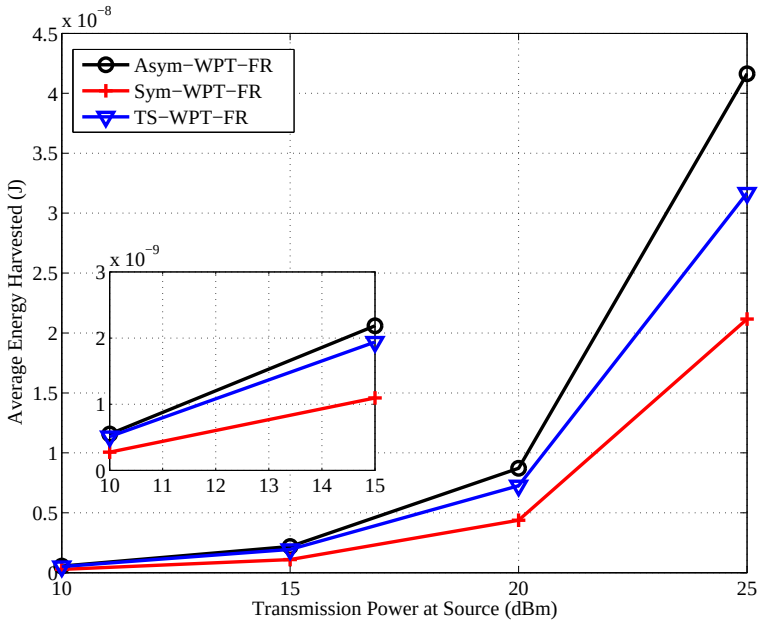

Figure 6.5: Impact of the transmission power on the energy harvested with $d_{SR} = d_{RD} = 50$ m.

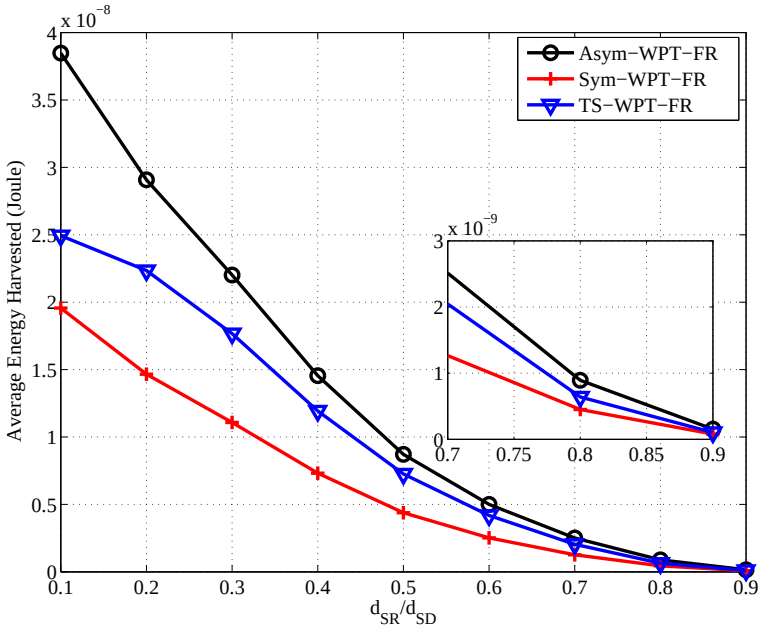

Figure 6.6: Impact of the normalised source-relay distance on the energy harvested with $d_{SD} = 100$ m and $p_s = 20$ dBm.

from both source and relay, which is naturally superior to the TS-WPT-FR system. As a comparison, the TS-WPT-FR system only harvests energy from the source, therefore it shows the lowest harvested energy, only a half of the energy harvested by our Asym-WPT-FR system.

Fig. 6.6, on the other hand, shows the amount of the harvested energy with different relay positions. The proposed Asym-WPT-FR system can harvest more energy than others. Also, it is obvious that the harvested energy decreases given a longer source-relay distance due to the significant signal attenuation.

6.5.3 Time Duration

Fig. 6.7 shows the value of $(T_2 - T_1)/T$ of three systems under different transmission power at the source. In the Asym-WPT-FR system, the length of the first time slot T_1 is slightly increased with a higher transmission power at source. It is because with a higher transmission power at the source, more energy at the relay can be harvested and the SINR of the relay-user link is also improved. System needs to reduce the length of the second time slot T_2 and replenish it to the first time slot T_1. On the contrary, T_1 decreases with a higher transmission power at the source in the TS-WPT-FR system. It is because time slot T_1 is only used for energy harvesting. Wireless energy may be collected quickly given a higher transmission power, and the system can spare more time to the second time slot T_2 for information transmission. While Sym-WPT-FR system allocates uniform time slots, and thus its SE of the source-relay link is wasted

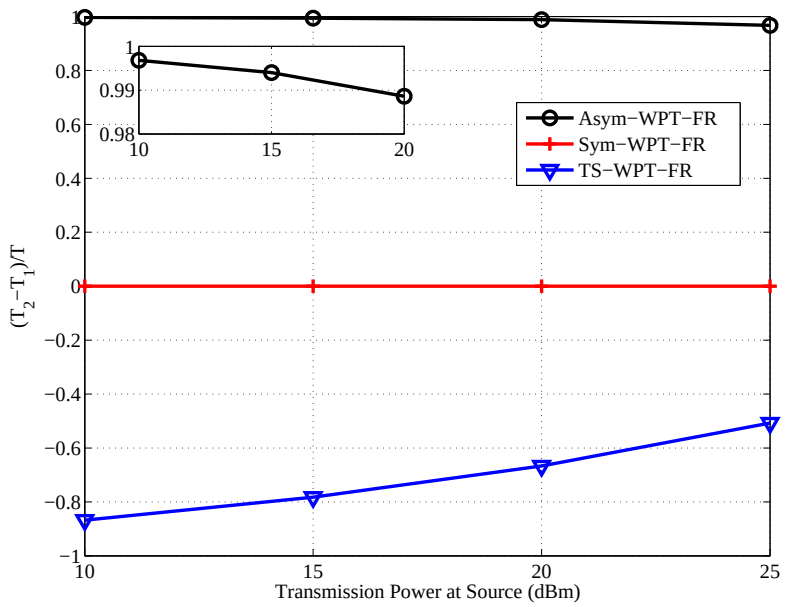

Figure 6.7: Impact of the transmission power on the value of $(T_2 - T_1)/T$ with $d_{SR} = d_{RD} = 50$ m.

partially.

Fig. 6.8 demonstrates the value of $(T_2 - T_1)/T$ with different relay's positions. In the Asym-WPT-FR system, when the relay moves to the middle point, the time slot T_1 is slightly decreased because of the reduced harvested power at the relay, and the system needs to allocate more time for T_2 to remedy the low SINR of the relay-user link. While if the distance of the relay-users link is much shorter than that of the source-relay link, the time slot T_1 begins to improve because the SINR of the source-relay is significantly degraded with a longer source-relay distance. Therefore, system needs to increase the value of T_1 to re-balance the SE of the two links. As comparisons, the Sym-WPT-FR system has uniform time slot duration, which is insensitive to the relay's position. While the TS-WPT-FR system shows converse trend compared to the Asym-WPT-FR algorithm, due to the different information transmission and energy harvesting mechanism.

6.5.4 Convergence Behaviour

Fig. 6.9 shows the convergence behaviour for searching optimal Lagrange multipliers. It can be observed that the optimal Lagrange multipliers can be found within a few iterations, confirming the fast convergence of the proposed algorithm.

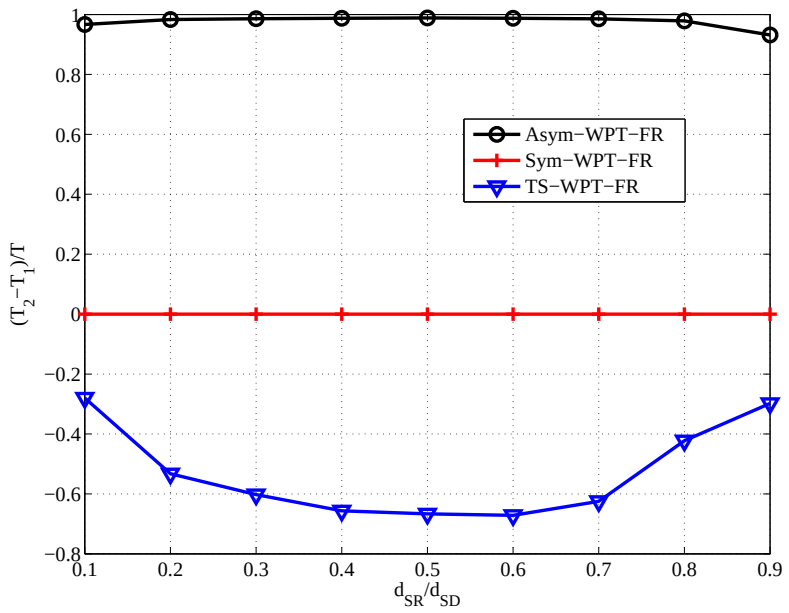

Figure 6.8: Impact of the normalised source-relay distance on the value of $(T_2 - T_1)/T$ with $d_{SD} = 100$ m and $p_s = 20$ dBm.

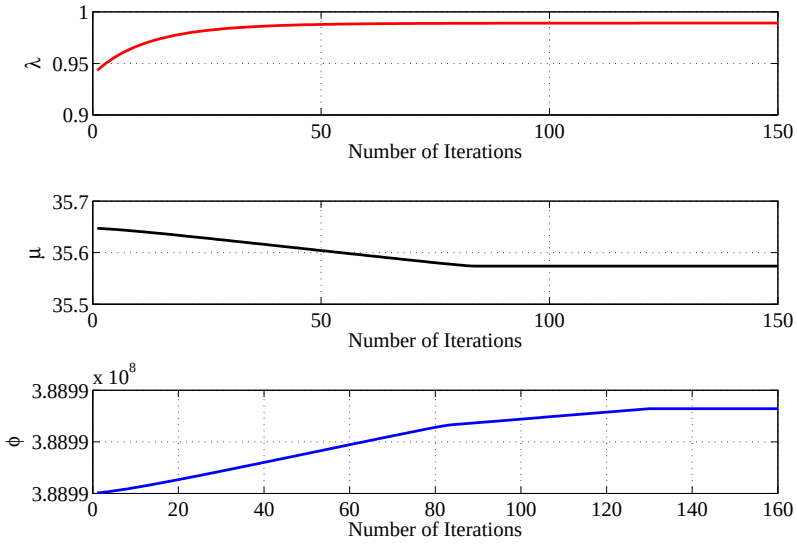

Figure 6.9: Iteration behaviour on finding λ^*, μ^*, and ϕ^*

6.6 Summary

To address the unbalanced SE performances of the source-relay and the relay-multiuser links in WPT-aided relay systems, a novel asymmetric structure has been proposed to allow non-uniform time slot durations for the two hops, achieving higher degree of freedom than the symmetric system [108] and the time-switching based system [105]. A corresponding algorithm is developed to maximise the system SE, by jointly allocating time slot durations and transmission power at the source and the relay, and subcarriers for multiuser. The closed-forms of the optimal results are given. Simulation shows that the proposed Asym-WPT-FR system can achieve approximately twice SE compared to the Sym-WPT-FR [108] and the TS-WPT-FR [105]. By utilising the self-interference at the FD relay, the energy harvested by the proposed Asym-WPT-FR system is 200% and 30% higher than that of the TS-WPT-FR and the Sym-WPT-FR, respectively, showing its high EE and applicability to WPT-supported relay systems. An intensive performance analysis is provided. It is shown that the length of the second time slot T_2 is normally longer than that of the first time slot T_1, due to the fact that the transmission power at the relay is much lower than that at the source caused by channel propagation loss and energy harvesting efficiency. It is also shown that, by harvesting energy from self-interference signal rather than cancelling it, more power is allocated to the subcarriers with higher self-interference channel frequency response. Differently, conventional grid-powered FD relay systems [114] [115] assign more power to the subcarriers with lower self-interference channel frequency response.

Chapter 7

Energy Efficiency Oriented Resource Management for Bi-Directional Full Duplex Distributed Antenna Systems

FD MIMO bi-directional communication [3] is regarded as a promising solution to meet the rapidly increasing demand for high data rate. Unlike the conventional HD MIMO, where uplink and downlink transmission are decoupled into orthogonal time slots or frequencies [116] [117], FD MIMO system allows communication devices to transmit and receive signals simultaneously over the same frequency [114], subject to effective SIC, i.e. natural isolation [42] and analogue/digital domain cancellation [118] [119]. Based on the state-of-the-art SIC operation, SE maximisation issue has been extensively researched to fully exploit the advantage of FD MIMO systems [41] [65] [66] [120]. In [65], an algorithm was proposed to maximise the system ergodic mutual information. In [66] [120], the SE of bidirectional FD MIMO systems were investigated, where a small cell FD BS communicates with multiple single-antenna users in downlink and uplink simultaneously. In [41], a single and multiuser FD MIMO precoding transceiver structure applicable for single-carrier and OFDM systems was presented to maximise SE. More literature review of FD MIMO systems is summarised in Tab. 7.1.

Some fundamental challenges, however, need to be addressed in FD MIMO systems. The first challenge is that both MIMO and FD techniques will require much higher power consumption, which is against the green evolution requirement proposed by the future communication systems. This is because a) MIMO increases the number of active transmit/receive chains, leading to much higher power consumption than SISO configuration [116]. b) For FD systems, additional power consumption is incurred by SIC [10] [16]. Therefore, how to ensure high EE transmission needs to be considered. However, most EE oriented research only focuses on HD one-directional transmission systems [53] [75] [91], which may not be directly applied to bi-directional

Table 7.1: Summary of MIMO FD NETWORKS

Reference	Precoding or decoding method used	Joint or separate beamforming design	Optimisation metric	Antenna array
[2]	ZF	Joint	Throughput maximisation	Co-located
[68]	ZF	Joint	Outage probability minimisation	Co-located
[121]	MMSE	Separate	Bit error rate minimisation	Co-located
[120]	n.a.	Joint	Throughput maximisation	Co-located
[66]	MMSE	Joint	Throughput maximisation	Co-located
[122]	ZF	Joint	Outage probability minimisation	Co-located
[123]	ZF	Separate	Throughput maximisation	Co-located
[124]	ZF	Joint	Outage probability minimisation	Co-located
[125]	ZF	Joint	Throughput maximisation	Co-located
[126]	ZF	Separate	SIC maximisation	Co-located

FD systems due to the residual self-interference, co-channel interference from uplink users to downlink users and multiuser self-interference. The second challenge is with the increased number of centralised antennas, SIC circuit design in analogue/digital domain becomes very complicated. The third challenge lies with the similar level of high PL and correlated small scale fading suffered by the co-located MIMO system.

To this end, centralised FD MIMO can be formulated into a distributed manner. Several advantages may be gained: a) Since the contributions of each distributed antenna (DA) may vary practically due to the location of the users [127], system power consumption can be significantly reduced by only activating those DAs contributing the most; b) With distributed deployment, SIC becomes much easier due to the fact that the self-interference among different DAs can be well controlled in the propagation domain, benefiting from the ideal natural isolation performance. As a result, the circuit design for SIC could be as easy as the SISO case within each FD DA itself; c) The DA system can reduce the large-scale fading impact and obtain blockage-free effect using the multiple DAs distributed geographically [128], helping extend coverage and maintain connectivity of networks. In summary, there is strong evidence showing that, DA system is a remarkable alternative for co-located FD MIMO system. FD cooperative multi-point system was studied in [129], where the antennas can be set to either FD mode or sleep mode based on the state-of-art switch on/off technique [47]. Having only these two modes may not be optimal in some scenarios. For example, if the active antennas are only close to uplink users while are very far from downlink users, these antennas may work in HD (receive) mode to incur lower power consumption and

absence of self-interference. In addition, the authors in [129] set total power minimisation as the optimisation target, which may not be equivalent to EE maximisation. Another EE research of FD systems only assume a SISO [10] [114] or co-located MIMO deployment [2] [60], which are limited in reducing high PL and blockage effect.

In this chapter, a bi-directional DA system is proposed where DAs are capable of working in hybrid duplex mode: FD, HD and sleep, and investigate its EE maximisation with dynamic hybrid duplexing, The effectiveness of the proposed system is verified by simulation results. Our work is different in the following aspects:

- Hybrid duplex mode enables higher degree of freedom and hence much higher EE compared to FD DA systems [129], with just marginal loss in SE. The proposed system also demonstrates significant EE and SE enhancement over FD co-located MIMO systems [66].

- Compared to FD DA and FD co-located MIMO systems, the proposed hybrid duplex system requires much simpler SIC for FD mode, due to less cross talks between distributed antennas.

- EE maximisation is investigated by considering both bi-directional SE and power consumption. This is different from the existing work on SE maximisation alone [65] [66] or total power consumption minimisation alone [129]. Various practical aspects are taken into account for the optimisation, such as residual self-interference at DAs in FD mode, co-channel interference from uplink users to downlink users, and multiuser interference in both uplink and downlink, whereas only self-interference was considered in our previous work on one-directional FD relay systems [10] [114]. Also, the PA dissipated power, circuit power, system fixed power and SIC power are all included in the power consumption model, which is more accurate than the existing models formulated for FD systems [86] [129].

- Low-complexity algorithms are proposed for EE maximisation of the hybrid-duplex system, where a channel gain based DA clustering algorithm is first performed to activate/deactivate transmit/receive chain, which highlights the characteristics of distributed antenna deployment, and a distributed hybrid duplexing (D-HD) based algorithm is then performed to optimise the downlink beamformer and the uplink transmission power.

Notation: Matrices and vectors are represented by boldface capital and lower case letters, respectively. $|\cdot|$ denotes the absolute value of a complex scalar. $||\cdot||$ denotes the Euclidean vector norm. $\boldsymbol{A}^H$ and $\mathrm{Tr}(\boldsymbol{A})$ denote the Hermitian transpose and trace of matrix $\boldsymbol{A}$. $\mathrm{Rank}(\boldsymbol{A})$ denote the rank of matrix $\boldsymbol{A}$. diag $(\boldsymbol{A})$ returns a diagonal matrix

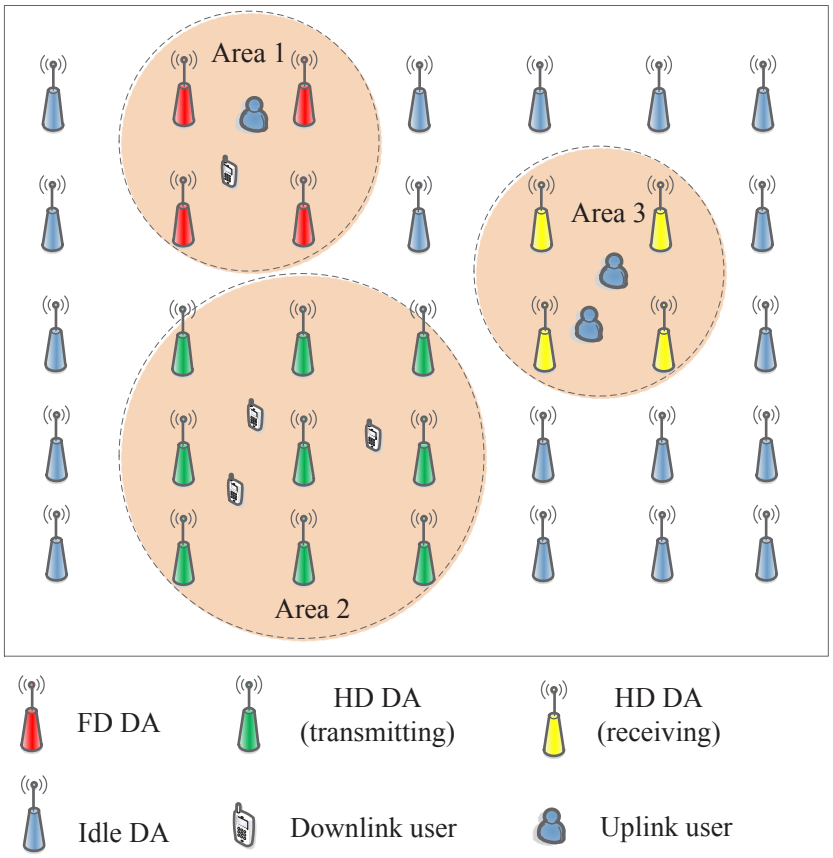

Figure 7.1: Bidirectional hybrid duplexing DA system, with multiple uplink/downlink users.

with diagonal elements from matrix $\boldsymbol{A}$. $\boldsymbol{A} \succeq 0$ means $\boldsymbol{A}$ is a positive semi-definite matrix. Superscript k or u denotes the downlink/uplink user's index.

7.1 System Model and Problem Formulation for Bi-Directional Full Duplex Distributed Antenna Systems

7.1.1 System Model

Assume a bi-directional DA system with one central signal processing unit, which consists of a baseband module and L DAs. All DA ports are connected to the central unit through a noise-free wired front-haul for cooperative communications. The DAs can work in FD, HD (transmit or receive) or sleep mode, while the users employ single-antenna HD for low hardware complexity. In particular, there are U uplink users and K downlink users. It is assumed that the perfect channel state information is obtained by the pilot assisted reciprocal channel estimation [128] [129]. The system model is depicted by Fig. 7.1.

Define a receive chain activation vector $\boldsymbol{r} \in \mathbb{C}^{L\times 1}$, whose $l-th$ element r_l is equal

to 1 if the $l-th$ DA's receive chain is activated, otherwise r_l is equal to 0. Similarly, define a transmit chain activation vector $\boldsymbol{t} \in \mathbb{C}^{L\times 1}$, whose $l-th$ element t_l is equal to 1 if the $l-th$ DA's transmit chain is activated, otherwise t_l is equal to 0. Accordingly, there are four states for each DA, which can be described as 4 tuples. (0, 0) means both receive and transmit chains are deactivated, and thus the DA is in sleep mode. (1, 0) means only receive chain is active while transmit chain is deactivated, and (0, 1) means only transmit chain is active while receive chain is deactivated. The above two cases mean the DA works in HD mode. (1, 1) means both receive and transmit chains are activated and thus the DA works in FD mode. Since the shared-antenna deployment has been extensively researched, where only one antenna set is adopted for simultaneous transmission and reception, and the received and transmitted signal are separated with the help of a duplexer [59], the configuration is reasonable in practice. Define $\boldsymbol{w_k} \in \mathbb{C}^{L\times 1}$ as beamformer at DAs for downlink user $\forall k \in K$. For each vector $\boldsymbol{w_k}$, its element w_k^l denotes the beamforming weight of antenna l for user k. Denote p_u as transmission power allocation at uplink users, for $\forall u \in U$.

7.1.2 Problem Formulation

To maximise the system EE, DA vectors $\boldsymbol{r}, \boldsymbol{t}$, beamformer $\boldsymbol{w_k}$, for $\forall k \in K$, and transmission power p_u, for $u \in U$ are jointly optimised. Define $\eta(\boldsymbol{r}, \boldsymbol{t}, \boldsymbol{w_k}, p_u)$ as EE (in bits/Joule), which is the ratio of the system throughput T_{total} to the incurred total power consumption P_{total}. Accordingly, the EE maximisation problem of the hybrid duplexing DA system is formulated as

$$
\begin{aligned}
P7.1: & \underset{\boldsymbol{r},\boldsymbol{t},\boldsymbol{w_k},p_u,k\in K,u\in U,l\in N}{\operatorname{argmax}} \frac{T_{\text{total}}}{P_{\text{total}}}, \\
s.t.\ & (C1): 0 \le \sum_{k=1}^{K} |w_k^l|^2 \le p_{DA}, \forall l \in L, \\
& (C2): 0 \le p_u \le p_{u,max}, \forall u \in U, \\
& (C3): r_l = \{0,1\}, \forall l \in L, \\
& (C4): t_l = \{0,1\}, \forall l \in L,
\end{aligned}
\tag{7.1}
$$

where constraint $(C1)$ denotes that the allocated transmission power at each DA is non-negative and is upper bounded by p_{DA}, for $\forall l \in L$. $(C2)$ denotes that the transmission power allocated at each uplink user u is non-negative and upper bounded by $p_{u,max}$, for $\forall u \in U$. $(C3)$ denotes the status of the receive chain of DA l, and $(C4)$ denotes the status of the transmit chain of DA l, for $\forall l \in L$.

7.2 Throughput and Power Consumption Analysis

The optimisation problem involves with throughput and power consumption in both downlink and uplink. In this section, the downlink and uplink throughput are analysed in subsection 7.2.1 and 7.2.2, respectively, and then the total power consumption is given in subsection 7.2.3.

7.2.1 Downlink Throughput

In each time slot, the received signal at downlink user k is given by

$$y_k^{DL} = \boldsymbol{h_k} \boldsymbol{w_k} d_k^{DL} + \underbrace{\sum_{k' \neq k}^{K} \boldsymbol{h_k} \boldsymbol{w_{k'}} d_{k'}^{DL}}_{\text{multiuser interference}} + \underbrace{\sum_{u=1}^{U} \sqrt{p_u} e_{u,k} d_u^{UL}}_{\text{co-channel interference}} + z_k, \tag{7.2}$$

where vector $\boldsymbol{h_k} \in \mathbb{C}^{1 \times L}$ is downlink channel between L DAs and downlink user k and captures the PL and small scale fading, whose $l-th$ element $(\boldsymbol{h_k})_l$ presents the channel condition between the $l-th$ DA and downlink user k. $d_k^{DL} \in \mathbb{C}$ is transmit data for downlink user k. $e_{u,k} \in \mathbb{C}$ denotes the channel condition from uplink user u to downlink user k. $d_u^{UL} \in \mathbb{C}$ is transmit data from uplink user u. $z_k \sim CN(0, \sigma_k^2)$ is the complex AWGN at downlink user k. Without loss of generality, it is assumed $\mathbb{E}\{|d_k^{DL}|^2\} = \mathbb{E}\{|d_u^{UL}|^2\} = 1$, for $\forall k \in K$ and $\forall u \in U$.

When the activation/deactivation of transmit chain is considered, the vector $\boldsymbol{t} \in \mathbb{C}^{L \times 1}$ is introduced into equation (7.2), which is transformed into

$$y_k^{DL} = \boldsymbol{h_k}(\boldsymbol{t} \circ \boldsymbol{w_k}) d_k^{DL} + \underbrace{\sum_{k' \neq k}^{K} \boldsymbol{h_k}(\boldsymbol{t} \circ \boldsymbol{w_{k'}}) d_{k'}^{DL}}_{\text{multiuser interference}} + \underbrace{\sum_{u=1}^{U} \sqrt{p_u} e_{u,k} d_u^{UL}}_{\text{co-channel interference}} + z_k, \tag{7.3}$$

where the operator $\circ$ denotes the pair-wise product of two vectors or matrices. For simplicity, auxiliary matrices $\boldsymbol{F_l} = diag\{\underbrace{0, ..., 0}_{l\text{-}1}, 1, \underbrace{0, ..., 0}_{L\text{-}l}\}$ are introduced to transform the pair-wise product $\boldsymbol{t} \circ \boldsymbol{w_k}$ into a simpler form $\boldsymbol{t} \circ \boldsymbol{w_k} = \sum_{l=1}^{L} t_l \boldsymbol{F_l} \boldsymbol{w_k}$. Therefore, equation (7.3) can be re-expressed as

$$y_k^{DL} = \boldsymbol{h_k}(\sum_{l=1}^{L} t_l \boldsymbol{F_l} \boldsymbol{w_k}) d_k^{DL} + \underbrace{\sum_{k' \neq k}^{K} \boldsymbol{h_k}(\sum_{l=1}^{L} t_l \boldsymbol{F_l} \boldsymbol{w_{k'}}) d_{k'}^{DL}}_{\text{multiuser interference}} + \underbrace{\sum_{u=1}^{U} \sqrt{p_u} e_{u,k} d_u^{UL}}_{\text{co-channel interference}} + z_k. \tag{7.4}$$

According to (7.4), the SINR of downlink user k is calculated as

$$\Gamma_k^{DL} = \frac{\left| \boldsymbol{h_k}(\sum_{l=1}^{L} t_l \boldsymbol{F_l} \boldsymbol{w_k}) \right|^2}{\sum_{k' \neq k}^{K} \left| \boldsymbol{h_k}(\sum_{l=1}^{L} t_l \boldsymbol{F_l} \boldsymbol{w_{k'}}) \right|^2 + \sum_{u=1}^{U} p_u \left| e_{u,k} \right|^2 + \sigma_k^2}. \tag{7.5}$$

The total downlink throughput is

$$T_{DL} = \sum_{k=1}^{K} \log_2(1 + \Gamma_k^{DL}), \tag{7.6}$$

where bandwidth is normalized for simplicity. To simplify the mathematical expression, (7.6) is transformed into the structure $\log(1 + \frac{A}{B}) = \log(A + B) - \log B$ as

$$\begin{aligned} T_{DL} = &\sum_{k=1}^{K} \log_2\Big(\sum_{k'=1}^{K} \Big| \boldsymbol{h_k}\Big(\sum_{l=1}^{L} t_l \boldsymbol{F_l} \boldsymbol{w_{k'}}\Big)\Big|^2 + \sum_{u=1}^{U} p_u |e_{u,k}|^2 + \sigma_k^2\Big) - \\ &\sum_{k=1}^{K} \log_2\Big(\sum_{k' \neq k}^{K} \Big| \boldsymbol{h_k}\Big(\sum_{l=1}^{L} t_l \boldsymbol{F_l} \boldsymbol{w_{k'}}\Big)\Big|^2 + \sum_{u=1}^{U} p_u |e_{u,k}|^2 + \sigma_k^2\Big). \end{aligned} \tag{7.7}$$

By defining matrices $\boldsymbol{H_k} = \boldsymbol{h_k^H h_k}$ and $\boldsymbol{W_k} = \boldsymbol{w_k w_k^H}$, the overall downlink throughput is given by (7.8).

$$\begin{aligned} T_{DL} = &\sum_{k=1}^{K} \log_2\Big(\sum_{k'=1}^{K} \mathrm{Tr}\Big(\sum_{m=1}^{L}\sum_{n=1}^{L} t_m t_n \boldsymbol{F_m} \boldsymbol{W_{k'}} \boldsymbol{F_n^H} \boldsymbol{H_k}\Big) + \sum_{u=1}^{U} p_u |e_{u,k}|^2 + \sigma_k^2\Big) \\ &- \sum_{k=1}^{K} \log_2\Big(\sum_{k' \neq k}^{K} \mathrm{Tr}\Big(\sum_{m=1}^{L}\sum_{n=1}^{L} t_m t_n \boldsymbol{F_m} \boldsymbol{W_{k'}} \boldsymbol{F_n^H} \boldsymbol{H_k}\Big) + \sum_{u=1}^{U} p_u |e_{u,k}|^2 + \sigma_k^2\Big). \end{aligned} \tag{7.8}$$

7.2.2 Uplink Throughput

In uplink, define self-interference channel matrix $\boldsymbol{h_{SI}} \in \mathbb{C}^{L \times L}$, whose element $(\boldsymbol{h_{SI}})_{ij}$ represents the channel condition from the $j-th$ DA to the $i-th$ DA. Specifically, the diagonal entry $(\boldsymbol{h_{SI}})_{ii}$, for $\forall i \in L$, represents the $i-th$ DA's self-interference channel. The self-interference signal is the downlink transmitted signal from the DAs, and thus can be calculated as $\sum_{k=1}^{K}\sum_{l=1}^{L} t_l \boldsymbol{F_l} \boldsymbol{w_k} d_k^{DL}$. Define an SIC amount α as the ratio of post-SIC self-interference power over the pre-SIC self-interference power. The residual self-interference after SIC is thus given by $\frac{1}{\sqrt{\alpha}} \boldsymbol{h_{SI}} \sum_{k=1}^{K}\sum_{l=1}^{L} t_l \boldsymbol{F_l} \boldsymbol{w_k} d_k^{DL}$, and the uplink received signal at the DAs is given by

$$\boldsymbol{y}^{UL} = \sum_{u=1}^{U} \sqrt{p_u} \boldsymbol{g_u} d_u^{UL} + \underbrace{\frac{1}{\sqrt{\alpha}} \boldsymbol{h_{SI}} \sum_{k=1}^{K}\sum_{l=1}^{L} t_l \boldsymbol{F_l} \boldsymbol{w_k} d_k^{DL}}_{\text{residual self-interference}} + \boldsymbol{z}, \tag{7.9}$$

where vector $\boldsymbol{g_u} \in \mathbb{C}^{L \times 1}$ is the uplink channel from user u to L DAs, whose element $(\boldsymbol{g_u})_l$ presents the channel condition between the $l-th$ DA and uplink user u. Vector $\boldsymbol{z} \in \mathbb{C}^{L \times 1}, \sim CN(0, \sigma^2 \boldsymbol{I_L})$ is the AWGN receive noise. It is assumed that the central

unit employs a linear maximum ratio combining (MRC) receiver [129] [1], $\boldsymbol{v_u} \in \mathbb{C}^{L\times 1}$, for decoding of the received $u-th$ uplink user information, which is given by $\boldsymbol{v_u} = \sum_{i=1}^{L} r_i \boldsymbol{F_i} \boldsymbol{g_u}$. It is obvious that $r_i = 0$ means the receive chain of the $i-th$ DA is deactivated. As a result, the equivalent SINR for uplink user u is given by (7.10)

$$\Gamma_u^{UL} = \frac{p_u |\boldsymbol{v_u}^H \boldsymbol{g_u}|^2}{\sum_{u'\neq u}^{U} p_{u'} |\boldsymbol{v_u}^H \boldsymbol{g_{u'}}|^2 + \frac{1}{\alpha}\left|\boldsymbol{v_u}^H \boldsymbol{h_{SI}} \sum_{k=1}^{K}\sum_{l=1}^{L} t_l \boldsymbol{F_l} \boldsymbol{w_k}\right|^2 + ||\boldsymbol{v_u}||^2 \sigma^2}. \tag{7.10}$$

Therefore, the total achievable uplink throughput is given by

$$T_{UL} = \sum_{u=1}^{U} \log_2(1+\Gamma_u^{UL}). \tag{7.11}$$

By defining $\boldsymbol{G_u} = \boldsymbol{g_u}\boldsymbol{g_u}^H$ and substituting $\boldsymbol{v_u} = \sum_{i=1}^{L} r_i \boldsymbol{F_i} \boldsymbol{g_u}$ into (7.11), the overall uplink throughput is finally given by (7.12)

$$\begin{aligned} T_{UL} = &\sum_{u=1}^{U} \log_2\Bigg(\sum_{u'=1}^{U} p_{u'} \mathrm{Tr}(\boldsymbol{G_{u'}} \sum_{i=1}^{L}\sum_{j=1}^{L} r_i r_j \boldsymbol{F_i} \boldsymbol{G_u} \boldsymbol{F_j}^H) + \sigma^2 \mathrm{Tr}(\sum_{i=1}^{L}\sum_{j=1}^{L} r_i r_j \mathbf{F}_i \mathbf{G}_u \mathbf{F}_j^H) \\ &+ \frac{1}{\alpha}\mathrm{Tr}\big(\mathrm{diag}(\boldsymbol{h_{SI}}(\sum_{k=1}^{K}\sum_{m=1}^{L}\sum_{n=1}^{L} t_m t_n \boldsymbol{F_m} \boldsymbol{W_k} \boldsymbol{F_n}^H)\boldsymbol{h_{SI}}^H)(\sum_{i=1}^{L}\sum_{j=1}^{L} r_i r_j \boldsymbol{F_i} \boldsymbol{G_u} \boldsymbol{F_j}^H)\big)\Bigg) \\ &- \sum_{u=1}^{U} \log_2\Bigg(\sum_{u'\neq u}^{U} p_{u'} \mathrm{Tr}(\boldsymbol{G_{u'}} \sum_{i=1}^{L}\sum_{j=1}^{L} r_i r_j \boldsymbol{F_i} \boldsymbol{G_u} \boldsymbol{F_j}^H) + \sigma^2 \mathrm{Tr}(\sum_{i=1}^{L}\sum_{j=1}^{L} r_i r_j \boldsymbol{F_i} \boldsymbol{G_u} \boldsymbol{F_j}^H) \\ &+ \frac{1}{\alpha}\mathrm{Tr}\big(\mathrm{diag}(\boldsymbol{h_{SI}}(\sum_{k=1}^{K}\sum_{m=1}^{L}\sum_{n=1}^{L} t_m t_n \boldsymbol{F_m} \boldsymbol{W_k} \boldsymbol{F_n}^H)\boldsymbol{h_{SI}}^H)(\sum_{i=1}^{L}\sum_{j=1}^{L} r_i r_j \boldsymbol{F_i} \boldsymbol{G_u} \boldsymbol{F_j}^H)\big)\Bigg) \end{aligned} \tag{7.12}$$

7.2.3 Power Consumption

The power consumption model mainly consists of: PA power consumption, circuit power consumption, system fixed power consumption and SIC power consumption [53] [62] [128].

a) The PA power is closely related to the beamforming weight at DAs, uplink transmission power at users and drain efficiency of PA, which is calculated as $\frac{1}{\omega}\big(\mathrm{Tr}(\sum_{k=1}^{K}\boldsymbol{W_k}) + \sum_{u=1}^{U} p_u\big)$ [129]. ω is the drain efficiency of PAs. Without loss of generality, it is assumed that all PAs (of DAs and users) have the same DE performance.

b) Circuit power consumption is proportional to the number of active transmit and receive chains, including the power consumed by DAC, filter, synthesiser, electrical/optical (E/O) converter, etc. Circuit power consumption can be calculated as

[1] It is known that MRC provides a performance close to minimum mean square error (MMSE) beamforming given a large number of antennas [130]. Besides, since the coupling between $\boldsymbol{r}, \boldsymbol{t}, \boldsymbol{W_k}$ and the residual self-interference at DAs, it is difficult to derive a tractable solution by applying MMSE or zero-forcing receive beamforming.

$\sum_{l=1}^{L}\big((1-r_l)(1-t_l)p_{idle}\big)+\sum_{l=1}^{L}(r_l p_{c,r})+\sum_{l=1}^{L}(t_l p_{c,t})$, where $p_{c,t}$ and $p_{r,t}$ denote the circuit power consumed by active receive and transmit chains, respectively. p_{idle} denotes the circuit power consumption of each sleeping DA.

c) System fixed power consumption p_{fix} is the power consumed by power supply, active cooling system at central unit and/or DAs, etc, which is independent of the state of transmit/receive chain.

d) For the DAs working in FD mode, i.e. $r_l = 1$ and $t_l = 1$, for $\forall l \in L$, additional power is required for SIC, which is related to the specific SIC circuit design [2], and can be considered as a constant value [43] [131]. Define p_{can} as the power required by SIC at each DA, and the overall power consumed by SIC is given as $\sum_{l=1}^{L}(r_l t_l p_{can})$ [3]. Finally, the total power consumption is given as

$$P_{\text{total}} = \underbrace{\frac{1}{\omega}\big(\text{Tr}(\sum_{k=1}^{K}\boldsymbol{W_k})+\sum_{u=1}^{U}p_u\big)}_{\text{PA power}}+\underbrace{\sum_{l=1}^{L}(t_l r_l p_{can})}_{\text{SIC power}}+p_{fix}+ \underbrace{\sum_{l=1}^{L}\big((1-r_l)(1-t_l)p_{idle}\big)+\sum_{l=1}^{L}(r_l p_{c,r})+\sum_{l=1}^{L}(t_l p_{c,t})}_{\text{circuit power}}. \tag{7.13}$$

7.3 EE Oriented Activation/Deactivation of Distributed Antennas, Downlink Beamformer and Uplink Transmission Power

According to the throughput and power consumption analysis in Section 7.2, the optimisation problem $P7.1$ is re-formulated into

[2] Generally speaking, complex SIC scheme needs more involved components and consumes higher power. For example, the AC operation design in [3] needs DAC, transmit radio unit and adder to mitigate self-interference. Another kind of AC design in [16] uses tunable attenuator and delay unit to route the estimated signal to the receiver for SIC.

[3] Herein, analogue or digital of SIC is only required within each FD DA itself, which is because the self-interference among different DAs can be well controlled in the propagation domain benefiting from the high PL. Also, SIC operation across different DAs imposes high complexity for hardware design. More details can be referred in [3] for co-located FD MIMO systems.

$$
\begin{aligned}
P7.2: & \underset{\boldsymbol{r},\boldsymbol{t},\boldsymbol{W_k},p_u,k\in K,u\in U,l\in L}{\operatorname{argmax}} \frac{T_{DL}(\boldsymbol{r},\boldsymbol{t},\boldsymbol{W_k},p_u)+T_{UL}(\boldsymbol{r},\boldsymbol{t},\boldsymbol{W_k},p_u)}{P_{\text{total}}(\boldsymbol{r},\boldsymbol{t},\boldsymbol{W_k},p_u)}, \\
s.t.\ & (\widetilde{C1}): \sum_{k=1}^{K} \text{Tr}(\boldsymbol{W_k}\boldsymbol{F_l}) \leq p_{DA}, \forall l \in L, \\
& (C2), (C3), (C4), \\
& (C5): \boldsymbol{W_k} \succeq 0, \forall k \in K, \\
& (C6): \text{Rank}(\boldsymbol{W_k}) = 1, \forall k \in K,
\end{aligned}
\tag{7.14}
$$

where constraint $(\widetilde{C1})$ denotes the transmission power at each DA is upper bounded by p_{DA}, for $\forall l \in L$. $(C5)$ and $(C6)$ are imposed to guarantee that $\boldsymbol{W_k} = \boldsymbol{w_k}\boldsymbol{w_k}^H$ holds after optimisation.

The problem in $P7.2$ is generally very difficult to solve. It involves a) vectors $\boldsymbol{r}, \boldsymbol{t}$ with binary elements in the objective function. Furthermore, the combinational constraints in $(C3), (C4)$ increase the difficulty in finding the optimal solution. b) product of binary variables t_m, t_n, r_i, r_j with continuous variables $\boldsymbol{W_k}, p_u$, for $\forall k \in K, u \in U$ and $\forall m, n, i, j \in L$. c) rank constraint in $(C6)$. Besides, with L DAs, there are 4^L possibilities of DA configurations. It is prohibitive to find the global optimum in terms of computational complexity and thus a low-complexity suboptimal algorithm is desirable. In the subsection 7.3.1, a channel-gain-based algorithm is first proposed to perform DAs activation/deactivation, which effectively removes the binary variables in the objective and in the constraints $(C3)$ $(C4)$, and the product between binary variables with continuous variables. After this, a novel D-HD algorithm is proposed to optimise beamformer $\boldsymbol{W_k}$, for $\forall k \in K$ and transmission power p_u, for $\forall u \in U$, in subsection 7.3.2. At last, total complexity is given in subsection 7.3.3.

7.3.1 Activation/Deactivation of Transmit/Receive Chains at Distributed Antennas

Intuitively, if the channel gain between the $l-th$ DA and uplink users is strong, while the channel gain between the DA and downlink users is poor, the $l-th$ DA should work in HD receive mode. Since if the DA works in FD mode, its downlink throughput contribution is marginal for all downlink users, while more power consumption is required. More importantly, the downlink transmission corrupts its uplink reception due to the introduced self-interference. Conversely, the DA should work in HD transmit mode, if the channel gain between the DA and uplink users is poor while the channel gain between the DA and downlink users is strong. Also, one DA can work in FD mode if it has good channel condition in both uplink and downlink, which contributes reasonable throughput bidirectionally with affordable power consumption. At last, the DA can be

turned-off to save power consumption if it has poor channel condition from all users.

To implement the DA clustering algorithm, a threshold, i.e. ψ, is needed for judgement. The threshold can be adjusted according to different QoS requirements and DA density. For example, one can increase ψ if power consumption requirement is stringent. It means less DAs will be activated and therefore power consumption is decreased. If users' SE requirement is stringent, on the other hand, one can decrease the value of ψ, it means more DAs will be activated. Also, for a dense DA deployment, the value of ψ could be higher than a sparse deployment. The whole DA clustering algorithm is presented in Algorithm 5, then downlink beamformer and uplink transmission power allocation are ready to perform.

Algorithm 5 DA clustering algorithm

Input: $\boldsymbol{h_k}, \boldsymbol{g_u}$ for $\forall k \in k, u \in U$, and the threshold ψ.
Output: Transmit/receive chains vector $\boldsymbol{r}^*$, $\boldsymbol{t}^*$.

for $l = 1, ..., L$ **do**
  for $u = 1, ..., U$ **do**
    Calculate the channel condition between the $l - th$ DA and uplink user u.
    if $(\boldsymbol{g_u})_l \geq \psi$ **then**
      $r_l = 1$, break.
    else
      $r_l = 0$.
    end if
  end for
  for $k = 1, ..., K$ **do**
    Calculate the channel condition between the $l - th$ DA and downlink user k.
    if $(\boldsymbol{h_k})_l \geq \psi$ **then**
      $t_l = 1$, break.
    else
      $t_l = 0$.
    end if
  end for
end for
return $\boldsymbol{r}^*$, $\boldsymbol{t}^*$.

7.3.2 Design of Downlink Beamformer at DAs and Uplink Transmission Power at Users

For simplicity, a super matrix $\boldsymbol{W} = \{\boldsymbol{W_1}, \boldsymbol{W_2}, ..., \boldsymbol{W_K}\}$ is defined, including all beamformer variables $\boldsymbol{W_k}, \forall k \in K$. Define a vector $\boldsymbol{p} = \{p_1, p_2, ..., p_U\}$, including all uplink transmission power variables $p_u, \forall u \in U$. The feasible domain confined by the constraints is expressed as $\boldsymbol{\Theta}$. Then the optimisation problem goes into

$$P7.3: \underset{\boldsymbol{W},\boldsymbol{p}\in\boldsymbol{\Theta}}{\operatorname{argmax}} \frac{T_{DL}(\boldsymbol{W},\boldsymbol{p})+T_{UL}(\boldsymbol{W},\boldsymbol{p})}{P_{\text{total}}(\boldsymbol{W},\boldsymbol{p})}, \quad s.t.\ (\widetilde{C1}),(C2),(C5),(C6). \tag{7.15}$$

For the overall throughput $T_{DL}(\boldsymbol{W},\boldsymbol{p})+T_{UL}(\boldsymbol{W},\boldsymbol{p})$, all the positive parts are collected into $f_1(\boldsymbol{W},\boldsymbol{p})$, while the negative parts are collected into $f_2(\boldsymbol{W},\boldsymbol{p})$. Then the overall throughput can be expressed as $f_1(\boldsymbol{W},\boldsymbol{p})-f_2(\boldsymbol{W},\boldsymbol{p})$, where $f_1(\boldsymbol{W},\boldsymbol{p})$ and $f_2(\boldsymbol{W},\boldsymbol{p})$ are given by (7.16) and (7.17), respectively.

$$\begin{aligned} f_1(\boldsymbol{W},\boldsymbol{p}) = &\sum_{k=1}^{K}\log_2\Big(\sum_{k'=1}^{K}\mathrm{Tr}(\sum_{m=1}^{L}\sum_{n=1}^{L}t_m t_n \boldsymbol{F_m}\boldsymbol{W_{k'}}\boldsymbol{F_n}^H\boldsymbol{H_k})+\sum_{u=1}^{U}p_u|e_{u,k}|^2+\sigma_k^2\Big)+\\ &\sum_{u=1}^{U}\log_2\Big(\sum_{u'=1}^{U}p_{u'}\mathrm{Tr}(\boldsymbol{G_{u'}}\sum_{i=1}^{L}\sum_{j=1}^{L}r_i r_j\boldsymbol{F_i}\boldsymbol{G_u}\boldsymbol{F_j}^H)+\sigma^2\mathrm{Tr}(\sum_{i=1}^{L}\sum_{j=1}^{L}r_i r_j\boldsymbol{F_i}\boldsymbol{G_u}\boldsymbol{F_j}^H)+\\ &\frac{1}{\alpha}\mathrm{Tr}\big(\mathrm{diag}(\boldsymbol{h_{SI}}(\sum_{k=1}^{K}\sum_{m=1}^{L}\sum_{n=1}^{L}t_m t_n\boldsymbol{F_m}\boldsymbol{W_k}\boldsymbol{F_n}^H)\boldsymbol{h_{SI}}^H)(\sum_{i=1}^{L}\sum_{j=1}^{L}r_i r_j\boldsymbol{F_i}\boldsymbol{G_u}\boldsymbol{F_j}^H)\big)\Big). \end{aligned} \tag{7.16}$$

$$\begin{aligned} f_2(\boldsymbol{W},\boldsymbol{p}) = &\sum_{k=1}^{K}\log_2\Big(\sum_{k'\neq k}^{K}\mathrm{Tr}(\sum_{m=1}^{L}\sum_{n=1}^{L}t_m t_n \boldsymbol{F_m}\boldsymbol{W_{k'}}\boldsymbol{F_n}^H\boldsymbol{H_k})+\sum_{u=1}^{U}p_u|e_{u,k}|^2+\sigma_k^2\Big)+\\ &\sum_{u=1}^{U}\log_2\Big(\sum_{u'\neq u}^{U}p_{u'}\mathrm{Tr}(\boldsymbol{G_{u'}}\sum_{i=1}^{L}\sum_{j=1}^{L}r_i r_j\boldsymbol{F_i}\boldsymbol{G_u}\boldsymbol{F_j}^H)+\sigma^2\mathrm{Tr}(\sum_{i=1}^{L}\sum_{j=1}^{L}r_i r_j\boldsymbol{F_i}\boldsymbol{G_u}\boldsymbol{F_j}^H)+\\ &\frac{1}{\alpha}\mathrm{Tr}\big(\mathrm{diag}(\boldsymbol{h_{SI}}(\sum_{k=1}^{K}\sum_{m=1}^{L}\sum_{n=1}^{L}t_m t_n\boldsymbol{F_m}\boldsymbol{W_k}\boldsymbol{F_n}^H)\boldsymbol{h_{SI}}^H)(\sum_{i=1}^{L}\sum_{j=1}^{L}r_i r_j\boldsymbol{F_i}\boldsymbol{G_u}\boldsymbol{F_j}^H)\big)\Big). \end{aligned} \tag{7.17}$$

Obviously, $f_1(\boldsymbol{W},\boldsymbol{p})$ and $f_2(\boldsymbol{W},\boldsymbol{p})$ are both jointly-concave with respect to the variables $\boldsymbol{W},\boldsymbol{p}$ in the considered domain $\boldsymbol{\Theta}$, and the FW method can be adopted to handle the difference of two concave functions. The Frank-Wolfe (FW) method approximates of the minus part $f_2(\boldsymbol{W},\boldsymbol{p})$ by its first order Taylor series $f_2^{(n)}(\boldsymbol{W},\boldsymbol{p})$, and updates the approximation $f_2^{(n)}(\boldsymbol{W},\boldsymbol{p})$ iteratively along the direction that approaches the original function $f_2(\boldsymbol{W},\boldsymbol{p})$ [66]. Suppose the value of $\boldsymbol{W},\boldsymbol{p}$ is denoted by $\boldsymbol{W^{(n)}},\boldsymbol{p^{(n)}}$ and $f_2(\boldsymbol{W},\boldsymbol{p})$ is approximated by $f_2^{(n)}(\boldsymbol{W},\boldsymbol{p})$ at the n-th iteration. Since the total throughput $f_1(\boldsymbol{W},\boldsymbol{p})-f_2^{(n)}(\boldsymbol{W},\boldsymbol{p})$ is the lower bound of the original one $f_1(\boldsymbol{W},\boldsymbol{p})-f_2(\boldsymbol{W},\boldsymbol{p})$, the variables $\boldsymbol{W^{(n)}},\boldsymbol{p^{(n)}}$ are iteratively updated and the lower bound increases after every iteration. Because of the power consumption is upper bounded by constraints, the iterative procedure is guaranteed to converge. Since $f_2(\boldsymbol{W},\boldsymbol{p})$ is concave and differentiable on the considered domain, one can easily find its first-order approximation by (7.18)

$$
\begin{aligned}
&f_2^{(n)}(\boldsymbol{W},\boldsymbol{p}) = f_2(\boldsymbol{W^{(n)}},\boldsymbol{p^{(n)}}) + \sum_{k=1}^{K}(a_k^{(n)})^{-1}\sum_{u=1}^{U}(p_u - p_u^{(n)})|e_{u,k}|^2 + \\
&\sum_{k=1}^{K}(a_k^{(n)})^{-1}\sum_{k'\neq k}^{K}\mathrm{Tr}\Big(\sum_{m=1}^{L}\sum_{n=1}^{L}t_m t_n \boldsymbol{F_m}(\boldsymbol{W_{k'}} - \boldsymbol{W_{k'}^{(n)}})\boldsymbol{F_n}^H\boldsymbol{H_k}\Big) + \\
&\sum_{u=1}^{U}(b_u^{(n)})^{-1}\sum_{u'\neq u}^{U}(p_{u'} - p_{u'}^{(n)})\mathrm{Tr}\big(\boldsymbol{G_{u'}}\sum_{i=1}^{L}\sum_{j=1}^{L}r_i r_j \boldsymbol{F_i}\boldsymbol{G_u}\boldsymbol{F_j^H}\big) + \\
&\sum_{u=1}^{U}\Bigg((b_u^{(n)})^{-1}\frac{1}{\alpha}\mathrm{Tr}\big(\mathrm{diag}(\boldsymbol{h_{SI}}(\sum_{k=1}^{K}\sum_{m=1}^{L}\sum_{n=1}^{L}t_m t_n \boldsymbol{F_m}(\boldsymbol{W_k} - \boldsymbol{W_k^{(n)}})\boldsymbol{F_n}^H)\boldsymbol{h_{SI}}^H) \\
&(\sum_{i=1}^{L}\sum_{j=1}^{L}r_i r_j \boldsymbol{F_i}\boldsymbol{G_u}\boldsymbol{F_j}^H)\big)\Bigg)
\end{aligned}
\tag{7.18}
$$

where $(a_k^{(n)}) = \sum_{k'\neq k}^{K}\mathrm{Tr}(\sum_{i=1}^{L}\sum_{j=1}^{L}t_m t_n \boldsymbol{F_m}\boldsymbol{W_{k'}^{(n)}}\boldsymbol{F_n}^H\boldsymbol{H_k}) + \sum_{u=1}^{U}p_u^{(n)}|e_{u,k}|^2 + \sigma_k^2$, and $(b_u^{(n)}) = \sigma^2\mathrm{Tr}(\sum_{i=1}^{L}\sum_{j=1}^{L}r_i r_j \boldsymbol{F_i}\boldsymbol{G_u}\boldsymbol{F_j}^H) + \sum_{u'\neq u}^{U}(p_{u'}^{(n)})\mathrm{Tr}(\sum_{i=1}^{L}\sum_{j=1}^{L}r_i r_j \boldsymbol{F_i}\boldsymbol{G_u}\boldsymbol{F_j}^H) + \frac{1}{\alpha}\mathrm{Tr}\big(\mathrm{diag}(\boldsymbol{h_{SI}}(\sum_{k=1}^{K}\sum_{m=1}^{L}\sum_{n=1}^{L}t_m t_n \boldsymbol{F_m}\boldsymbol{W_k^{(n)}}\boldsymbol{F_n}^H)\boldsymbol{h_{SI}}^H)(\sum_{i=1}^{L}\sum_{j=1}^{L}r_i r_j \boldsymbol{F_i}\boldsymbol{G_u}\boldsymbol{F_j}^H)\big)$.

Now, the overall throughput is re-expressed as $f_1(\boldsymbol{W},\boldsymbol{p}) - f_2^{(n)}(\boldsymbol{W},\boldsymbol{p})$, which is jointly-concave with respect to the variables. It is because $f_1(\boldsymbol{W},\boldsymbol{p})$ is jointly-concave, and $f_2^{(n)}(\boldsymbol{W},\boldsymbol{p})$ is affine with respect to all variables $\boldsymbol{W},\boldsymbol{p} \in \{\boldsymbol{\Theta}\}$. The optimisation problem can be expressed as

$$
\begin{aligned}
&P7.4 : \underset{\boldsymbol{W},\boldsymbol{p}\in\boldsymbol{\Theta}.}{\mathrm{argmax}}\ \frac{f_1(\boldsymbol{W},\boldsymbol{p}) - f_2^{(n)}(\boldsymbol{W},\boldsymbol{p})}{P_{\mathrm{total}}(\boldsymbol{W},\boldsymbol{p})}, \\
&s.t.\ (\widetilde{C1}), (C2), (C5), (C6).
\end{aligned}
\tag{7.19}
$$

Since the problem P7.4 is the ratio between a concave function and an affine function in the consider domain, Theorem 7.1 is introduced to solve the problem.

Theorem 7.1: The reformulated EE, $\dfrac{f_1(\boldsymbol{W},\boldsymbol{p}) - f_2^{(n)}(\boldsymbol{W},\boldsymbol{p})}{P_{\mathrm{total}}(\boldsymbol{W},\boldsymbol{p})}$, is jointly quasi-concave with respect to the variables $\boldsymbol{W},\boldsymbol{p}$ in the feasible domain.

Proof of Theorem 7.1 is similar to the proof or Theorem 4,1, and thus is omitted.

Theorem 7.1 confirms that there is a global optimal EE in the feasible domain. For the fractional structured quasi-concave problem in (19), $\beta = \frac{f_1(\boldsymbol{W},\boldsymbol{p}) - f_2^{(n)}(\boldsymbol{W},\boldsymbol{p})}{p_{\mathrm{total}}(\boldsymbol{W},\boldsymbol{p})}$, can be associated with a subtract programming $f_1(\boldsymbol{W},\boldsymbol{p}) - f_2^{(n)}(\boldsymbol{W},\boldsymbol{p}) - \beta p_{\mathrm{total}}(\boldsymbol{W},\boldsymbol{p})$ [132] [71]. Assume that β^* is the optimal value of (7.19), it is obvious that maximising (7.19) is equivalent to finding the root of $f_1(\boldsymbol{W},\boldsymbol{p}) - f_2^{(n)}(\boldsymbol{W},\boldsymbol{p}) - \beta^* P_{\mathrm{total}}(\boldsymbol{W},\boldsymbol{p})$, as proven in Appendix H. Therefore, with the equivalent subtract programming, the problem turns into solving $f_1(\boldsymbol{W},\boldsymbol{p}) - f_2^{(n)}(\boldsymbol{W},\boldsymbol{p}) - \beta^* P_{\mathrm{total}}(\boldsymbol{W},\boldsymbol{p})$ with a given β.

$$
\begin{aligned}
&P7.5: \underset{\boldsymbol{W},\boldsymbol{p}\in\boldsymbol{\Theta}.}{\operatorname{argmax}} f_1(\boldsymbol{W},\boldsymbol{p}) - f_2^{(n)}(\boldsymbol{W},\boldsymbol{p}) - \beta P_{\text{total}}(\boldsymbol{W},\boldsymbol{p}),\\
&s.t.\ (\widetilde{C1}), (C2), (C5), (C6).
\end{aligned} \tag{7.20}
$$

For the rank constraint in $(C6)$, rank relaxation can be applied [132] [133]. In particular, with the condition that the channel variables are statistically independent, the solution of original problem is rank-one, which is proved in Appendix I. In DA systems, the channel is independent [128], which is different from the co-located antennas systems. Accordingly, the rank-one constraint $(C6)$ is dropped benefiting from the DA deployment.

The problem P7.5 after rank one relaxation is a standard concave maximisation problem with semi-definite programming (SDP). Therefore, the CVX solver can be adopted to solve the problem [4]. Finally, a distributed hybrid duplexing-based (D-HD) EE maximisation algorithm is proposed to concurrently optimise $\boldsymbol{W},\boldsymbol{p}$, which solves the SDP problem P7.5 in the inner layer and updates β in the outer layer (The convergence in inner layer is proven in Appendix J). The D-HD algorithm is summarised as Algorithm 6.

Algorithm 6 D-HD algorithm

Input: Antenna configuration vectors $\boldsymbol{r},\boldsymbol{t}$, left/right bounds β_l and β_r, channel condition, i.e. $\boldsymbol{h_k},\boldsymbol{g_u},e_{u,k},\boldsymbol{h_{SI}}$, for $\forall k\in k, u\in U$, and power consumption parameters, i.e. $\eta, p_{idle}, p_{c,t}, p_{c,r}, p_{can}, p_{fix}, p_{DA}, p_{u,max}$.

Output: Optimal beamforming weight $\boldsymbol{W_k^*}$, for $\forall k\in k$, and optimal uplink transmission power p_u^*, $\forall u\in U$.

1: Set accuracy factor $\epsilon>0$, and suppose $\mathcal{F}(\beta)$ is the optimal value of $f_1(\boldsymbol{W},\boldsymbol{p}) + f_2^{(n)}(\boldsymbol{W},\boldsymbol{p}) - \beta P_{\text{total}}(\boldsymbol{W},\boldsymbol{p})$. Initialise left bound β_l and right bound β_r that ensure the $\mathcal{F}(\beta_l)\cdot\mathcal{F}(\beta_r)<0$.
2: **while** $\beta_r-\beta_l>\epsilon$ **do**
3: $\beta=\frac{\beta_r+\beta_l}{2}$.
4: Solve the problem $P5$ with the FW method until convergence.
5: **if** $\mathcal{F}(\beta_l)\cdot\mathcal{F}(\beta)<0$ **then**
6: $\beta_r=\beta$.
7: **else**
8: $\beta_l=\beta$.
9: **end if**
10: **end while**

7.4 Complexity Analysis

The complexity of the two algorithms are first analysed and then the overall complexity is given. In the DA clustering algorithm, at most $L(K+U)$ comparisons

[4]The CVX contains multiple solvers for SDP optimisation, e.g. SEDuMi, SDPT3 and MOSEK. By claiming variables, objective function (maximisation of concave function or minimisation of convex function) and constraints, the SDP optimisation can be readily solved.

Table 7.2: Simulation Setup

Central carrier frequency	2 GHz
Bandwidth	1 MHz
AWGN power spectral density	-174 dBm/Hz
Cell model	square grid 100 m^2
DE of PA η	25%
Rician factor	5 dB
p_{idle}, $p_{c,r}$ and $p_{c,t}$	10 mW, 100 mW and 100 mW
p_{can} and p_{fix}	50 mW and 500 mW
p_{DA} and $p_{u,max}$	100 mW and 40 mW
Cancellation amount α	α = 60-100 dB
Antenna Gain	0 dBi
Number of users	4
Uplink users' location	(92,10), (85,86)
Downlink users' location	(5,76), (78,16)

is required to find $\boldsymbol{r}^*$ and $\boldsymbol{t}^*$. After this, the D-HD algorithm is performed to allocate beamformer at DAs and transmission power at uplink users. The fractional-structure $\frac{f_1(\boldsymbol{W},\boldsymbol{p})-f_2^{(n)}(\boldsymbol{W},\boldsymbol{p})}{P_{\text{total}}(\boldsymbol{W},\boldsymbol{p})}$ is transformed into a more tractable difference-structure $f_1(\boldsymbol{W},\boldsymbol{p}) - f_2^{(n)}(\boldsymbol{W},\boldsymbol{p}) - \beta P_{\text{total}}(\boldsymbol{W},\boldsymbol{p})$. Bisection search is used in the outer layer for finding optimal β^*. With ϵ as the accuracy required for bisection search, at most $\log_2(\frac{\beta_r-\beta^*}{\epsilon})$ iterations can guarantee convergence. In the inner layer, CVX is called to solve the SDP optimisation $f_1(\boldsymbol{W},\boldsymbol{p}) - f_2^{(n)}(\boldsymbol{W},\boldsymbol{p}) - \beta P_{\text{total}}(\boldsymbol{W},\boldsymbol{p})$, whose complexity is indexed as ξ [5]. Thus the complexity of the DHD algorithm is $\mathcal{O}(\log_2(\frac{\beta_r-\beta^*}{\epsilon}) \cdot \xi)$. As a result, the total complexity is given by $\mathcal{O}\big(L(K+U) + \log_2(\frac{\beta_r-\beta^*}{\epsilon}) \cdot \xi\big)$. As can be seen, the associated bisection search in the outer layer has the largest impact on the complexity of the whole algorithm, more insight on the number of iterations of the associated bisection search will be demonstrated in Section. 7.5.

7.5 Simulation Results

Numerical results are used to verify our analysis. The simulation setup is shown in Tab. 7.2. The PL model PL = $145.4 + 37.5\log_{10}(d/1000)$ is adopted [135], which is featured in 3GPP LTE communications. Besides, to evaluate the performance of the proposed hybrid duplexing system, two benchmarks are added as comparisons. The first one is the distributed FD (D-FD) [129], where all DAs are only capable of working in FD or sleep modes. The other is co-located FD (C-FD) MIMO [132]. Since all antennas have identical PL to users due to the co-located antenna deployment, the activation/deactivation of transmit/receive chains is disabled in the C-FD system.

Figs. 7.2(a) demonstrates the average optimal EE performance under D-HD, D-FD and C-FD systems. The centralised antennas of C-FD system are located in the centre of

[5] Since the FW method is adopted for the inner layer iteration, the convergence rate is $\mathcal{O}(\frac{1}{n})$ [134]. In the n-th update in the inner layer, the CVX SDPT3 solver implements an interior-point method to solve the SDP problem, which belongs to the class of path-following method and leads a fast convergence.

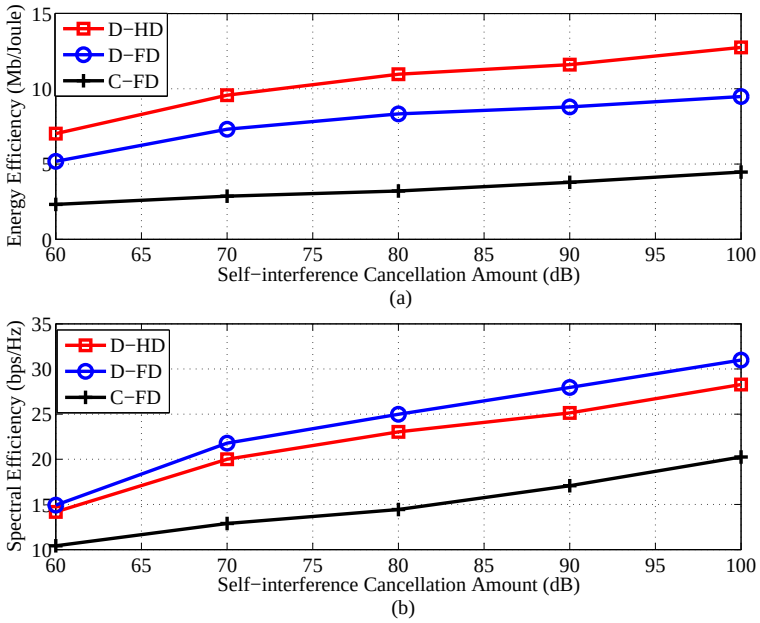

Figure 7.2: Average EE and SE performance vs. different SIC amount, with 16 DAs and $\psi = 0.5 \times 10^{-8}$.

the map. It can be seen that the proposed D-HD algorithm outperforms others in terms of EE at all SIC settings. It is because under the proposed D-HD algorithm, the DAs with poor channel condition are deactivated, hence power waste is avoided. Besides, the activated DAs can work in HD modes (only transmit or receive) if the DAs have only reasonable channel gain in one direction. Differently, under the D-FD algorithm, all activated DAs work in FD mode. This leads to much higher power consumption than the proposed D-HD, but not all DAs can contribute acceptable throughput bi-directly, hence the EE is degraded. For the C-FD with centralised antennas, all co-located antennas suffer similar PL, leading to poor throughput performance. Besides, high power consumption is incurred due to the fully activated antennas. As a result, the EE performance is the lowest among the three systems. Also, it can be seen that, for all the three systems, EE will be improved with increased SIC amount. Fig. 7.2(b) shows the average SE performance for the three systems. D-FD shows the highest SE performance due to the fact that all antennas work in FD. However, our proposed D-HD has only marginal SE loss compared to the D-FD, but with much less power consumption. The C-FD algorithm demonstrates the poorest SE performance, which is because the co-located antenna deployment is sensitive to the distance between users and antennas and has limited ability in reducing PL. The co-located antenna deployment has also resulted in the strongest self-interference among different antennas. Therefore, the co-located antenna system requires higher SIC amount than the DA systems. As a result, the C-FD SE increases more slowly than the DA systems.

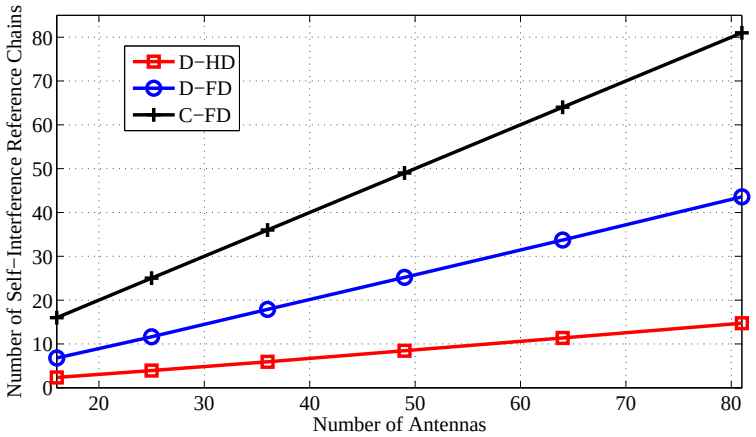

Figure 7.3: Average required number of reference chains for SIC operation, with $\psi = 1 \times 10^{-9}$.

Fig. 7.3 shows the required number of self-interference reference chains by the three systems. Since the analogue and digital domain cancellation needs to tap reference signal from every transmit chain and feed it to all receive chains for SIC operation [3], the required number of self-interference reference chains has significant impact on the SIC circuit design. It can be seen that, the proposed hybrid duplexing DA system requires the fewest self-interference reference chains. It is because DAs may sleep or work in HD mode, where SIC operation is not needed. Besides, benefiting from the distributed deployment, propagation domain cancellation guarantees a reasonable SIC amount across different DAs, and thus the analogue and digital domain SIC is not required across different DAs. As a comparison, all antennas are active and work in FD mode by the conventional C-FD system, where the number of self-interference reference chains increases linearly with numbers of antenna.

Fig. 7.4(a) shows the total power consumption of the three systems with different number of antennas. The proposed D-HD consumes the lowest power. Since the DAs may work in HD or sleep mode, power consumption can be reduced effectively due to the less circuit power consumption. Also, no SIC power consumption is incurred in non-FD DAs, while the C-FD consumes the highest power because of the fully-activated antennas and the high transmission power to overcome the PL. Besides, it obvious that a denser DA deployment results in higher power consumption because more DAs are activated. On the other side, as shown by Fig. 7.4(b), EE is not necessarily higher with a denser DA deployment due to the increased power consumption. It means that, one may appropriately decrease the threshold value given a denser DA deployment in terms of EE oriented design, which is further analysed by Fig. 7.5.

Fig. 7.5 shows the power consumption and SE performance with different value of ψ. It can be seen that, less power and lower throughput are demonstrated by a higher threshold, since fewer DAs are activated. This indicates that the threshold value can

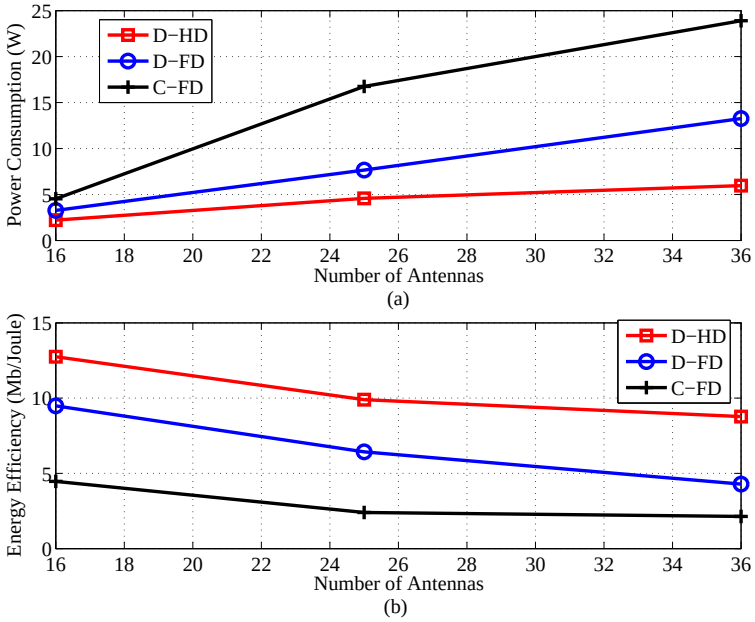

Figure 7.4: Average power consumption and EE vs. different number of antennas, with $\alpha = 100$ dB and $\psi = 1 \times 10^{-9}$.

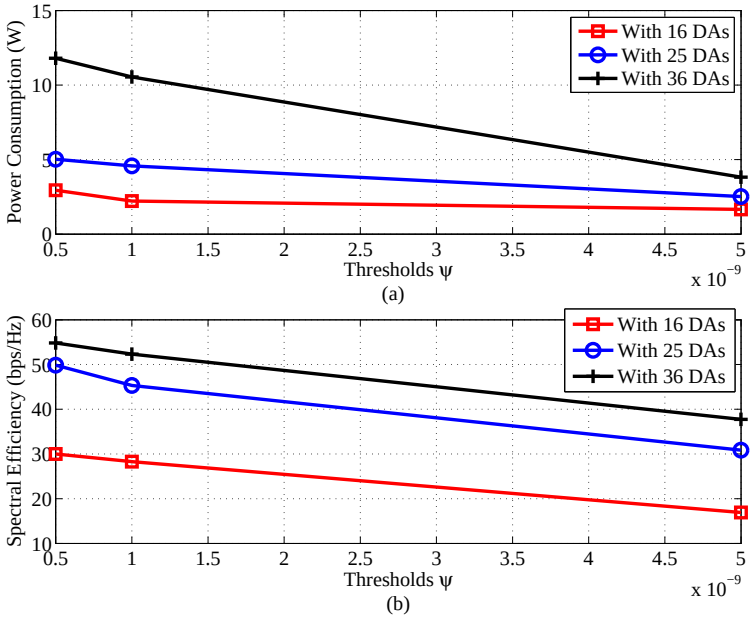

Figure 7.5: Average power consumption and SE performance vs. different DA clustering threshold values, with $\alpha = 100$ dB.

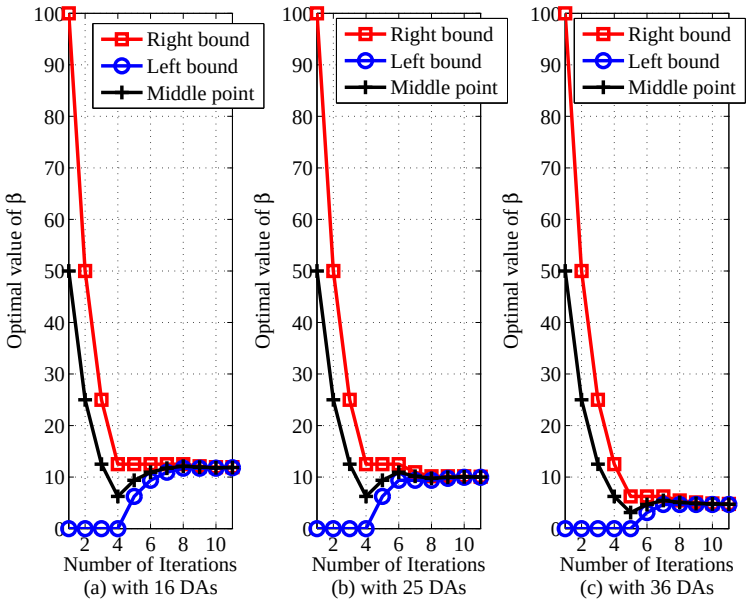

Figure 7.6: The number of iterations on finding optimal β^* by bisection searching, with left bound $\beta_l = 0$ and right bound $\beta_r = 100$.

be adjusted to reduce the power consumption, at the cost of SE. On the other hand, a lower threshold allows a better SE performance, while power consumption is relatively higher, which corresponds to a stringent SE QoS scenario. This confirms our analysis in the DA clustering algorithm that by changing the threshold value ψ, the number of activated DAs can be well controlled towards different QoS requirement. Besides, with more DAs, SE can be significantly improved, with increased power consumption. As a result, the EE is not necessarily improved, which shows the similar observation in Fig. 7.4(b).

Fig. 7.6 shows the iteration behaviour of the proposed D-HD algorithm on finding the optimal β^* with different number of DAs. It can be seen that at most around 10 iterations are needed to get convergence, which confirms the low complexity of the proposed algorithm.

7.6 Summary

In this chapter, a novel hybrid duplexing DA system has been proposed, which features high EE, low power consumption, and simple SIC circuit design. Based on the proposed system, the EE oriented resource allocation has been investigated by jointly designing activation/deactivation of transmit/receive chains, downlink beamformer and uplink transmission power. Simulation results show that the proposed design demonstrates significant EE enhancement and power saving over the co-located FD MIMO system and the sole-FD duplex DA system, achieving a reasonable balance between low power

consumption and high SE. Moreover, since DAs can flexibly adjust their duplexing and working modes due to the enhanced degree of freedom, the proposed hybrid duplexing DA system obtains a much simpler SIC circuit design compared to the two benchmarks in [129] and [132].

Chapter 8

Conclusion and Future Work

8.1 Conclusion

This thesis has investigated the EE oriented resource management in FD wireless communication systems, including FD AF relay system, FD DF relay multiuser system with cross layer design, WPT-aided FD DF relay multiuser system, and bi-directional FD DA system.

In Chapter 4, the EE gain regions among FD (PSAC), FD (PS) and HD have been investigated. The closed-forms of EE gain regions among three modes have been given. To optimise the EE of AF FD relay systems, transmission power adaptation and opportunistic relay selection have been proposed. By the proposed algorithms, the average optimal EE of FD AF relay systems can be up to 1.4 Gb/Joule higher than that of HD AF relay system. Also, the SE achieved by FD AF relay system is 1.3$\sim$2 times of that of HD AF relay systems, provided the SIC amount varies from 40$\sim$60 dB. At last, some properties have been discussed, e.g. with low drain efficiency or high static circuit power, FD (PSAC) is preferable over FD (PS) and HD in terms of EE.

In Chapter 5, addressing the characteristic of mm-wave, e.g. the intermittent blockage and the out-of-the-date channel estimation, the cross-layer design has been studied for FD DF multiuser systems with OFDMA technique. To maximise the system EE and satisfy the cross-layer design constraints, a so-called Q-FERA algorithm has been proposed, by joint allocation of transmission power, subcarriers and throughput. It has been shown that the proposed algorithm achieves higher EE than its counterpart, FD DF relay system with SE oriented algorithm [2], with marginal SE loss. Besides, the throughput outage probability of the proposed algorithm is much lower than that of the algorithm in [2], making the proposed cross-layer algorithm more robust against channel estimation errors and applicable in mm-wave communications. At last, some properties have been discussed, e.g. the impact of transmission power on EE, EE oriented water-filling power allocation, EE-SE trade-off for two-hop FD relay systems, the suitability of the Q-FERA algorithm for 60 GHz applications and the impact of outage probability constraint on EE.

In Chapter 6, the resource management in WPT-aided FD DF relay multiuser systems has been researched, where the relay is powered by WPT from the source. To better balance the SE of the source-relay and relay-destinations hops, an asymmetric system has been proposed, which allows nonuniform time slot durations for the two hops and therefore obtains higher degree of freedom than the symmetric system [108] and the time-switching based system [105]. Based on the asymmetric structure, a so-called Asym-WPT-FR algorithm has been developed by jointly allocating time slot durations and transmission power at the source and the relay, and subcarriers for multiuser. The closed-form of the optimal results has been derived. Simulation shows that the proposed Asym-WPT-FR system can achieve approximately twice SE compared to the Sym-WPT-FR [108] and the TS-WPT-FR [105]. Also the energy harvested by the proposed Asym-WPT-FR system is 200% and 30% higher than that of the TS-WPT-FR and the Sym-WPT-FR, respectively, showing its high EE and applicability to WPT-supported relay systems. Last but not least, it has been pointed out that, by harvesting energy from self-interference signal rather than cancelling it, more power is allocated to the subcarriers with higher self-interference channel frequency response, while conventional grid-powered FD relay systems [114] [115] assign more power to the subcarriers with lower self-interference channel frequency response.

In Chapter 7, FD technique has been incorporated with DA systems to further improve the SE and EE performance, where antennas are distributed geographically rather than co-located. Benefited from the distributed deployment, PL and blockage can be significantly relieved over the conventional co-located MIMO systems. EE oriented resource allocation has been researched by jointly designing the status of DAs, downlink beamformer and uplink transmission power. Since the DAs are capable of working in hybrid modes, higher degrees of freedom can be readily obtained compared to sole-FD systems [129] and co-located FD MIMO systems [132]. By the proposed algorithm, both higher EE and SE are achieved compared to conventional co-located FD MIMO systems [132], and higher EE is achieved over the sole-FD DA systems [129] with marginal SE loss. Besides, SIC design is much simplified by the proposed algorithm, becoming as easy as that in SISO scenario.

8.2 Future Work

In the research on FD systems presented in this thesis, it has been been assumed that multiuser access is orthogonal. The other access technique, non-orthogonal frequency multiple access (NOMA) also has attracted much attention, which even demonstrates higher SE than orthogonal multiuser access (OMA) by proper design. Besides, ultra-dense and heterogeneous systems are two key deployments in 5G systems, which provides seamless network coverage and features low money cost and low power consumption. However, how to incorporate FD with NOMA, ultra-dense or heterogeneous

systems is still challenging. Hence, the future research topics are summarised in the following.

- The key concept of NOMA is that it allows multiuser occupy the same frequency, time and code. Users' signals are linearly superimposed and transmitted at the BS. At receiver end, the user with better channel condition decodes the data of another user with worse channel condition, and performs successive interference cancellation to subtract the multiuser interference before detecting its own signal. Recently, in order to further improve the SE performance of NOMA systems, HD cooperative NOMA systems have been proposed, where strong user acts as a HD relay node. As mentioned above, HD relay systems need two orthogonal time slots and inevitably lead to SE loss. As a result, FD cooperative NOMA systems will be addressed in the future.

- FD transmission in ultra-dense small cell or heterogeneous systems has not been investigated. High density of small cell increases the possibility of inter-cell interference. The performance of FD transmission may be significantly degraded by noise, self-interference, inter-cell interference and multiuser interference. How to determine the density of small cell, how to organise adjacent small cells for cooperative communications and interference management are challenging and will be investigated thoroughly.

Appendix A

Proof of Theorem 4.1

Hereby the concavity of the EE of FD (PSAC) is proven with respect to the total transmission power P_s (FD (PS) and HD can be seen as special cases). Define $\boldsymbol{B} = \{T_{FD(PSAC)} | T_{FD(PSAC)} \in (0, \infty)\}$ as the set of the overall throughput, while $\boldsymbol{A} = \{P_s | P_s \in (0, \infty)\}$ is the corresponding total transmission power. With a specific mapping function (power allocation method) $f : P_s \xrightarrow{f} T_{FD(PSAC)}$, the total transmission power and the overall throughput is one-to-one mapped ($f : \boldsymbol{A} \xrightarrow{f} \boldsymbol{B}$) and higher transmission power leads to higher throughput. Therefore, if EE $\eta_{FD(PSAC)}$ is strictly quasi-concave with respect to the overall throughput $T_{FD(PSAC)}$, it is also quasi-concave with respect to the total transmission power P_s. The superlevel sets of $\eta_{FD(PSAC)}$ is defined as $S_\Upsilon = \{T_{FD(PSAC)} > 0 | \eta_{FD(PSAC)} > \Upsilon\}$. According to [136], $\eta_{FD(PSAC)}$ is strictly quasi-concave with respect to $T_{FD(PSAC)}$ if S_Υ is strictly convex for any real number Υ. If $\Upsilon < 0$, there is no physical meaning. If $\Upsilon \geq 0$, S_Υ is equivalent to $S_\Upsilon = \{T_{FD(PSAC)} > 0 | \Upsilon(P_s/\omega) \sum_{n=1}^{N} \tilde{\lambda}_n + \Upsilon(P_{c,sta} + P_{AC}) + (\Upsilon\varepsilon - 1) T_{FD(PSAC)} \leq 0\}$. It is known that P_s is strictly convex with respect to $T_{FD(PSAC)}$ given a sufficiently large number of subcarriers [2] [53] and with good SIC. The linear part $\Upsilon(P_{c,sta} + P_{AC}) + (\Upsilon\varepsilon - 1) T_{FD(PSAC)}$ is convex (not strictly) with respect to throughput $T_{FD(PSAC)}$. Therefore, the summation $\Upsilon(P_s/\omega) \sum_{n=1}^{N} \tilde{\lambda}_n + \Upsilon(P_{c,sta} + P_{AC}) + (\Upsilon\varepsilon - 1) T_{FD(PSAC)}$ is strictly convex with respect to throughput $T_{FD(PSAC)}$. In conclusion, $\eta_{FD(PSAC)}$ is strictly quasi-concave with respect to $T_{FD(PSAC)}$, and is strictly quasi-concave with respect to P_s. Under a small maximum transmission power constraint P_{max}, $\eta_{FD(PSAC)}$ may be mono-increasing with respect to the total transmission power P_s.

Appendix B

Derivative Calculation of EE with respect to the Total Transmission Power

Hereby we take FD (PSAC) as example to show the derivative calculation of EE with respect to the total transmission power (FD (PS) and HD can be seen as special cases). For the strictly-continuous function $\eta_{FD(PSAC)}$ in the region $P_s \in (0, P_{max}]$, the limit of the difference quotient when ΔP_s approaches zero, if existing, should represent the slope of the tangent line to (P_s, $\eta_{FD(PSAC)}$), which is calculated as

$$\frac{\partial \eta_{FD(PSAC)}}{\partial P_s}|_{P_s} = \lim_{\Delta P_s \to 0} \frac{\eta_{FD(PSAC)}(P_s + \Delta P_s) - \eta_{FD(PSAC)}(P_s)}{\Delta P_s}. \tag{B.1}$$

With a minimal increment ΔP_s that approaches 0, the values of $\eta_{FD(PSAC)}$ and $\eta_{FD(PSAC)}$ can be obtained at points $P_s + \Delta P_s$ and P_s, respectively. Substituting the two terms into (B.1), $\partial \eta_{FD(PSAC)}/\partial P_s$ can be found. Therefore, calculating $\frac{\partial \eta}{\partial P_s}$ can be transferred into calculating $\eta_{FD(PSAC)}$ at transmission powers P_s and $P_s + \Delta P_s$.

Appendix C

Energy Efficiency Gain Regions among FD(PSAC) FD(PS) and HD

C.1 Energy Efficiency Gain Region between FD (PSAC) and FD (PS)

The difference between the EEs of FD (PSAC) and FD (PS) is calculated as

$$\eta_{FD(PSAC)} - \eta_{FD(PS)} = \frac{1}{\left(\frac{P_s}{\omega}\sum_{n=1}^{N}\tilde{\lambda}_n + \varepsilon T_{FD(PS)} + P_{c,sta}\right)} \times \frac{\left(\frac{P_s}{\omega}\sum_{n=1}^{N}\tilde{\lambda}_n + P_{c,sta}\right)\left(\frac{T_{FD(PSAC)}}{T_{FD(PS)}} - 1\right) - P_{AC}}{T_{FD(PS)}\left(\frac{P_s}{\omega}\sum_{n=1}^{N}\tilde{\lambda}_n + \varepsilon T_{FD(PSAC)} + P_{c,sta} + P_{AC}\right)}, \tag{C.1}$$

where $T_{FD(PSAC)}$ and $T_{FD(PS)}$ represent the throughputs achieved by FD (PSAC) and FD (PS), respectively. Obviously, the sign of (C.1) is the same as the sign of its numerator.

C.2 Energy Efficiency Gain Region between FD (PSAC) and HD

The difference between the EEs of FD (PSAC) and HD is calculated as

$$\eta_{FD(PSAC)} - \eta_{HD} = \frac{\left(\frac{P_s}{\omega}\sum_{n=1}^{N}\tilde{\lambda}_n + P_{c,sta}\right)\left(\frac{T_{FD(PSAC)}}{T_{HD}} - 1\right) - P_{AC}}{T_{HD}\left(\frac{P_s}{\omega}\sum_{n=1}^{N}\tilde{\lambda}_n + \varepsilon T_{FD(PSAC)} + P_{c,sta} + P_{AC}\right)} \frac{1}{\left(\frac{P_s}{\omega}\sum_{n=1}^{N}\tilde{\lambda}_n + \varepsilon T_{HD} + P_{c,sta}\right)}, \tag{C.2}$$

where $T_{FD(PSAC)}$ and T_{HD} are throughputs achieved by FD (PSAC) and HD, respectively.

Specially, with near-perfect SIC, the throughput of FD (PSAC) is nearly twice as high as that of HD. Hence, (C.2) reduces to

$$\eta_{FD(PSAC)} - \eta_{HD} = \frac{\left(\frac{P_s}{\omega}\sum_{n=1}^{N}\tilde{\lambda}_n + P_{c,sta}\right) - P_{AC}}{T_{HD}\left(\frac{P_s}{\omega}\sum_{n=1}^{N}\tilde{\lambda}_n + \varepsilon T_{FD(PSAC)} + P_{c,sta} + P_{AC}\right)} \frac{1}{\left(\frac{P_s}{\omega}\sum_{n=1}^{N}\tilde{\lambda}_n + \varepsilon T_{HD} + P_{c,sta}\right)}. \tag{C.3}$$

C.3 Energy Efficiency Gain Region between FD (PS) and HD

FD (PS) uses antenna shielding or directional antenna to mitigate self-interference, and therefore it does not consume additional power on SIC. With the same transmission power, the EE difference between FD (PS) and HD is calculated as

$$\eta_{FD(PS)} - \eta_{HD} = \frac{\left(\frac{P_s}{\omega}\sum_{n=1}^{N}\tilde{\lambda}_n + P_{c,sta}\right)(T_{FD(PS)} - T_{HD})}{T_{HD}\left(\frac{P_s}{\omega}\sum_{n=1}^{N}\tilde{\lambda}_n + \varepsilon T_{FD(PS)} + P_{c,sta}\right)} \frac{1}{\left(\frac{P_s}{\omega}\sum_{n=1}^{N}\tilde{\lambda}_n + \varepsilon T_{HD} + P_{c,sta}\right)}, \tag{C.4}$$

where $T_{FD(PS)}$ and T_{HD} are the throughputs achieved by FD (PS) and HD, respectively. The sign of (C.4) is the same as the sign of $T_{FD(PS)} - T_{HD}$, i.e. FD (PS) is more energy efficient than HD if FD (PS) achieves a higher throughput than HD.

Appendix D

Derivation of Lemma 5.2

Shannon capacity $c_{k,n}$ is the maximum rate of reliable communication supported by subcarrier n for user k. The quantity of $c_{k,n}$ is a function of the random channel gains and is therefore random. Suppose the source sends data at a rate $t_{k,n}$. If the arranged rate $t_{k,n}$ is higher than its upper bound $c_{k,n}$, then whatever code that was used by the transmitter, the decoding error probability cannot be made arbitrarily small. The transmission on subcarrier n is said to be in outage [19].

The outage probability in (C5) of problem P5.2 is equivalent to

$$\begin{aligned} &Pr[2\gamma_{RR,k,n}(2^{t_{k,n}-1}) > \sqrt{4p_{k,n}\gamma_{SR,k,n}\gamma_{RD,k,n}\gamma_{RR,k,n} + (\gamma_{SR,k,n}+\gamma_{RD,k,n})^2} \\ &\quad - (\gamma_{SR,k,n}+\gamma_{RD,k,n}) \mid \hat{h_{RD,k,n}}] = \theta^k. \end{aligned} \tag{D.1}$$

The left hand of (D.1) can be re-sorted to

$$Pr[\gamma_{RR,k,n}(2^{t_{k,n}}-1)^2 + (2^{t_{k,n}}-1)\gamma_{SR,k,n} > \gamma_{RD,k,n}(p_{k,n}\gamma_{SR,k,n} - (2^{t_{k,n}}-1)) \mid \hat{h_{RD,k,n}}]. \tag{D.2}$$

Note that since $p_{r,k,n}\gamma_{RR,kk,n} \geq 0$ and $p_{k,n} = p_{s,k,n} + p_{r,k,n}$, it can be derived that $log_2(1+\frac{p_{s,k,n}\gamma_{SR,k,n}}{1+p_{r,k,n}\gamma_{RR,k,n}}) \leq log_2(1+p_{k,n}\gamma_{SR,k,n})$. Since perfect CSI of link S-R is available at the source, $t_{k,n}$ will not exceed the real capacity of the S-R link as the corresponding perfect CSI is available at the scheduler, i.e. $t_{k,n} \leq log_2(1+\frac{p_{s,k,n}\gamma_{SR,k,n}}{1+p_{r,k,n}\gamma_{RR,k,n}}) \leq log_2(1+p_{k,n}\gamma_{SR,k,n})$. Therefore, $2^{t_{k,n}} - 1 < p_{k,n}\gamma_{SR,k,n}$ is readily obtained. Therefore, (D.2) is transformed into

$$Pr\left[|h_{RD,k,n}|^2 < \frac{(2^{t_{k,n}}-1)^2\gamma_{RR,k,n} + (2^{t_{k,n}}-1)\gamma_{SR,k,n}}{p_{k,n}\gamma_{SR,k,n} - (2^{t_{k,n}}-1)} \frac{\sigma^2}{l_{RD,k}} \mid \hat{h_{RD,k,n}}\right]. \tag{D.3}$$

Since (D.3) is a conditional probability, the estimated channel $\hat{h_{RD,k,n}}$ and $h_{RD,k,n} = \hat{h_{RD,k,n}} + \Delta h_{RD,k,n}$ can be known. Therefore, (D.3) is equivalent to

$$Pr\left[|\hat{h_{RD,k,n}} + \Delta h_{RD,k,n}|^2 < \frac{(2^{t_{k,n}}-1)^2\gamma_{RR,k,n} + (2^{t_{k,n}-1})\gamma_{SR,k,n}}{p_{k,n}\gamma_{SR,k,n} - (2^{t_{k,n}}-1)} \frac{\sigma^2}{l_{RD,k}} \mid \hat{h_{RD,k,n}}\right]. \tag{D.4}$$

(D.4) can be seen as the cdf of a non-central chi-square distributed variable. Substituting (D.4) into (D.1), we get

$$F\left(\frac{(2^{t_{k,n}}-1)^2\gamma_{RR,k,n}+(2^{t_{k,n}}-1)\gamma_{SR,k,n}}{p_{k,n}\gamma_{SR,k,n}-(2^{t_{k,n}}-1)}\frac{2\sigma^2}{l_{RD,k}\sigma^2_{error}}\right)=\theta^k, \tag{D.5}$$

where the operator $F(\cdot)$ denotes the cdf of the corresponding non-central chi-square function [88], with degree of freedom 2 and non-central parameter $\frac{2|\hat{h_{RD,k,n}}|^2}{\sigma^2_{error}}$ [94] [137]. Finally, (D.5) leads to Lemma 5.2.

The inverse function $F^{-1}(\cdot)$ is mono-increasing with respect to the non-central parameter, which is $\frac{2|\hat{h_{RD,k,n}}|^2}{\sigma^2_{error}}$ as derived. Hence, better channel estimation quality (smaller variance of channel estimation error σ^2_{error}) leads to more aggressive throughput assignment and higher EE with a given outage probability constraint. A similar impact of channel estimation error on system metrics can be found in [94] for CR networks.

Appendix E

Proof of Concavity of the Problem in (5.15)

For the proof purpose, a new variable $X_{k,n} = \sqrt{4p_{k,n}\Phi_{k,n} + \Psi_{k,n}^2} - \Psi_{k,n}$ is defined for simplicity. The objective function is transformed to $u1(\rho_{k,n}, X_{k,n}) = \rho_{k,n} log_2(1 + \frac{X_{k,n}-\Psi_{k,n}}{2\rho_{k,n}\gamma_{RR,k,n}})$. It is proven that the objective function is jointly-concave in terms of $\rho_{k,n}$ and $X_{k,n}$. The Hessian matrix of the objective is

$$\boldsymbol{H}(u1(\rho_{k,n}, X_{k,n})) = \begin{pmatrix} \frac{-\rho_{k,n}}{ln(2)\varphi_{k,n}} & \frac{X_{k,n}-\Psi_{k,n}}{ln(2)\varphi_{k,n}} \\ \frac{X_{k,n}-\Psi_{k,n}}{ln(2)\varphi_{k,n}} & \frac{(X_{k,n}-\Psi_{k,n})^2}{\rho_{k,n}} \\ & \frac{}{ln(2)\varphi_{k,n}} \end{pmatrix}, \tag{E.1}$$

where $\varphi_{k,n} = (2\rho_{k,n}\gamma_{RR,k,n} + X_{k,n} - \Psi_{k,n})^2$. (E.1) can be further reduced to

$$\boldsymbol{H}(u1(\rho_{k,n}, X_{k,n})) = \frac{X_{k,n} - \Psi_{k,n}}{ln(2)\varphi_{k,n}} \begin{pmatrix} \frac{-\rho_{k,n}}{X_{k,n}-\Psi_{k,n}} & 1 \\ 1 & \frac{X_{k,n}-\Psi_{k,n}}{-\rho_{k,n}} \end{pmatrix}. \tag{E.2}$$

It is straightforward (E.2) is a negative semi-definite matrix, indicating $u1$ is jointly-concave in terms of $\rho_{k,n}$ and $X_{k,n}$. Since $X_{k,n} = \sqrt{4p_{k,n}\Phi_{k,n} + \Psi_{k,n}^2} - \Psi_{k,n}$ is non-decreasing in terms of $p_{k,n}$, $u1(\rho_{k,n}, X_{k,n}) = \rho_{k,n} log_2(1 + \frac{X_{k,n}-\Psi_{k,n}}{2\rho_{k,n}\gamma_{RR,k,n}})$ is non-decreasing in terms of $p_{k,n}$. As a result, $u1$ is jointly-concave in terms of $\rho_{k,n}$ and $p_{k,n}$. Finally, it is easy to prove that $\sum_{k=1}^{K}(1-\theta^k)\sum_{n=1}^{N}\rho_{k,n} log_2(1 + \frac{\Lambda_{k,n}}{\rho_{k,n}})$ is joint-concave in terms of $\rho_{k,n}$ and $p_{k,n}$.

Appendix F

Theoretic Analysis of the Branch-and-Bound Approach

The BnB approach guarantees the global optimum of the original problem. Therefore, the BnB approach is adopted as a benchmark to evaluate the optimality of the proposed Q-FERA algorithm.

With N subcarriers and K users, the enumeration tree is given by Fig. F.1, which contains all possible subcarrier allocations (K^N possibilities). For brevity, the power allocation ($p_{k,n}$ for $\forall k \in K$ and $n \in N$) is not drawn. As demonstrated by Fig. F.1, each parent node has K child nodes, meaning there are K choices for each subcarrier allocation. The $k-th$ child node at the $n-th$ level represents that subcarrier n is allocated to user k ($\rho_{k,n} = 1$ and $\rho_{k',n} = 0$ for $\forall k' \neq k$ and $k' \in K$). Obviously, the node value is related with the current node (subcarriers to be decided), as well as the associated searching path from the root node to its parent node (subcarriers have been allocated) [96]. For notational convenience, the definitions and the rules used in the BnB approach are introduced.

Definition F.1: Complete path and partial path

A complete path $l_N = \{nod_1, nod_2, ..., nod_N\}$ is from the root node to a leaf node, which means all subcarriers have been allocated to particular users (therefore $\rho_{k,n} = \{0, 1\}$, for $\forall n \in N, k \in K$), where nod_n is the $n-th$ node visited along the particular path l_N. A partial (incomplete) path $l_n = \{nod_1, nod_2, ..., nod_n\}$ is defined as the part of a complete path that starts at the root node and ends at some internal node along the particular path l_n, where $n < N$.

Rule F.1: The rule for calculating node value

The node value (EE, in bits/Joule) along a path l_n is denoted as $EE(l_n)$, which is calculated as: solve the problem P5.4 with constraints $(C2)$, $(C3)$, $(C8)$ and remove the subcarrier allocation constraints along the searched path l_n (from subcarrier 1 to current subcarrier n, which means these nodes have been searched and therefore the subcarriers have been allocated), while the constraints of undecided subcarriers (from

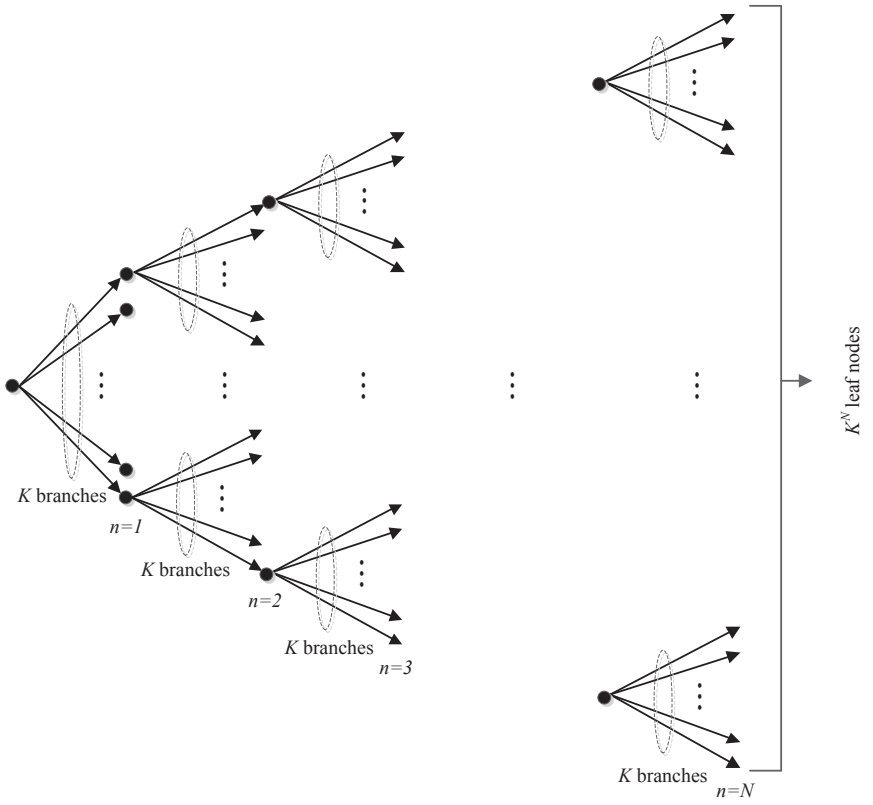

Figure F.1: An enumeration tree for the BnB approach

$n+1$ to N) are relaxed to [0, 1].

According to Definition F.1 and Rule F.1, Definition F.2, Rule F.2 and Rule F.3 are given.

Definition F.2: Upper bound and candidate solution

For an internal node n ($n < N$), its node value $EE(l_n)$ can be seen as an upper bound (since part of subcarrier constraints is relaxed), which represents the best estimate of all subsequent searches. For a leaf node ($n = N$), the node value $EE(l_N)$ can be seen as a candidate solution (since all subcarriers have been allocated along the searched path l_N).

Rule F.2: The rule for visiting order of child nodes

The order of visiting K child nodes of a given parent node should be the same as the ascending order of the corresponding child node values [96]. In other words, one should visit the child node with the highest node value, since the optimal solution is most likely to occur in the branch.

Rule F.3: The rule for pruning node

When visiting a node n along a partial path l_n, we calculate its node value and compare it with the candidate solution O^*. If $EE(l_n) \geq O^*$, it means that a better

solution is likely to occur in this branch and then we search its child nodes according to Rule F.2. If $EE(l_n) < O^*$, it means the upper bound of this path is lower than the candidate solution and it is not worth searching its child nodes any more. Therefore, we prune the node and begin to search the next unvisited child node at the same level or backtrack to the next unexplored nodes in the previous level.

To reduce the complexity of the BnB approach, it is better to prune the non-promising sub-trees as early as possible. Therefore, a near-optimal candidate solution is needed, with which we can prune the non-promising sub-trees as early as possible and significantly reduce the searching time. As said in chapter 5, our proposed Q-FERA algorithm is near-optimal given a large number of subcarriers. Therefore, the Q-FERA algorithm can be used to get a candidate solution for initialization purpose. The whole BnB approach is described as follows.

Algorithm 7 Branch-and-Bound (BnB) Approach

1: Call the Q-FERA algorithm to get a candidate solution O^*. Set the initial level at $j = 0$ (the root node).
2: Calculate the child node values of $j - th$ level according to Rule 1 and visit one of child node according to Rule 2. Set $j = j + 1$ if no backtrack is needed or set $j = j - 1$ according to Rule 3.
3: **if** $j < N$ **then**
4: Go to Step 2.
5: **else**
6: Update the candidate solution $O^* = max\{O^*, EE(l_N)\}$ according to Definition 2.
7: **end if**
8: BnB searching terminates if all nodes have been visited or pruned. Otherwise, set $j = j - 1$ and go to Step 2.

Appendix G

Proof of Theorem 6.1

T_1 and T_2 can be calculated as

$$T_1 = \frac{T\sum_{k=1}^{K}\sum_{n=1}^{N}\beta_{k,n}log_2(1+\frac{p_{r,k,n}\gamma_{rd,k,n}}{\beta_{k,n}})}{\sum_{k=1}^{K}\sum_{n=1}^{N}\beta_{k,n}log_2(1+\frac{p_{s,k,n}\gamma_{sr,k,n}}{\beta_{k,n}})+\sum_{k=1}^{K}\sum_{n=1}^{N}\beta_{k,n}log_2(1+\frac{p_{r,k,n}\gamma_{rd,k,n}}{\beta_{k,n}})} \tag{G.1}$$

$$T_2 = \frac{T\sum_{k=1}^{K}\sum_{n=1}^{N}\beta_{k,n}log_2(1+\frac{p_{s,k,n}\gamma_{sr,k,n}}{\beta_{k,n}})}{\sum_{k=1}^{K}\sum_{n=1}^{N}\beta_{k,n}log_2(1+\frac{p_{s,k,n}\gamma_{sr,k,n}}{\beta_{k,n}})+\sum_{k=1}^{K}\sum_{n=1}^{N}\beta_{k,n}log_2(1+\frac{p_{r,k,n}\gamma_{rd,k,n}}{\beta_{k,n}})} \tag{G.2}$$

Substituting (G.1) and (G.2) into (6.9), an equivalent object function is obtained as

$$\underset{T_1,T_2,\boldsymbol{p_s},\boldsymbol{p_r},\boldsymbol{\beta}}{\operatorname{argmax}} \frac{2\big(\sum_{k=1}^{K}\sum_{n=1}^{N}\beta_{k,n}log_2(1+\frac{p_{s,k,n}\gamma_{sr,k,n}}{\beta_{k,n}})\big)\big(\sum_{k=1}^{K}\sum_{n=1}^{N}\beta_{k,n}log_2(1+\frac{p_{r,k,n}\gamma_{rd,k,n}}{\beta_{k,n}})\big)}{\sum_{k=1}^{K}\sum_{n=1}^{N}\beta_{k,n}log_2(1+\frac{p_{s,k,n}\gamma_{sr,k,n}}{\beta_{k,n}})+\sum_{k=1}^{K}\sum_{n=1}^{N}\beta_{k,n}log_2(1+\frac{p_{r,k,n}\gamma_{rd,k,n}}{\beta_{k,n}})} \tag{G.3}$$

Then the objective function can be transformed into

$$\underset{T_1,T_2,\boldsymbol{p_s},\boldsymbol{p_r},\boldsymbol{\beta}}{\operatorname{argmin}} \frac{1}{2}\Bigg(\frac{1}{\sum_{k=1}^{K}\sum_{n=1}^{N}\beta_{k,n}log_2(1+\frac{p_{s,k,n}\gamma_{sr,k,n}}{\beta_{k,n}})}+\frac{1}{\sum_{k=1}^{K}\sum_{n=1}^{N}\beta_{k,n}log_2(1+\frac{p_{r,k,n}\gamma_{rd,k,n}}{\beta_{k,n}})}\Bigg) \tag{G.4}$$

Consider two inter functions $u = \sum_{k=1}^{K}\sum_{n=1}^{N}\beta_{k,n}log_2(1+\frac{p_{s,k,n}\gamma_{sr,k,n}}{\beta_{k,n}})$ and $v = \sum_{k=1}^{K}\sum_{n=1}^{N}\beta_{k,n}log_2(1+\frac{p_{r,k,n}\gamma_{rd,k,n}}{\beta_{k,n}})$. The Hessian matrix of function u is given as

$$\boldsymbol{H}\big(u(T_1, T_2, \boldsymbol{p_s}, \boldsymbol{p_r}, \boldsymbol{\beta})\big) = \frac{p_{s,k,n}\gamma_{sr,k,n}^2}{(\beta_{k,n} + p_{s,k,n}\gamma_{sr,k,n})^2} \begin{pmatrix} -\frac{p_{s,k,n}}{\beta_{k,n}} & 1 \\ 1 & -\frac{\beta_{k,n}}{p_{s,k,n}} \end{pmatrix}. \tag{G.5}$$

It is obvious that (G.5) is a negative semi-definite matrix, meaning u is a concave function. Also, the Hessian matrix of function v is given as

$$\boldsymbol{H}\big(v(T_1, T_2, \boldsymbol{p_s}, \boldsymbol{p_r}, \boldsymbol{\beta})\big) = \frac{p_{r,k,n}\gamma_{rd,k,n}^2}{(\beta_{k,n} + p_{r,k,n}\gamma_{rd,k,n})^2} \begin{pmatrix} -\frac{p_{r,k,n}}{\beta_{k,n}} & 1 \\ 1 & -\frac{\beta_{k,n}}{p_{r,k,n}} \end{pmatrix}, \tag{G.6}$$

which is also a negative semi-definite matrix, indicating that v is a concave function. Since functions u and v are both concave and positive, it is concluded that the equivalent function $\frac{1}{2}(\frac{1}{u} + \frac{1}{v})$ is a convex function with one and only one optimal solution in the considered domain.

Appendix H

Proof of Convergence in Outer Layer

Suppose that $(\boldsymbol{W^*}, \boldsymbol{p^*})$ is the optimal solution of (7.20), with the optimal β^*. Define β_0 as the root of $f_1(\boldsymbol{W}, \boldsymbol{p}) - f_2^{(n)}(\boldsymbol{W}, \boldsymbol{p}) - \beta p_{\text{total}}(\boldsymbol{W}, \boldsymbol{p}) = 0$.

If $f_1(\boldsymbol{W}, \boldsymbol{p}) - f_2^{(n)}(\boldsymbol{W}, \boldsymbol{p}) - \beta_0 p_{\text{total}}(\boldsymbol{W}, \boldsymbol{p}) = 0$ is obtained at $(\boldsymbol{W_0}, \boldsymbol{p_0}) \in \boldsymbol{\Theta}$, it can be known that there is at least one solution $(\boldsymbol{W_0}, \boldsymbol{p_0})$ satisfying $f_1(\boldsymbol{W_0}, \boldsymbol{p_0}) - f_2^{(n)}(\boldsymbol{W_0}, \boldsymbol{p_0}) - \beta_0 p_{\text{total}}(\boldsymbol{W_0}, \boldsymbol{p_0}) = 0$. Also, we have

$$\beta^* \geq \frac{f_1(\boldsymbol{W_0}, \boldsymbol{p_0}) - f_2^{(n)}(\boldsymbol{W_0}, \boldsymbol{p_0})}{p_{\text{total}}(\boldsymbol{W_0}, \boldsymbol{p_0})} = \beta_0. \tag{H.1}$$

Due to the optimality, $f_1(\boldsymbol{W}, \boldsymbol{p}) - f_2^{(n)}(\boldsymbol{W}, \boldsymbol{p}) - \beta_0 p_{\text{total}}(\boldsymbol{W}, \boldsymbol{p}) = 0$ means $f_1(\boldsymbol{W}, \boldsymbol{p}) - f_2^{(n)}(\boldsymbol{W}, \boldsymbol{p}) - \beta_0 p_{\text{total}}(\boldsymbol{W}, \boldsymbol{p}) \leq 0$ for all $\boldsymbol{W}, \boldsymbol{p} \in \boldsymbol{\Theta}$, including $\boldsymbol{W^*}, \boldsymbol{p^*}$. Therefore, we have $\beta^* \leq \beta_0$. As a result, $\beta_* = \beta_0$ is readily lead.

On the other hand, if $\beta = \beta^*$, at least we have $f_1(\boldsymbol{W^*}, \boldsymbol{p^*}) - f_2^{(n)}(\boldsymbol{W^*}, \boldsymbol{p^*}) - \beta p_{\text{total}}(\boldsymbol{W^*}, \boldsymbol{p^*}) = 0$ and thus $f_1(\boldsymbol{W}, \boldsymbol{p}) - f_2^{(n)}(\boldsymbol{W}, \boldsymbol{p}) - \beta^* p_{\text{total}}(\boldsymbol{W}, \boldsymbol{p}) \geq 0$. Also, because β^* is optimal, for all feasible $(\boldsymbol{W}, \boldsymbol{p}) \in \boldsymbol{\Theta}$, $f_1(\boldsymbol{W}, \boldsymbol{p}) - f_2^{(n)}(\boldsymbol{W}, \boldsymbol{p}) - \beta^* p_{\text{total}}(\boldsymbol{W}, \boldsymbol{p}) \leq 0$ holds. As a result, the equality $\beta = \beta^*$ derives that $f_1(\boldsymbol{W}, \boldsymbol{p}) - f_2^{(n)}(\boldsymbol{W}, \boldsymbol{p}) - \beta^* p_{\text{total}}(\boldsymbol{W}, \boldsymbol{p}) = 0$.

In conclusion, the sufficient and necessary condition of $\beta = \beta^*$ is $f_1(\boldsymbol{W}, \boldsymbol{p}) - f_2^{(n)}(\boldsymbol{W}, \boldsymbol{p}) - \beta p_{\text{total}}(\boldsymbol{W}, \boldsymbol{p}) = 0$.

Appendix I

Proof of Rank One

The SDP relaxed problem in (7.20) satisfies the Slater's constraint qualification. To obtain the dual problem, the Lagrange function of the primal problem is given in (J.4). According to (J.4), the KKT conditions used for the proof are given by (I.1)

$$\begin{aligned}
&\frac{K\sum_{m=1}^{L}\sum_{n=1}^{L}t_m t_n \boldsymbol{F_m^T}(\boldsymbol{F_n^H})^T\boldsymbol{H_k}}{\Gamma^*}-\sum_{k'\neq K}^{K}\frac{\sum_{m=1}^{L}\sum_{n=1}^{L}t_m t_n \boldsymbol{F_m^T}(\boldsymbol{F_n^H})^T\boldsymbol{H_{k'}}}{a_{k'}^{(n)}}+\\
&\frac{U\mathrm{Tr}\big(\mathrm{diag}(\boldsymbol{h_{SI}}(\sum_{k=1}^{K}\sum_{m=1}^{L}\sum_{n=1}^{L}t_m t_n \boldsymbol{F_m^T}(\boldsymbol{F_n^H}))^T\boldsymbol{h_{SI}^H})(\sum_{i=1}^{L}\sum_{j=1}^{L}r_i r_j \boldsymbol{F_i G_u F_j^H})\big)}{\alpha\Lambda^*}\\
&-\sum_{u=1}^{U}\frac{\mathrm{diag}(\boldsymbol{h_{SI}}(\sum_{k=1}^{K}\sum_{m=1}^{L}\sum_{n=1}^{L}t_m t_n \boldsymbol{F_m^T}(\boldsymbol{F_n^H}))^T\boldsymbol{h_{SI}^H})(\sum_{i=1}^{L}\sum_{j=1}^{L}r_i r_j \boldsymbol{F_i G_u F_j^H})\big)}{\alpha b_u^{(n)}}\\
&-\frac{\beta}{\eta}\boldsymbol{I}-\sum_{l=1}^{L}\zeta_l^*\boldsymbol{F_l}^T+\boldsymbol{Z_k^*}=0;\boldsymbol{W_k^*Z_k^*}=\boldsymbol{0};\boldsymbol{Z_k^*}\succeq\boldsymbol{0};\zeta_l^*\geq 0;
\end{aligned}\tag{I.1}$$

where $\Gamma^*=\sum_{k=1}^{K}\log_2\Big(\sum_{k'=1}^{K}\mathrm{Tr}(\sum_{m=1}^{L}\sum_{n=1}^{L}t_m t_n \boldsymbol{F_m W_{k'}^* F_n^H H_k})+\sum_{u=1}^{U}p_u^*|e_{u,k}|^2+\sigma_k^2\Big)$, $\Lambda^*=\sum_{u=1}^{U}\log_2\Big(\sum_{u'\neq u}^{U}p_{u'}^*\mathrm{Tr}(\boldsymbol{G_{u'}}\sum_{i=1}^{L}\sum_{j=1}^{L}r_i r_j \boldsymbol{F_i G_u F_j^H})+\sigma^2\mathrm{Tr}(\sum_{i=1}^{L}\sum_{j=1}^{L}r_i r_j \boldsymbol{F_i G_u F_j^H})+\frac{1}{\alpha}\mathrm{Tr}\big(\mathrm{diag}(\boldsymbol{h_{SI}}(\sum_{k=1}^{K}\sum_{m=1}^{L}\sum_{n=1}^{L}t_m t_n \boldsymbol{F_m W_k^* F_n^H})\boldsymbol{h_{SI}^H})(\sum_{i=1}^{L}\sum_{j=1}^{L}r_i r_j \boldsymbol{F_i G_u F_j^H})\big)\Big)$ are both scalars. For simplicity, the equation (I.1) can be re-expressed by (I.2), which is also shown at the top of the next page. By pre-multiplying both side of the first equality in (I.2) by $\boldsymbol{W_k^*}$, we have

$$\boldsymbol{Z}_{\boldsymbol{k}}^{*}=\boldsymbol{A}_{\boldsymbol{k}}^{*}-\frac{K\sum_{m=1}^{L}\sum_{n=1}^{L}t_m t_n \boldsymbol{F}_{\boldsymbol{m}}^{T}(\boldsymbol{F}_{\boldsymbol{n}}^{H})^{T}\boldsymbol{H}_{\boldsymbol{k}}}{\Gamma^{*}},$$
$$\boldsymbol{A}_{\boldsymbol{k}}^{*}=\sum_{k'\neq K}^{K}\frac{\sum_{m=1}^{L}\sum_{n=1}^{L}t_m t_n \boldsymbol{F}_{\boldsymbol{m}}^{T}(\boldsymbol{F}_{\boldsymbol{n}}^{H})^{T}\ \boldsymbol{H}_{\boldsymbol{k'}}}{a_{k'}^{(n)}}+\frac{\beta}{\eta}\boldsymbol{I}+\sum_{l=1}^{L}\zeta_{l}^{*}\boldsymbol{F}_{\boldsymbol{l}}^{T}+$$
$$\sum_{u=1}^{U}\frac{\mathrm{diag}(\boldsymbol{h}_{\boldsymbol{SI}}(\sum_{k=1}^{K}\sum_{m=1}^{L}\sum_{n=1}^{L}t_m t_n \boldsymbol{F}_{\boldsymbol{m}}^{T}(\boldsymbol{F}_{\boldsymbol{n}}^{H}))^{T}\boldsymbol{h}_{\boldsymbol{SI}}^{H})(\sum_{i=1}^{L}\sum_{j=1}^{L}r_i r_j \boldsymbol{F}_{\boldsymbol{i}}\boldsymbol{G}_{\boldsymbol{u}}\boldsymbol{F}_{\boldsymbol{j}}^{H}))}{\alpha b_{u}^{(n)}}$$
$$-\frac{U\mathrm{Tr}\big(\mathrm{diag}(\boldsymbol{h}_{\boldsymbol{SI}}(\sum_{k=1}^{K}\sum_{m=1}^{L}\sum_{n=1}^{L}t_m t_n \boldsymbol{F}_{\boldsymbol{m}}^{T}(\boldsymbol{F}_{\boldsymbol{n}}^{H}))^{T}\boldsymbol{h}_{\boldsymbol{SI}}^{H})(\sum_{i=1}^{L}\sum_{j=1}^{L}r_i r_j \boldsymbol{F}_{\boldsymbol{i}}\boldsymbol{G}_{\boldsymbol{u}}\boldsymbol{F}_{\boldsymbol{j}}^{H})\big)}{\alpha\Lambda^{*}} \tag{I.2}$$

$$\boldsymbol{W}_{\boldsymbol{k}}^{*}\boldsymbol{A}_{\boldsymbol{k}}^{*}=\boldsymbol{W}_{\boldsymbol{k}}^{*}\frac{K\sum_{m=1}^{L}\sum_{n=1}^{L}t_m t_n \boldsymbol{F}_{\boldsymbol{m}}^{T}(\boldsymbol{F}_{\boldsymbol{n}}^{H})^{T}\boldsymbol{H}_{\boldsymbol{k}}}{\Gamma}. \tag{I.3}$$

Since all channel variables in the system are statistically independent, the matrices span the whole signal space and it can be known that $\boldsymbol{A}_{\boldsymbol{k}}^{*}$ is a full-rank matrix [133]. According to the properties of matrix calculus, we have

$$\begin{aligned}
&\mathrm{Rank}(\boldsymbol{W}_{\boldsymbol{k}}^{*})=\mathrm{Rank}(\boldsymbol{W}_{\boldsymbol{k}}^{*}\boldsymbol{A}_{\boldsymbol{k}})\\
&=\mathrm{Rank}(\boldsymbol{W}_{\boldsymbol{k}}^{*}\frac{K\sum_{m=1}^{L}\sum_{n=1}^{L}t_m t_n \boldsymbol{F}_{\boldsymbol{m}}^{T}(\boldsymbol{F}_{\boldsymbol{n}}^{H})^{T}\boldsymbol{H}_{\boldsymbol{k}}}{\Gamma})\\
&\leq \min\{\mathrm{Rank}(\boldsymbol{W}_{\boldsymbol{k}}^{*}),\mathrm{Rank}(\frac{K\sum_{m=1}^{L}\sum_{n=1}^{L}t_m t_n \boldsymbol{F}_{\boldsymbol{m}}^{T}(\boldsymbol{F}_{\boldsymbol{n}}^{H})^{T}\boldsymbol{H}_{\boldsymbol{k}}}{\Gamma})\}\\
&\leq \mathrm{Rank}(\frac{K\sum_{m=1}^{L}\sum_{n=1}^{L}t_m t_n \boldsymbol{F}_{\boldsymbol{m}}^{T}(\boldsymbol{F}_{\boldsymbol{n}}^{H})^{T}\boldsymbol{H}_{\boldsymbol{k}}}{\Gamma}).
\end{aligned} \tag{I.4}$$

Since $\mathrm{Rank}(\frac{K\sum_{m=1}^{L}\sum_{n=1}^{L}t_m t_n \boldsymbol{F}_{\boldsymbol{m}}^{T}(\boldsymbol{F}_{\boldsymbol{n}}^{H})^{T}\boldsymbol{H}_{\boldsymbol{k}}}{\Gamma})\leq 1$, it is derived that the rank of matrix $\boldsymbol{W}_{\boldsymbol{k}}^{*}$ is smaller or equal to 1. It is well known that only a null matrix has rank 0 while $\boldsymbol{W}_{\boldsymbol{k}}^{*}\neq\boldsymbol{0}$. Thus, $\mathrm{Rank}(\boldsymbol{W}_{\boldsymbol{k}}^{*})=1$ is obtained.

Appendix J

Proof of Convergence in Inner Layer

The proof of convergence of FW method follows the similar approach in [66]. Let $\Upsilon^{(n+1)}$ denote the optimal value of P7.5 at the $n+1th$ iteration. According to the updating method in FW, we have

$$\begin{aligned}\Upsilon^{(n+1)} &= f_1(\boldsymbol{W^{(n+1)}}, \boldsymbol{p^{(n+1)}}) - f_2^{(n)}(\boldsymbol{W^{(n+1)}}, \boldsymbol{p^{(n+1)}}) - \beta P_{\text{total}}(\boldsymbol{W^{(n+1)}}, \boldsymbol{p^{(n+1)}}) \\ &= \underset{\boldsymbol{W},\boldsymbol{p}\in\boldsymbol{\Theta}.}{\text{argmax}}\, f_1(\boldsymbol{W},\boldsymbol{p}) - f_2^{(n)}(\boldsymbol{W},\boldsymbol{p}) - \beta P_{\text{total}}(\boldsymbol{W},\boldsymbol{p}).\end{aligned} \tag{J.1}$$

$\Upsilon^{(n+1)}$ is the optimal value at the $(n+1)-th$ iteration, which is greater than any other solution in the feasible domain. Therefore, we have the following inequality

$$\begin{aligned}&\underset{\boldsymbol{W},\boldsymbol{p}\in\boldsymbol{\Theta}.}{\text{argmax}}\, f_1(\boldsymbol{W},\boldsymbol{p}) - f_2^{(n)}(\boldsymbol{W},\boldsymbol{p}) - \beta P_{\text{total}}(\boldsymbol{W},\boldsymbol{p}) \geq \\ &f_1(\boldsymbol{W^{(n)}}, \boldsymbol{p^{(n)}}) - f_2^{(n)}(\boldsymbol{W^{(n)}}, \boldsymbol{p^{(n)}}) - \beta P_{\text{total}}(\boldsymbol{W^{(n)}}, \boldsymbol{p^{(n)}})\end{aligned} \tag{J.2}$$

Since we have the equalities that $f_2^{(n)}(\boldsymbol{W^{(n)}}, \boldsymbol{p^{(n)}}) = f_2(\boldsymbol{W^{(n)}}, \boldsymbol{p^{(n)}})$ and $\nabla f_2^{(n)}(\boldsymbol{W^{(n)}}, \boldsymbol{p^{(n)}}) = \nabla f_2(\boldsymbol{W^{(n)}}, \boldsymbol{p^{(n)}})$, (J.2) can be further derived as

$$\begin{aligned}&f_1(\boldsymbol{W^{(n)}}, \boldsymbol{p^{(n)}}) - f_2^{(n)}(\boldsymbol{W^{(n)}}, \boldsymbol{p^{(n)}}) - \beta P_{\text{total}}(\boldsymbol{W^{(n)}}, \boldsymbol{p^{(n)}}) \\ &= f_1(\boldsymbol{W^{(n)}}, \boldsymbol{p^{(n)}}) - f_2(\boldsymbol{W^{(n)}}, \boldsymbol{p^{(n)}}) - \beta P_{\text{total}}(\boldsymbol{W^{(n)}}, \boldsymbol{p^{(n)}}) \\ &\geq f_1(\boldsymbol{W^{(n)}}, \boldsymbol{p^{(n)}}) - f_2^{(n-1)}(\boldsymbol{W^{(n)}}, \boldsymbol{p^{(n)}}) - \beta P_{\text{total}}(\boldsymbol{W^{(n)}}, \boldsymbol{p^{(n)}}) = \Upsilon^{(n)}.\end{aligned} \tag{J.3}$$

As a result, it indicates that $\Upsilon^{(n+1)} \geq \Upsilon^{(n)}$, meaning the value of (7.20) is non-decreasing after each iteration. Also, the value of (7.20) is upper bounded by the transmission power constraints $(\widetilde{C1})$ and $(C2)$, and thus the FW method confirms the convergence.

Then it is proven that the convergence leads to a KKT point. The Lagrange function of (7.20) is established as

$$\begin{aligned} L = & f_1(\boldsymbol{W}, \boldsymbol{p}) - f_2^{(n)}(\boldsymbol{W}, \boldsymbol{p}) - \beta P_{\text{total}}(\boldsymbol{W}, \boldsymbol{p}) + \lambda_u p_u + \\ & \sum_{l=1}^{L} \zeta_l (p_{DA} - \sum_{k=1}^{K} Tr(\boldsymbol{W_k} \boldsymbol{F_l})) + \boldsymbol{W_k} \boldsymbol{Z_k} + \varsigma_u (p_{u,max} - p_u). \end{aligned} \tag{J.4}$$

The KKT condition of the optimal value at iteration n is given by

$$\begin{aligned} & \nabla_{\boldsymbol{W_k}} f_1(\boldsymbol{W^{(n)}}, \boldsymbol{p^{(n)}}) - \nabla_{\boldsymbol{W_k}} f_2^{(n)}(\boldsymbol{W^{(n)}}, \boldsymbol{p^{(n)}}) + \boldsymbol{Z_k} - \nabla_{\boldsymbol{W_k}} \beta P_{\text{total}}(\boldsymbol{W^{(n)}}, \boldsymbol{p^{(n)}}) - \\ & \sum_{l=1}^{L} \zeta_l \boldsymbol{F_l} = 0, \\ & \nabla_{p_u} f_1(\boldsymbol{W^{(n)}}, \boldsymbol{p^{(n)}}) - \nabla_{p_u} f_2^{(n)}(\boldsymbol{W^{(n)}}, \boldsymbol{p^{(n)}}) - \varsigma_u + \lambda_u - \nabla_{p_u} \beta P_{\text{total}}(\boldsymbol{W^{(n)}}, \boldsymbol{p^{(n)}}) = 0, \\ & \zeta_l (p_{DA} - \sum_{k=1}^{K} Tr(\boldsymbol{W_k^{(n)}} \boldsymbol{F_l})) = 0, Tr(\boldsymbol{W_k^{(n)}} Z_k) = 0, \\ & \varsigma_u (p_{u,max} - p_u^{(n)}) = 0, \lambda_u p_u^{(n)} = 0, \end{aligned} \tag{J.5}$$

for $\forall k \in K$, $\forall u \in U$, and $\forall l \in L$. According to the equality that $\nabla f_2^{(n)}(\boldsymbol{W^{(n)}}, \boldsymbol{p^{(n)}}) = \nabla f_2(\boldsymbol{W^{(n)}}, \boldsymbol{p^{(n)}})$, $\nabla_{\boldsymbol{W_k}} f_2^{(n)}(\boldsymbol{W^{(n)}}, \boldsymbol{p^{(n)}})$ and $\nabla_{p_u} f_2^{(n)}(\boldsymbol{W^{(n)}}, \boldsymbol{p^{(n)}})$ can be replaced by $\nabla_{\boldsymbol{W_k}} f_2(\boldsymbol{W^{(n)}}, \boldsymbol{p^{(n)}})$ and $\nabla_{p_u} f_2(\boldsymbol{W^{(n)}}, \boldsymbol{p^{(n)}})$, which is exactly the KKT condition of the original problem $f_1(\boldsymbol{W}, \boldsymbol{p}) - f_2(\boldsymbol{W}, \boldsymbol{p}) - P_{\text{total}}(\boldsymbol{W}, \boldsymbol{p})$.

Bibliography

[1] D. Sabella, A. de Domenico, E. Katranaras, M. A. Imran, M. di Girolamo, U. Salim, M. Lalam, K. Samdanis, and A. Maeder, "Energy efficiency benefits of ran-as-a-service concept for a cloud-based 5g mobile network infrastructure," *IEEE Access*, vol. vol. 2, pp. 1586–1597, December 2014.

[2] D. W. K. Ng, E. S. Lo, and R. Schober, "Dynamic resource allocation in mimo-ofdma systems with full-duplex and hybrid relaying," *IEEE Transactions on Communications*, vol. 60, no. 5, pp. 1291–1304, May 2012.

[3] M. Duarte, A. Sabharwal, V. Aggarwal, R. Jana, K. K. Ramakrishnan, C. W. Rice, and N. K. Shankaranarayanan, "Design and characterization of a full-duplex multiantenna system for wifi networks," *IEEE Transactions on Vehicular Technology*, vol. 63, no. 3, pp. 1160–1177, March 2014.

[4] C. Marcu, D. Chowdhury, C. Thakkar, J. D. Park, L. K. Kong, M. Tabesh, Y. Wang, B. Afshar, A. Gupta, A. Arbabian, S. Gambini, R. Zamani, E. Alon, and A. M. Niknejad, "A 90 nm cmos low-power 60 ghz transceiver with integrated baseband circuitry," *IEEE Journal of Solid-State Circuits*, vol. 44, no. 12, pp. 3434–3447, December 2009.

[5] A. Siligaris, Y. Hamada, C. Mounet, C. Raynaud, B. Martineau, N. Deparis, N. Rolland, M. Fukaishi, and P. Vincent, "A 60 ghz power amplifier with 14.5 dbm saturation power and 25% peak pae in cmos 65 nm soi," *IEEE Journal of Solid-State Circuits*, vol. 45, no. 7, pp. 1286–1294, July 2010.

[6] V. H. Do, V. Subramanian, W. Keusgen, and G. Boeck, "A 60 ghz sige-hbt power amplifier with 20% pae at 15 dbm output power," *IEEE Microwave and Wireless Components Letters*, vol. 18, no. 3, pp. 209–211, March 2008.

[7] K. Okada, K. Kondou, M. Miyahara, M. Shinagawa, H. Asada, R. Minami, T. Yamaguchi, A. Musa, Y. Tsukui, Y. Asakura, S. Tamonoki, H. Yamagishi, Y. Hino, T. Sato, H. Sakaguchi, N. Shimasaki, T. Ito, Y. Takeuchi, N. Li, Q. Bu, R. Murakami, K. Bunsen, K. Matsushita, M. Noda, and A. Matsuzawa, "Full

four-channel 6.3-gb/s 60-ghz cmos transceiver with low-power analog and digital baseband circuitry," *IEEE Journal of Solid-State Circuits*, vol. 48, no. 1, pp. 46–65, January 2013.

[8] T. S. Rappaport, R. W. Heath, R. C. Daniels, and J. N. Murdock, "millimeter wave wireless communications," *Englewood Cliffs, NJ, USA: Prentice-Hall*, 2015.

[9] S. Geng, J. Kivinen, X. Zhao, and P. Vainikainen, "Millimeter-wave propagation channel characterization for short-range wireless communications," *IEEE Transactions on Vehicular Technology*, vol. 58, no. 1, pp. 3–13, January 2009.

[10] Z. Wei, X. Zhu, S. Sun, Y. Huang, L. Dong, and Y. Jiang, "Full-duplex versus half-duplex amplify-and-forward relaying: Which is more energy efficient in 60-ghz dual-hop indoor wireless systems?" *IEEE Journal on Selected Areas in Communications*, vol. 33, no. 12, pp. 2936–2947, December 2015.

[11] S. T. Choi, K. S. Yang, S. Nishi, S. Shimizu, K. Tokuda, and Y. H. Kim, "A 60-ghz point-to-multipoint millimeter-wave fiber-radio communication system," *IEEE Transactions on Microwave Theory and Techniques*, vol. 54, no. 5, pp. 1953–1960, May 2006.

[12] T. Dinc and H. Krishnaswamy, "A t/r antenna pair with polarization-based reconfigurable wideband self-interference cancellation for simultaneous transmit and receive," in *Proceeding of 2015 IEEE International Conference on International Microwave Symposium*, Phoenix, USA, May 2015, pp. 1–4.

[13] D. J. van den Broek, E. A. M. Klumperink, and B. Nauta, "An in-band full-duplex radio receiver with a passive vector modulator downmixer for self-interference cancellation," *IEEE Journal of Solid-State Circuits*, vol. 50, no. 12, pp. 3003–3014, December 2015.

[14] L. Li, K. Josiam, and R. Taori, "Feasibility study on full-duplex wireless millimeter-wave systems," in *Proceeding of 2014 IEEE International Conference on Acoustics, Speech and Signal Processing*, Florence, Italy, May 2014, pp. 2769–2773.

[15] V. V. Mai, J. Kim, S. W. Jeon, S. W. Choi, B. Seo, and W. Y. Shin, "Degrees of freedom of millimeter wave full-duplex systems with partial csit," *IEEE Communications Letters*, vol. 20, no. 5, pp. 1042–1045, May 2016.

[16] M. Jain, "Practical, real-time, full duplex," in *Proceeding of 2011 ACM International Conference on Mobile Computing and Networking*, HK, China, Sepetember 2011, pp. 301–312.

[17] T. S. Rappaport, S. Sun, R. Mayzus, H. Zhao, Y. Azar, K. Wang, G. N. Wong, J. K. Schulz, M. Samimi, and F. Gutierrez, "Millimeter wave mobile communications for 5g cellular: It will work!" *IEEE Access*, vol. 1, pp. 335–349, May 2013.

[18] N. Zhou, "Dynamic resource management for next generation broadband wireless communication systems," PhD Thesis, The University of Liverpool, Liverpool, UK, September 2010.

[19] D. Tse and P. Viswanath, *Fundamentals of Wireless Communication*, 2nd ed. Cambridge, U.K: Cambridge University Press, 2005.

[20] L. Dong, "Resource allocation for relay based green communication systems," PhD Thesis, The University of Liverpool, Liverpool, UK, September 2013.

[21] Z. Pi and F. Khan, "An introduction to millimeter-wave mobile broadband systems," *IEEE Communications Magazine*, vol. 49, no. 6, pp. 101–107, June 2011.

[22] IEEE 802.15.3c Part 15.3: Wireless medium access control (MAC) and physical layer (PHY) specifications for high rate wireless personal area networks (WPANs) amendment 2: Millimeter-wave-based alternative physical layer extension, October 2009.

[23] Z. Lan, C.-S. Sum, J. Wang, T. Baykas, F. Kojima, H. Nakase, and H. Harada, "Relay with deflection routing for effective throughput improvement in gbps millimeter-wave wpan systems," *IEEE Journal on Selected Areas in Communications*, vol. 27, no. 8, pp. 1453–1465, October 2009.

[24] C. W. Pyo and H. Harada, "Throughput analysis and improvement of hybrid multiple access in ieee 802.15.3c mm-wave wpan," *IEEE Journal on Selected Areas in Communications*, vol. 27, no. 8, pp. 1414–1424, October 2009.

[25] J. Qiao, L. X. Cai, X. S. Shen, and J. W. Mark, "Enabling multi-hop concurrent transmissions in 60 ghz wireless personal area networks," *IEEE Transactions on Wireless Communications*, vol. 10, no. 11, pp. 3824–3833, November 2011.

[26] A. Osseiran, F. Boccardi, V. Braun, K. Kusume, P. Marsch, M. Maternia, O. Queseth, M. Schellmann, H. Schotten, H. Taoka, H. Tullberg, M. A. Uusitalo, B. Timus, and M. Fallgren, "Scenarios for 5g mobile and wireless communications: the vision of the metis project," *IEEE Communications Magazine*, vol. 52, no. 5, pp. 26–35, May 2014.

[27] C. Dehos, J. L. Gonzlez, A. D. Domenico, D. Ktnas, and L. Dussopt, "Millimeter-wave access and backhauling: the solution to the exponential data traffic in-

crease in 5g mobile communications systems?" *IEEE Communications Magazine*, vol. 52, no. 9, pp. 88–95, September 2014.

[28] H. Xu, V. Kukshya, and T. S. Rappaport, "Spatial and temporal characteristics of 60-ghz indoor channels," *IEEE Journal on Selected Areas in Communications*, vol. 20, no. 3, pp. 620–630, April 2002.

[29] N. Moraitis and P. Constantinou, "Measurements and characterization of wideband indoor radio channel at 60 ghz," *IEEE Transactions on Wireless Communications*, vol. 5, no. 4, pp. 880–889, April 2006.

[30] S. Wyne, K. Haneda, S. Ranvier, F. Tufvesson, and A. F. Molisch, "Beamforming effects on measured mm-wave channel characteristics," *IEEE Transactions on Wireless Communications*, vol. 10, no. 11, pp. 3553–3559, November 2011.

[31] T. Manabe, Y. Miura, and T. Ihara, "Effects of antenna directivity and polarization on indoor multipath propagation characteristics at 60 ghz," *IEEE Journal on Selected Areas in Communications*, vol. 14, no. 3, pp. 441–448, April 1996.

[32] H. Shokri-Ghadikolaei, C. Fischione, G. Fodor, P. Popovski, and M. Zorzi, "Millimeter wave cellular networks: A mac layer perspective," *IEEE Transactions on Communications*, vol. 63, no. 10, pp. 3437–3458, October 2015.

[33] S. Singh, F. Ziliotto, U. Madhow, E. Belding, and M. Rodwell, "Blockage and directivity in 60 ghz wireless personal area networks: from cross-layer model to multihop mac design," *IEEE Journal on Selected Areas in Communications*, vol. 27, no. 8, pp. 1400–1413, October 2009.

[34] K. Dong, X. Liao, and S. Zhu, "Link blockage analysis for indoor 60ghz radio systems," *Electronics Letters*, vol. 48, no. 23, pp. 1506–1508, November 2012.

[35] V. K. Sakarellos, D. Skraparlis, A. D. Panagopoulos, and J. D. Kanellopoulos, "Cooperative diversity performance in millimeter wave radio systems," *IEEE Transactions on Communications*, vol. 60, no. 12, pp. 3641–3649, December 2012.

[36] D. Dardari and V. Tralli, "High-speed indoor wireless communications at 60 ghz with coded ofdm," *IEEE Transactions on Communications*, vol. 47, no. 11, pp. 1709–1721, November 1999.

[37] H. Ju, E. Oh, and D. Hong, "Improving efficiency of resource usage in two-hop full duplex relay systems based on resource sharing and interference cancellation," *IEEE Transactions on Wireless Communications*, vol. 8, no. 8, pp. 3933–3938, August 2009.

[38] I. Krikidis, H. A. Suraweera, P. J. Smith, and C. Yuen, "Full-duplex relay selection for amplify-and-forward cooperative networks," *IEEE Transactions on Wireless Communications*, vol. 11, no. 12, pp. 4381–4393, December 2012.

[39] H. Cui, M. Ma, L. Song, and B. Jiao, "Relay selection for two-way full duplex relay networks with amplify-and-forward protocol," *IEEE Transactions on Wireless Communications*, vol. 13, no. 7, pp. 3768–3777, July 2014.

[40] A. Ikhlef, J. Kim, and R. Schober, "Mimicking full-duplex relaying using half-duplex relays with buffers," *IEEE Transactions on Vehicular Technology*, vol. 61, no. 7, pp. 3025–3037, September 2012.

[41] S. Huberman and T. Le-Ngoc, "Mimo full-duplex precoding: A joint beamforming and self-interference cancellation structure," *IEEE Transactions on Wireless Communications*, vol. 14, no. 4, pp. 2205–2217, April 2015.

[42] E. Everett, A. Sahai, and A. Sabharwal, "Passive self-interference suppression for full-duplex infrastructure nodes," *IEEE Transactions on Wireless Communications*, vol. 12, no. 2, pp. 680–694, February 2014.

[43] V. Syrjala, M. Valkama, L. Anttila, T. Riihonen, and D. Korpi, "Analysis of oscillator phase-noise effects on self-interference cancellation in full-duplex ofdm radio transceivers," *IEEE Transactions on Wireless Communications*, vol. 13, no. 6, pp. 2977–2990, June 2014.

[44] Z. He, S. Shao, Y. Shen, C. Qing, and Y. Tang, "Performance analysis of rf self-interference cancellation in full-duplex wireless communications," *IEEE Wireless Communications Letters*, vol. 3, no. 4, pp. 405–408, August 2014.

[45] B. Franois and P. Reynaert, "A fully integrated transformer-coupled power detector with 5 ghz rf pa for wlan 802.11ac in 40 nm cmos," *IEEE Journal of Solid-State Circuits*, vol. 50, no. 5, pp. 1237–1250, May 2015.

[46] K. Yamamoto, T. Moriwaki, T. Fujii, J. Otsuji, M. Miyashita, Y. Miyazaki, and K. Nishitani, "A 2.2-v operation, 2.4-ghz single-chip gaas mmic transceiver for wireless applications," *IEEE Journal of Solid-State Circuits*, vol. 34, no. 4, pp. 502–512, April 1999.

[47] R. Bolla, R. Bruschi, F. Davoli, and F. Cucchietti, "Energy efficiency in the future internet: A survey of existing approaches and trends in energy-aware fixed network infrastructures," *IEEE Communications Surveys Tutorials*, vol. 13, no. 2, pp. 223–244, Second Quarter 2011.

[48] E. Ahmed, A. M. Eltawil, and A. Sabharwal, "Rate gain region and design tradeoffs for full-duplex wireless communications," *IEEE Transactions on Wireless Communications*, vol. 12, no. 7, pp. 3556–3565, July 2013.

[49] W. Li, J. Lilleberg, and K. Rikkinen, "On rate region analysis of half- and full-duplex ofdm communication links," *IEEE Journal on Selected Areas in Communications*, vol. 32, no. 9, pp. 1688–1698, September 2014.

[50] L. Dong, S. Sun, X. Zhu, and Y. K. Chia, "Power efficient 60 ghz wireless communication networks with relays," in *Proceeding of 2013 IEEE Annual International Symposium on Personal, Indoor, and Mobile Radio Communications*, Sept 2013, pp. 2808–2812.

[51] G. Miao, N. Himayat, and G. Y. Li, "Energy-efficient link adaptation in frequency-selective channels," *IEEE Transactions on Communications*, vol. 58, no. 2, pp. 545–554, February 2010.

[52] S. Cui, A. J. Goldsmith, and A. Bahai, "Energy-efficiency of mimo and cooperative mimo techniques in sensor networks," *IEEE Journal on Selected Areas in Communications*, vol. 22, no. 6, pp. 1089–1098, August 2004.

[53] C. Xiong, G. Y. Li, S. Zhang, Y. Chen, and S. Xu, "Energy- and spectral-efficiency tradeoff in downlink ofdma networks," *IEEE Transactions on Wireless Communications*, vol. 10, no. 11, pp. 3874–3886, November 2011.

[54] Y. Li, M. Reisslein, and C. Chakrabarti, "Energy-efficient video transmission over a wireless link," *IEEE Transactions on Vehicular Technology*, vol. 58, no. 3, pp. 1229–1244, March 2009.

[55] O. Waqar, M. A. Imran, M. Dianati, and R. Tafazolli, "Energy consumption analysis and optimization of ber-constrained amplify-and-forward relay networks," *IEEE Transactions on Vehicular Technology*, vol. 63, no. 3, pp. 1256–1269, March 2014.

[56] D. Quintas and V. Friderikos, "Energy efficient relaying within a cell: Multi path versus shortest path routing," in *Proceeding of 2010 IEEE International Conference on Computer Communications Workshops*, Atlanta, USA, March 2010, pp. 1–2.

[57] Q. Liu, W. Zhang, X. Ma, and G. T. Zhou, "Designing peak power constrained amplify-and-forward relay networks with cooperative diversity," *IEEE Transactions on Wireless Communications*, vol. 11, no. 5, pp. 1733–1743, May 2012.

[58] V. K. Sakarellos, D. Skraparlis, A. D. Panagopoulos, and J. D. Kanellopoulos, "Optimum placement of radio relays in millimeter-wave wireless dual-hop networks [wireless corner]," *IEEE Antennas and Propagation Magazine*, vol. 51, no. 2, pp. 190–199, April 2009.

[59] G. Liu, F. R. Yu, H. Ji, V. C. M. Leung, and X. Li, "In-band full-duplex relaying: A survey, research issues and challenges," *IEEE Communications Surveys Tutorials*, vol. 17, no. 2, pp. 500–524, Second Quarter 2015.

[60] T. Riihonen, S. Werner, and R. Wichman, "Hybrid full-duplex/half-duplex relaying with transmit power adaptation," *IEEE Transactions on Wireless Communications*, vol. 10, no. 9, pp. 3074–3085, September 2011.

[61] O. Arnold, F. Richter, G. Fettweis, and O. Blume, "Power consumption modeling of different base station types in heterogeneous cellular networks," in *Proceeding of 2010 IEEE International Conference on Future Network Mobile Summit*, Florence, Italy, June 2010, pp. 1–8.

[62] S. Cui, A. J. Goldsmith, and A. Bahai, "Energy-constrained modulation optimization," *IEEE Transactions on Wireless Communications*, vol. 4, no. 5, pp. 2349–2360, September 2005.

[63] P. Grover, K. Woyach, and A. Sahai, "Towards a communication-theoretic understanding of system-level power consumption," *IEEE Journal on Selected Areas in Communications*, vol. 29, no. 8, pp. 1744–1755, September 2011.

[64] K. Yamamoto, K. Haneda, H. Murata, and S. Yoshida, "Optimal transmission scheduling for a hybrid of full- and half-duplex relaying," *IEEE Communications Letters*, vol. 15, no. 3, pp. 305–307, March 2011.

[65] A. C. Cirik, Y. Rong, and Y. Hua, "Achievable rates of full-duplex mimo radios in fast fading channels with imperfect channel estimation," *IEEE Transactions on Signal Processing*, vol. 62, no. 15, pp. 3874–3886, August 2014.

[66] D. Nguyen, L. N. Tran, P. Pirinen, and M. Latva-aho, "On the spectral efficiency of full-duplex small cell wireless systems," *IEEE Transactions on Wireless Communications*, vol. 12, no. 9, pp. 4896–4910, September 2014.

[67] C. Nam, C. Joo, and S. Bahk, "Joint subcarrier assignment and power allocation in full-duplex ofdma networks," *IEEE Transactions on Wireless Communications*, vol. 14, no. 6, pp. 3108–3119, June 2015.

[68] H. A. Suraweera, I. Krikidis, G. Zheng, C. Yuen, and P. J. Smith, "Low-complexity end-to-end performance optimization in mimo full-duplex relay sys-

tems," *IEEE Transactions on Wireless Communications*, vol. 13, no. 2, pp. 913–927, February 2014.

[69] H. Kim, S. Lim, H. Wang, and D. Hong, "Optimal power allocation and outage analysis for cognitive full duplex relay systems," *IEEE Transactions on Wireless Communications*, vol. 11, no. 10, pp. 3754–3765, October 2012.

[70] C. Xiong, L. Lu, and G. Y. Li, "Energy-efficient spectrum access in cognitive radios," *IEEE Journal on Selected Areas in Communications*, vol. 32, no. 3, pp. 550–562, March 2014.

[71] X. Xiao, X. Tao, and J. Lu, "Energy-efficient resource allocation in lte-based mimo-ofdma systems with user rate constraints," *IEEE Transactions on Vehicular Technology*, vol. 64, no. 1, pp. 185–197, January 2015.

[72] X. Hong, Y. Jie, C. X. Wang, J. Shi, and X. Ge, "Energy-spectral efficiency trade-off in virtual mimo cellular systems," *IEEE Journal on Selected Areas in Communications*, vol. 31, no. 10, pp. 2128–2140, October 2013.

[73] X. Ge, X. Huang, Y. Wang, M. Chen, Q. Li, T. Han, and C. X. Wang, "Energy-efficiency optimization for mimo-ofdm mobile multimedia communication systems with qos constraints," *IEEE Transactions on Vehicular Technology*, vol. 63, no. 5, pp. 2127–2138, June 2014.

[74] C. Xiong, G. Y. Li, S. Zhang, Y. Chen, and S. Xu, "Energy-efficient resource allocation in ofdma networks," *IEEE Transactions on Communications*, vol. 60, no. 12, pp. 3767–3778, December 2012.

[75] C. Xiong, G. Y. Li, Y. Liu, Y. Chen, and S. Xu, "Energy-efficient design for downlink ofdma with delay-sensitive traffic," *IEEE Transactions on Wireless Communications*, vol. 12, no. 6, pp. 3085–3095, June 2013.

[76] F. Haider, C. X. Wang, H. Haas, E. Hepsaydir, X. Ge, and D. Yuan, "Spectral and energy efficiency analysis for cognitive radio networks," *IEEE Transactions on Wireless Communications*, vol. 14, no. 6, pp. 2969–2980, June 2015.

[77] G. Yu, Q. Chen, R. Yin, H. Zhang, and G. Y. Li, "Joint downlink and uplink resource allocation for energy-efficient carrier aggregation," *IEEE Transactions on Wireless Communications*, vol. 14, no. 6, pp. 3207–3218, June 2015.

[78] G. Yu, Y. Jiang, L. Xu, and G. Y. Li, "Multi-objective energy-efficient resource allocation for multi-rat heterogeneous networks," *IEEE Journal on Selected Areas in Communications*, vol. 33, no. 10, pp. 2118–2127, October 2015.

[79] F. Z. Kaddour, E. Vivier, L. Mroueh, M. Pischella, and P. Martins, "Green opportunistic and efficient resource block allocation algorithm for lte uplink networks," *IEEE Transactions on Vehicular Technology*, vol. 64, no. 10, pp. 4537–4550, October 2015.

[80] A. Aijaz, M. Tshangini, M. R. Nakhai, X. Chu, and A. H. Aghvami, "Energy-efficient uplink resource allocation in lte networks with m2m/h2h co-existence under statistical qos guarantees," *IEEE Transactions on Communications*, vol. 62, no. 7, pp. 2353–2365, July 2014.

[81] F. D. Cardoso, S. Petersson, M. Boldi, S. Mizuta, G. Dietl, R. Torrea-Duran, C. Desset, J. Leinonen, and L. M. Correia, "Energy efficient transmission techniques for lte," *IEEE Communications Magazine*, vol. 51, no. 10, pp. 182–190, October 2013.

[82] G. Wu, C. Yang, S. Li, and G. Y. Li, "Recent advances in energy-efficient networks and their application in 5g systems," *IEEE Wireless Communications*, vol. 22, no. 2, pp. 145–151, April 2015.

[83] Z. Gao, L. Dai, D. Mi, Z. Wang, M. A. Imran, and M. Z. Shakir, "Mmwave massive-mimo-based wireless backhaul for the 5g ultra-dense network," *IEEE Wireless Communications*, vol. 22, no. 5, pp. 13–21, October 2015.

[84] X. Ge, S. Tu, G. Mao, C. X. Wang, and T. Han, "5g ultra-dense cellular networks," *IEEE Wireless Communications*, vol. 23, no. 1, pp. 72–79, February 2016.

[85] X. Ge, J. Ye, Y. Yang, and Q. Li, "User mobility evaluation for 5g small cell networks based on individual mobility model," *IEEE Journal on Selected Areas in Communications*, vol. 34, no. 3, pp. 528–541, March 2016.

[86] G. Liu, F. R. Yu, H. Ji, and V. C. M. Leung, "Energy-efficient resource allocation in cellular networks with shared full-duplex relaying," *IEEE Transactions on Vehicular Technology*, vol. 64, no. 8, pp. 3711–3724, August 2015.

[87] L. J. Rodrguez, N. H. Tran, and T. Le-Ngoc, "Performance of full-duplex af relaying in the presence of residual self-interference," *IEEE Journal on Selected Areas in Communications*, vol. 32, no. 9, pp. 1752–1764, September 2014.

[88] D. W. K. Ng and R. Schober, "Cross-layer scheduling for ofdma amplify-and-forward relay networks," *IEEE Transactions on Vehicular Technology*, vol. 59, no. 3, pp. 1443–1458, March 2010.

[89] G. Caire, G. Taricco, and E. Biglieri, "Optimum power control over fading channels," *IEEE Transactions on Information Theory*, vol. 45, no. 5, pp. 1468–1489, July 1999.

[90] W. Yu and R. Lui, "Dual methods for nonconvex spectrum optimization of multicarrier systems," *IEEE Transactions on Communications*, vol. 54, no. 7, pp. 1310–1322, July 2006.

[91] D. W. K. Ng, E. S. Lo, and R. Schober, "Energy-efficient resource allocation in ofdma systems with large numbers of base station antennas," *IEEE Transactions on Wireless Communications*, vol. 11, no. 9, pp. 3292–3304, September 2012.

[92] N. Zhou, X. Zhu, and Y. Huang, "Optimal asymmetric resource allocation and analysis for ofdm-based multidestination relay systems in the downlink," *IEEE Transactions on Vehicular Technology*, vol. 60, no. 3, pp. 1307–1312, March 2011.

[93] T. Zwick, T. J. Beukema, and H. Nam, "Wideband channel sounder with measurements and model for the 60 ghz indoor radio channel," *IEEE Transactions on Vehicular Technology*, vol. 54, no. 4, pp. 1266–1277, July 2005.

[94] S. Mallick, R. Devarajan, R. A. Loodaricheh, and V. K. Bhargava, "Robust resource optimization for cooperative cognitive radio networks with imperfect csi," *IEEE Transactions on Wireless Communications*, vol. 14, no. 2, pp. 907–920, February 2015.

[95] Wireless LAN medium access control (MAC) and physical layer (PHY) specifications amendment 3: enhancements for very high throughput in the 60 GHz band, March 2014. [Online]. Available: http: www.iso.org/iso/catalogue-detail.htm.csnumber=64876.

[96] Y. B. Lin, T. H. Chiu, and Y. T. Su, "Optimal and near-optimal resource allocation algorithms for ofdma networks," *IEEE Transactions on Wireless Communications*, vol. 8, no. 8, pp. 4066–4077, August 2009.

[97] S. Li, W. Li, J. Deng, T. D. Nguyen, and C. C. Mi, "A double-sided lcc compensation network and its tuning method for wireless power transfer," *IEEE Transactions on Vehicular Technology*, vol. 64, no. 6, pp. 2261–2273, June 2015.

[98] I. Krikidis, S. Timotheou, S. Nikolaou, G. Zheng, D. W. K. Ng, and R. Schober, "Simultaneous wireless information and power transfer in modern communication systems," *IEEE Communications Magazine*, vol. 52, no. 11, pp. 104–110, November 2014.

[99] J. Wang, C. Jiang, Z. Han, Y. Ren, and L. Hanzo, "Network association strategies for an energy harvesting aided super-wifi network relying on measured solar activity," *IEEE Journal on Selected Areas in Communications*, vol. 34, no. 12, pp. 3785–3797, December 2016.

[100] Q. Li, Q. Zhang, and J. Qin, "Secure relay beamforming for simultaneous wireless information and power transfer in nonregenerative relay networks," *IEEE Transactions on Vehicular Technology*, vol. 63, no. 5, pp. 2462–2467, June 2014.

[101] A. A. Nasir, X. Zhou, S. Durrani, and R. A. Kennedy, "Relaying protocols for wireless energy harvesting and information processing," *IEEE Transactions on Wireless Communications*, vol. 12, no. 7, pp. 3622–3636, July 2013.

[102] Z. Ding, I. Krikidis, B. Sharif, and H. V. Poor, "Wireless information and power transfer in cooperative networks with spatially random relays," *IEEE Transactions on Wireless Communications*, vol. 13, no. 8, pp. 4440–4453, August 2014.

[103] G. Amarasuriya, E. G. Larsson, and H. V. Poor, "Wireless information and power transfer in multiway massive mimo relay networks," *IEEE Transactions on Wireless Communications*, vol. 15, no. 6, pp. 3837–3855, June 2016.

[104] H. Ju and R. Zhang, "Optimal resource allocation in full-duplex wireless-powered communication network," *IEEE Transactions on Communications*, vol. 62, no. 10, pp. 3528–3540, October 2014.

[105] C. Zhong, H. A. Suraweera, G. Zheng, I. Krikidis, and Z. Zhang, "Wireless information and power transfer with full duplex relaying," *IEEE Transactions on Communications*, vol. 62, no. 10, pp. 3447–3461, October 2014.

[106] M. Mohammadi, B. K. Chalise, H. A. Suraweera, C. Zhong, G. Zheng, and I. Krikidis, "Throughput analysis and optimization of wireless-powered multiple antenna full-duplex relay systems," *IEEE Transactions on Communications*, vol. 64, no. 4, pp. 1769–1785, April 2016.

[107] Z. Wen, X. Liu, N. C. Beaulieu, R. Wang, and S. Wang, "Joint source and relay beamforming design for full-duplex mimo af relay swipt systems," *IEEE Communications Letters*, vol. 20, no. 2, pp. 320–323, February 2016.

[108] Y. Zeng and R. Zhang, "Full-duplex wireless-powered relay with self-energy recycling," *IEEE Wireless Communications Letters*, vol. 4, no. 2, pp. 201–204, April 2015.

[109] D. Hwang, K. C. Hwang, D. I. Kim, and T. J. Lee, "Self-energy recycling for rf powered multi-antenna relay channels," *IEEE Transactions on Wireless Communications*, vol. 16, no. 2, pp. 812–824, February 2017.

[110] Y. Zeng and R. Zhang, "Optimized training design for wireless energy transfer," *IEEE Transactions on Communications*, vol. 63, no. 2, pp. 536–550, February 2015.

[111] M. Maso, C. F. Liu, C. H. Lee, T. Q. S. Quek, and L. S. Cardoso, "Energy-recycling full-duplex radios for next-generation networks," *IEEE Journal on Selected Areas in Communications*, vol. 33, no. 12, pp. 2948–2962, December 2015.

[112] Y. Zeng, H. Chen, and R. Zhang, "Bidirectional wireless information and power transfer with a helping relay," *IEEE Communications Letters*, vol. 20, no. 5, pp. 862–865, May 2016.

[113] D. W. K. Ng, E. S. Lo, and R. Schober, "Wireless information and power transfer: Energy efficiency optimization in ofdma systems," *IEEE Transactions on Wireless Communications*, vol. 12, no. 12, pp. 6352–6370, December 2013.

[114] Z. Wei, X. Zhu, S. Sun, and Y. Huang, "Energy-efficiency-oriented cross-layer resource allocation for multiuser full-duplex decode-and-forward indoor relay systems at 60 ghz," *IEEE Journal on Selected Areas in Communications*, vol. 34, no. 12, pp. 3366–3379, December 2016.

[115] Z. Wei, X. Zhu, S. Sun, Y. Huang, A. Al-Tahmeesschi, and Y. Jiang, "Energy-efficiency of millimeter-wave full-duplex relaying systems: Challenges and solutions," *IEEE Access*, vol. 4, pp. 4848–4860, July 2016.

[116] X. Zhu and R. D. Murch, "Layered space-frequency equalization in a single-carrier mimo system for frequency-selective channels," *IEEE Transactions on Wireless Communications*, vol. 3, no. 3, pp. 701–708, May 2004.

[117] H. Xie, F. Gao, S. Zhang, and S. Jin, "A unified transmission strategy for tdd/fdd massive mimo systems with spatial basis expansion model," *IEEE Transactions on Vehicular Technology*, vol. 66, no. 4, pp. 3170–3184, April 2017.

[118] B. Radunovic, D. Gunawardena, P. Key, A. Proutiere, N. Singh, V. Balan, and G. Dejean, "Rethinking indoor wireless mesh design: Low power, low frequency, full-duplex," in *Proceeding of 2010 IEEE International Workshop on Wireless Mesh Networks*, Boston, UAS, June 2010, pp. 1–6.

[119] A. Almradi and K. A. Hamdi, "On the outage probability of mimo full-duplex relaying: Impact of antenna correlation and imperfect csi," *IEEE Transactions on Vehicular Technology*, vol. 66, no. 5, pp. 3957–3965, May 2017.

[120] B. P. Day, A. R. Margetts, D. W. Bliss, and P. Schniter, "Full-duplex bidirectional mimo: Achievable rates under limited dynamic range," *IEEE Transactions on Signal Processing*, vol. 60, no. 7, pp. 3702–3713, July 2012.

[121] T. Riihonen, S. Werner, and R. Wichman, "Mitigation of loopback self-interference in full-duplex mimo relays," *IEEE Transactions on Signal Processing*, vol. 59, no. 12, pp. 5983–5993, December 2011.

[122] G. Amarasuriya, C. Tellambura, and M. Ardakani, "Two-way amplify-and-forward multiple-input multiple-output relay networks with antenna selection," *IEEE Journal on Selected Areas in Communications*, vol. 30, no. 8, pp. 1513–1529, September 2012.

[123] J. H. Lee and O. S. Shin, "Full-duplex relay based on distributed beamforming in multiuser mimo systems," *IEEE Transactions on Vehicular Technology*, vol. 62, no. 4, pp. 1855–1860, May 2013.

[124] G. Amarasuriya, C. Tellambura, and M. Ardakani, "Multi-way mimo amplify-and-forward relay networks with zero-forcing transmission," *IEEE Transactions on Communications*, vol. 61, no. 12, pp. 4847–4863, December 2013.

[125] H. Q. Ngo, H. A. Suraweera, M. Matthaiou, and E. G. Larsson, "Multipair full-duplex relaying with massive arrays and linear processing," *IEEE Journal on Selected Areas in Communications*, vol. 32, no. 9, pp. 1721–1737, September 2014.

[126] B. Yin, M. Wu, C. Studer, J. R. Cavallaro, and J. Lilleberg, "Full-duplex in large-scale wireless systems," in *Proceeding of 2013 Asilomar International Conference on Signals, Systems and Computers*, CA, USA, Nov 2013, pp. 1623–1627.

[127] X. Gao, O. Edfors, F. Tufvesson, and E. G. Larsson, "Massive mimo in real propagation environments: Do all antennas contribute equally?" *IEEE Transactions on Communications*, vol. 63, no. 11, pp. 3917–3928, November 2015.

[128] J. Joung, Y. K. Chia, and S. Sun, "Energy-efficient, large-scale distributed-antenna system (l-das) for multiple users," *IEEE Journal of Selected Topics in Signal Processing*, vol. 8, no. 5, pp. 954–965, October 2014.

[129] D. W. K. Ng, Y. Wu, and R. Schober, "Power efficient resource allocation for full-duplex radio distributed antenna networks," *IEEE Transactions on Wireless Communications*, vol. 15, no. 4, pp. 2896–2911, April 2016.

[130] L. Lu, G. Y. Li, A. L. Swindlehurst, A. Ashikhmin, and R. Zhang, "An overview of massive mimo: Benefits and challenges," *IEEE Journal of Selected Topics in Signal Processing*, vol. 8, no. 5, pp. 742–758, October 2014.

[131] T. Riihonen, S. Werner, and R. Wichman, "Optimized gain control for single-frequency relaying with loop interference," *IEEE Transactions on Wireless Communications*, vol. 8, no. 6, pp. 2801–2806, June 2009.

[132] D. Nguyen, L. N. Tran, P. Pirinen, and M. Latva-aho, "Precoding for full duplex multiuser mimo systems: Spectral and energy efficiency maximization," *IEEE Transactions on Signal Processing*, vol. 61, no. 16, pp. 4038–4050, August 2013.

[133] Y. Sun, D. W. K. Ng, J. Zhu, and R. Schober, "Multi-objective optimization for robust power efficient and secure full-duplex wireless communication systems," *IEEE Transactions on Wireless Communications*, vol. 15, no. 8, pp. 5511–5526, August 2016.

[134] M. Jaggi, "Revisiting frank-wolfe projection-free sparse convex optimization," in *Proceeding of 2013 IEEE International Conference on Machine Learning*, Atlanta, USA, June 2013, pp. 427–435.

[135] Y. Cheng, M. Pesavento, and A. Philipp, "Joint network optimization and downlink beamforming for comp transmissions using mixed integer conic programming," *IEEE Transactions on Signal Processing*, vol. 61, no. 16, pp. 3972–3987, August 2013.

[136] S. Boyd and L. Vandenberghe, *Convex Optimization*, 1st ed. Cambridge, U.K: Cambridge University Press, 2004.

[137] S. Mallick, R. Devarajan, M. M. Rashid, and V. K. Bhargava, "Resource allocation for selective relaying based cellular wireless system with imperfect csi," *IEEE Transactions on Communications*, vol. 61, no. 5, pp. 1822–1834, May 2013.